Analysis of Phase Behavior for Steam-Solvent Coinjection for Bitumen Recovery

by

Kai Sheng

A thesis submitted in partial fulfillment of the requirements for the degree of

Master of Science

in

Petroleum Engineering

Department of Civil and Environmental Engineering
University of Alberta

Abstract

Steam-solvent coinjection, if properly implemented, can improve the bitumen recovery efficiency of steam-only injection methods, such as steam-assisted gravity drainage (SAGD). Previous studies have shown that steam-solvent coinjection can reduce residual oil saturation lower than that of SAGD. However, the phase behavior of reservoir fluids during steam-solvent coinjection has not been studied systematically to understand the enhanced displacement efficiency in steam-solvent coinjection. The main objective of this research is to develop a thermodynamics tool to explain the enhanced displacement efficiency obtained by steam-solvent coinjection compared to SAGD.

Isobaric ternary phase behavior of water/bitumen/solvent is analyzed to give a general classification method for solvent-containing reservoir fluids. Then, the mechanism of enhanced displacement efficiency by steam-solvent coinjection is explained in a unified way based on the systematic phase behavior study of reservoir fluids. The unified explanation incorporates the phase behavior study of reservoir fluids, mass transfer of the volatile components in reservoir fluids from liquids to vapor, and phase transitions. Finally, the unified explanation of distillation is applied to dimethyl ether (DME), a solvent that has not been studied for steam-solvent coinjection.

Two types of phase behavior can be defined for water/bitumen/n-alkane systems for steam-solvent coinjection. For Ternary Type 1, a solvent-rich oleic phase may separate from a bitumen-rich oleic phase in the vicinity of chamber edge, resulting in inefficient dilution of bitumen with the solvent. In contrast, Ternary Type 2 does not show the oleic phase separation, which indicates more effective dissolution of the solvent in bitumen. At

35 bars with the specific bitumen studied, n-C_4 and lighter alkanes are classified as Ternary Type 1, and those heavier than n-C_4 are classified as Ternary Type 2. Dimethyl ether is classified as a Ternary Type 1 solvent using the same classification scheme.

It is found that Ternary Type 1 n-alkanes can yield lower residual oil saturations than Ternary Type 2 n-alkanes under the same operation conditions. Analysis on distillation based on the thermodynamic tool indicates that the enhanced displacement efficiency because of distillation is a result of temperature increase and competition between water and solvent to evaporate. Coinjection of steam with a solvent that has a larger temperature increase during the distillation and is more volatile relative to water can achieve a lower residual oil saturation.

Coinjection of steam and DME through the analytical study shows its possible advantage over C_3, which is an alkane similar to dimethyl ether in terms of vapor pressure. Compared to C_3, DME has a smaller temperature increase for distillation, higher chamber edge temperature, higher displacement efficiency, and lower solvent retention. However, more research is required for more experimental data and modeling to investigate the applicability of DME.

The novelties of this research reside in the following items. The phase behavior classification and visualization of water/oil/solvent phase behavior is effectively used to explain the distillation mechanism and solvent dilution in steam-solvent coinjection. The analytical solution developed in this research is a first thermodynamics tool to estimate the displacement efficiency in steam-solvent coinjection, without performing numerical simulation. This research also gives a preliminary study of steam-DME coinjection.

Acknowledgements

I would like to express my most sincere gratitude to my supervisor, Dr. Ryosuke Okuno, for his guidance and financial support throughout my master program. As a researcher, he is indeed a real life model for me to follow. I have definitely learnt from him the essential qualities of being a good researcher, good attitude, hard work and integrity. What I have learnt would be of life-long benefits.

I would also like to thank the discussion and help of my loving colleagues and seniors, Arun Venkatramani, Ashutosh Kumar and Di Zhu. I respect them as smart, diligent and competent researchers. As goes the famous saying of Confucius translated by James Legge, “when I walk along with two others, they may serve me as my teachers. I will select their good qualities and follow them, their bad qualities and avoid them.”

I would also like to express my thanks to the love and support of my friends who share similar values. Many of them I have known for years and luckily I can still see them every day because of similar interests.

Last but not least, I would hereby address my deepest appreciation to my parents for their selfless love. I am lucky to live in a family that values education and knowledge more than anything else. That is why I have long been indoctrinated how education can change one’s fate.

Table of Contents

List of Tables

List of Figures

Nomenclature

Roman symbols

a, b	attraction and repulsion parameters of cubic EOS
A, B, C, D, E	constants of Rackett's equations
c_1, c_2, c_3, c_4	constants of BIP correlation
C_1	methane
C_3	propane
C_4	normal butane
C_5	normal pentane
C_6	normal hexane
C_7	normal heptane
C_{10}	normal decane
C_{12}	normal dodecane
H	enthalpy
$\underline{H}^{EXCESS}$	molar excess enthalpy
$\underline{H}_i^{IG}$	ideal gas molar enthalpy of component i
$\underline{H}_j$	molar enthalpy of phase j
$\underline{H}^t$	total molar enthalpy
K	K value
L1	bitumen-rich oleic phase
L2	solvent-rich oleic phase
Nc	number of components
Np	number of phases

P	pressure
P_c	critical pressure
P_{ref}	reference pressure
R	Regnault constant
S	saturation
S_g	gas saturation
S_{gr}	residual gas saturation
S_o	oil saturation
S_{or}	residual oil saturation
S_w	water saturation
S_{wr}	residual water saturation
T	temperature
T_{3p}	three-phase temperature
T_c	critical temperature
T_{edge}	chamber edge temperature
T_{ref}	reference temperature
T_{Swr}	temperature at S_{wr}
V	vapor phase
V_c	critical molar volume
W	aqueous phase
X	component mole fraction
x_{ij}	component i mole fraction in phase j
z	overall composition
Z	compressibility factor
z_i	overall composition of component i

Greek symbols

$\alpha_1, \alpha_2, \alpha_3, \alpha_4$	liquid density correlation constants in the CMG STARS (2013)
Λ, ζ	parameters of van Konynenburg and Scott's binary classification
β	phase mole fraction
β_j	mole fraction of phase j
ρ	molar density
ρ_i	pure component molar density of component i
ω	acentric factor

Abbreviations

AARD	average absolute relative deviation
BIP	binary interaction parameter
CP	critical point
DME	dimethyl ether
EOR	enhanced oil recovery
EOS	equation of state
PR EOS	the Peng-Robinson equation of state
GOR	surface gas oil ratio
IFT	interfacial tension
IG	ideal gas
K-S	van Konynenburg and Scott
LCEP	lower critical endpoint
MW	molecular weight
NPV	net present value
PC	pseudo component

RR	Rachford-Rice
SAGD	steam-assisted gravity drainage
ES-SAGD	expanded-solvent steam-assisted gravity drainage
SAP	solvent-aided process
SOR	steam-oil ratio
CSOR	cumulative steam-oil ratio
UCEP	upper critical endpoint
vdW	van der Waals
VLLE	vapor-liquid-liquid equilibrium

Superscripts and Subscripts

Bit	bitumen component
g	vapor phase
i	component index
HC	hydrocarbon
j	phase index
o	oleic phase
-r	residual variable
Sol	solvent component
w	water component
W	aqueous phase

Chapter 1 Introduction

1.1 Backgrounds and Problem Statements

The depletion of traditional fossil fuel and ever increasing energy demand have driven the exploration of unconventional resources, such as bitumen and heavy oil. Efficient recovery of those unconventional resources requires to increase the mobility of bitumen and heavy oil in situ. Thermal enhanced oil recovery (EOR) methods using steam such as SAGD and cyclic steam stimulation (CSS) have been proved to be successful techniques. The steam injected into a bitumen reservoir condenses at thermal fronts. Then, the latent heat is released to effectively reduce the bitumen viscosity, and therefore oil mobility is increased. Mobilized bitumen and heavy oil are then able to drain into the production well by gravity as in SAGD or by other mechanisms (Butler, 1997).

If properly implemented, an addition of a small amount of solvent into steam is able to increase production rate and bitumen recovery compared to SAGD in a series of pilot tests. Some successful pilot tests have reported increased bitumen drainage rate and reduced energy demand to recover one barrel of bitumen, such as the Imperial Oil's pilot test at the Cold Lake using heptane or C_7 (Leaute 2002; Leaute and Carey, 2005) and EnCana's pilot at the Senlac and the Christina Lake using butane or C_4 (Gupta and Gittins, 2006). In contrast, less successful pilots have also been reported in Nexen's Long Lake pilot using a mixture of hydrocarbons from C_7 to C_{12} and Suncor's Firebag pilot using naphtha (Orr 2009).

One of the benefits of steam-solvent coinjection is a higher bitumen drainage rate compared to SAGD. It has been reported that coinjection of a solvent can reduce the chamber edge temperature. The chamber edge temperature of lighter n-alkane is lower, if the same amount of solvent is added to the steam and complete condensation of water and solvent on the chamber edge is considered (Dong, 2012; Keshavarz et al., 2015b). However, the dissolved solvent and

water in the oleic phase near a chamber edge can reduce bitumen viscosity and may offset the negative impact brought by the lowered temperature on the oleic-phase mobility (Keshavarz et al., 2015b). Orr et al. (2003) reported hexane and heptane to be the optimum solvents that gave greatest incremental drainage rate because their volatility was similar to water. However, in the research of Gates (2007), C_6 could be even worse than SAGD in drainage rate. In the research of Govind et al. (2008), C_4 was reported to be the best in bitumen drainage rate. Other studies have revealed that the optimum solvent in terms of drainage rate is dependent upon the operation conditions, properties of bitumen and reservoirs. Heavier solvents are better than lighter ones in more viscous bitumen recovery and lower operation pressure conditions (Ardali et al., 2010; Keshavarz et al., 2015a). There has to be a unified framework to explain these different observations. A systematic understanding of phase behavior that occurs near a chamber edge is required to explain in a unified way and predict the performance of a solvent in terms of bitumen drainage rate as a result of solvent dissolution in the vicinity of steam chamber.

Steam-solvent injection also helps improve displacement efficiency compared to SAGD. Oil saturation (S_o) inside the chamber, or residual oil saturation (S_{or}), lower than the endpoint oil saturation, which is a reservoir rock property, has been reported by a number of researchers. Oil saturations lower than the endpoint oil saturation were firstly observed by Willman et al. (1961) in their steam injection experiment. They explained the lowered saturation as a result of the shrinkage of residual oil due to light components' distillation in heavy oil. In most simulations studies so far, heavy oil has been considered non-distillable. Steam-solvent coinjection can share similar mechanisms in oil saturation reduction if solvent can be sufficiently mixed with bitumen in situ. Nasr and Ayodele (2006) reported lowered residual oil saturation in ES-SAGD compared with SAGD using a mixture of light n-alkanes. Li et al. (2011b) reported a similar observation using a mixture of C_7 and dimethyl benzene. Also, Li et al. (2011a) concluded through numerical simulation that a mixture of solvents should be used because lighter solvents have better sweep efficiency while heavy ones have better displacement efficiency. Jha et al. (2013) gave an

opposite conclusion that the most volatile solvent C_4 used in their study yielded the lowest inside-chamber oil saturation as a result of solvent evaporation, similar to Willman et al.'s (1966) explanation. Keshavarz et al. (2015b) confirmed this observation by showing the process of volume shrinkage through ternary diagrams using C_5, and they (2015a) also observed volatile solvent yields lower oil saturation.

As discussed above, different researchers indicated different optimum solvents for displacement efficiency and production rate. The mixing of solvent with bitumen near a chamber edge is an important premise for solvent distillation and enhanced drainage rate. The mechanism of solvent distillation involves phase transition on the chamber edge: from all oleic and aqueous phases outside chamber to vapor-containing multiphase inside chamber. During the phase transition, solvent and water evaporate from liquid phases; however, distillation as a result of the mass transfer from liquids to vapor has not yet been explained in the literatures. In order to do analysis on the mass transfer from liquids to vapor, a systematic understanding of chamber edge conditions for water-solvent-bitumen is required. Yet, such a systematic phase behavior study of water-solvent-bitumen systems is also missing in the literatures. It helps to explain and predict performance of solvent in a unified way to understand water/bitumen/solvent ternary phase behavior and solvent distillation as a result of mass transfer from liquids to vapor.

Besides, the most commonly used solvents for steam-solvent coinjection are the n-alkanes, which have negligible solubility in water. If water-soluble solvent is used, the solvent is distillable from both the aqueous phase and oleic phase, unlike n-alkanes which can only be distilled from the oleic phase. This research is also interested in applying the systematic phase behavior study and distillation quantification to steam-solvent coinjection using water-soluble solvents.

1.2 Research Objectives

The objectives of this research are

- To give a systematic analysis of water-solvent-bitumen systems' multiphase behavior in steam-solvent coinjection;
- To give a thermodynamic understanding of enhanced displacement efficiency achieved by different solvents in steam-solvent coinjection;
- To develop a calculation method to quantify solvent and water transfer from liquids to vapor and the resulting residual oil saturation during the distillation process in steam-solvent coinjection; and
- To explore the possible usage of water-soluble solvent in steam-solvent coinjection based on the developed calculation method and numerical simulation.

1.3 Thesis Configuration

Chapter 2 presents a generic phase behavior classification method for ternary system based on three-phase behavior of reservoir fluid in temperature-composition space. Then, water/bitumen/n-alkane system is systematically studied, both as a ternary and a multicomponent system respectively, to show application of the classification method.

In Chapter 3, a thermodynamic tool is proposed to predict displacement efficiency enhanced by solvent distillation. The algorithm solves analytical residual oil saturation with few inputs, compared to numerical simulation. The tool is based on the thorough phase behavior study including multiphase and multicomponent. This model helps explain reduced residual oil saturation in steam or steam/solvent injection comprehensively. Differences between two types of n-alkanes proposed in Chapter 2 are discussed.

In Chapter 4, water/bitumen/DME ternary phase behavior is studied. Then, steam/DME coinjection is discussed via both analytical solution and numerical simulation. Its performance is compared with n-alkanes in terms of displacement efficiency, economic analysis and solvent efficiency in terms of bitumen recovery, steam-oil ratio and solvent retention.

In Chapter 5, important conclusions derived from this research are reiterated and their industrial significances are emphasized. Suggestions on future works are also presented based on observations in this research.

Chapter 2 Classification of Ternary Phase Behavior for Reservoir Fluids

2.1 Introduction

In EOR methods, such as steam injection, multiphase behavior and phase transitions are important for the explanation of improved oil recovery. In order to understand the phase behavior on the boundaries, equation of state (EOS), which is the mathematical description of phase behavior, should be used. Numerous modeling studies have been conducted in literatures regarding multiphase behavior, using a variety of EOS. One of the most famous classification by van Konynenburg and Scott (1980) gave a systematic overview on binary phase behavior. Such classification of phase behavior is helpful in behavior prediction of materials and mixtures that have not been fully understood.

In this chapter, a generic phase behavior classification method for ternary system is proposed based on three-phase behavior of reservoir fluid in temperature-composition (T-x) space. Then, water/bitumen/n-alkane system is thoroughly studied, both as a ternary and a multicomponent system respectively, to show application of the classification method.

2.1.1 Van Konynenburg and Scott Classification for Binary Phase Behavior

Van Konynenburg and Scott (1980) gave a systematic classification of binary systems on the basis of pressure-temperature (P-T) projections. In particular, they were concerned with the existence of three-phase and azeotrope lines and their relative positions to vapor pressure curves, and the ways critical lines were connected between critical points and critical endpoints.

Projections of phase boundaries in P-T space were reflected by two parameters in the research by van Konynenburg and Scott (K-S), Λ and ζ (Scott and van Konynenburg, 1970),

$$\zeta = (\frac{a_{22}}{b_{22}^2} - \frac{a_{11}}{b_{11}^2})/(\frac{a_{22}}{b_{22}^2} + \frac{a_{11}}{b_{11}^2}) \quad (2.1)$$

$$\Lambda = (\frac{a_{11}}{b_{11}^2} - \frac{2a_{12}}{b_{11}b_{22}} + \frac{a_{22}}{b_{22}^2})/(\frac{a_{22}}{b_{22}^2} - \frac{a_{11}}{b_{11}^2}) \quad (2.2)$$

where ζ represents the differences of critical pressure between two components in a binary system, and Λ is proportional to the excess molar enthalpy at 0 K. These two parameters are functions of a and b, the attraction and repulsion parameters. In their study, the van der Waals (vdW) EOS with the vdW mixing rules was used for phase behavior study and therefore, pure component a and b, i.e. a_{ii} and b_{ii} in equation 2.1 and 2.2, are only determined by critical properties of pure components.

By investigating all possible a_{12} and b_{12}, five types of binaries were classified in terms of ζ-Λ relation. Their classification is reproduced in **Figure 2.1**. The compact region in the vicinity of Λ=0 is enlarged and shown in **Figure 2.2**. Binary phase behavior can be classified into five types, from Type I to V, with subtypes possible within each type (van Konynenburg and Scott, 1980).

2.1.2 Experimental Evidence of Konynenburg-Scott Classification

The K-S classification was revisited by Deiters and Kraska (2011) in their monograph based on experimental data. Experiments have shown that Types I to V were remarkably predicted by the vdW EOS, despite its simplicity. A few more subtypes were added to complement the original K-S classification.

However, Types VI, VII and VIII were additionally found by experiments in some rare cases concerning non-spherical binaries, isotope-contained substances, ionic liquids and so on. These types have closed-loop immiscibility zones that cannot be properly predicted by simple EOS's, such as the vdW EOS (Bashkov, 1987; Schneider, 2002).

2.1.3 Introduction to Type III and Its Variants

According to the K-S definition, a Type III system is defined as a heteroazeotrope with two critical curves: one of the critical curve should connect one of critical point (CP1) and upper critical endpoint (UCEP); the other critical curve should connect the second critical point (CP2) while the other end goes to infinity as pressure increases. To clarify, heteroazeotrope is defined as a binary of which azeotrope happens inside miscibility gap, i.e. three-phase line exists for the binary.

Depending on the relative position of three-phase line to the vapor pressure curves, two variations of Type III are further presented by van Konynenburg and Scott (1980). If three-phase line lies to the left of both vapor pressure curves, it is classified as Type III-HA (**Figure 2.3**), and if three-phase line lies between two vapor pressure curves, it is classified as a Type III (**Figure 2.4**). To further classify, if the unbounded critical curve is S-shaped, it is further classified as Type III_m or Type III-HA_m.

Water/n-alkane is a typical Type III-HA system. Brunner (1990) further classified water/n-alkane as subtypes a (C1-C26) and b (C27 and heavier). For subtype a, the bounded critical curve connects UCEP and the CP of n-alkane, while for subtype b, the bounded critical curve connects UCEP and CP of water. Venkatramani and Okuno (2014) further pointed out differences between those two subtypes: for subtype a, L-V two-phase region becomes one phase at UCEP; for subtype b, W-V two-phase region becomes one phase at UCEP. Further explanation can be found in their paper.

Type III and its variants are of great interest in the petroleum industry. A number of binary systems fall into this category when one of the components is water or hydrocarbon.

The majority of water/hydrocarbon systems fall into Type III with a few exceptions (Qian et al., 2013). Examples can be found in literatures, such as binaries containing water and one of the following hydrocarbons: n-alkanes, n-alkenes, single-ring aromatics such as benzene and toluene (Robert and Kay, 1959; Connolly, 1966; Brunner, 1990; Brunner et al., 2006; Qian et al., 2013). Water/inorganics such as CO_2, H_2, H_2S and N_2 also falls into Type III. Water and multi-ring

aromatic binaries fall into Type II, which shares great similarities with Type III as will be introduced later (Brunner et al., 2006).

2.1.4 Similarities between Type II, III_m and IV

As shown in **Figure 2.1** and **Figure 2.2**, the transition zone from Type II to Type III_m via Type IV is a rather narrow region in Λ-ζ space. This results in great similarities of phase behavior in those types. **Figure 2.5** shows schematics of P-T projections for those three types.

By definition of the K-S classification, Type II is defined as a heteroazeotrope with one critical curve connecting two critical points (CP) and the other critical curve connecting upper critical endpoint (UCEP) and infinity. A three-phase line is between two vapor pressure curves, and the UCEP is below either of the critical points. Type IV has a discontinuous three-phase line and three critical curves: CP1 to UCEP; UCEP to infinity; lower critical endpoint (LCEP) to CP2. By inspection of **Figure 2.5** (1) to (3), it can be concluded that, the intersection of the S-shaped critical curve with three-phase line or vapor pressure curve results in three different types of phase behavior, and yet very similar.

Schematic T-x diagrams for Type III_m and Type III-HA are shown in **Figure 2.6**. Types II and IV resemble Type III_m in T-x diagram in that phase boundaries between all the two-phase regions disappear if pressure is increased. In contrast, Type III-HA phase boundaries are not prone to disappear with increased pressure.

One of the examples for the transition between Type II, III_m via IV is the case of hydrocarbon/inorganics binary. CO_2/n-alkane may fall into different categories, largely depending on the volatility of the hydrocarbon component. For an example, CO_2/n-C_{10} is classified as Type II, CO_2/n-C_{13} Type IV and CO_2/n-C_{14} Type III_m (Brunner, 1988).

Another good example is the case of hydrocarbon/hydrocarbon binaries. The category to which a specific binary belongs is decided by the volatility of both of the hydrocarbon. For instance,

Λ-ζ pairs of n-alkane/n-alkane systems are narrowly scattered around the borders between II, III_m and IV shown in **Figure 2.2** (van Konynenburg and Scott, 1980).

2.2 Classification of Ternary Phase Behavior

A generic classification method of ternary phase behaviors should be based on the observations of binary phase behaviors. Different binaries show different sensitivities to thermodynamic conditions in terms of phase behavior, as was described in **§2.1**. The binary in a ternary system that is prone to have separated two-phase regions with changing pressure should be examined when a ternary system is studied.

It is proposed here a classification method for ternary phase behavior based on the effect of binary behavior on ternary tie triangles. In the ternary classification method, the isobaric phase behavior is considered. Also, since the ternary phase behavior classification for water/bitumen/solvent should be used to serve phase behavior related study for steam-solvent coinjection, an operation temperature range should be applied in this classification. The upper temperature limit of the temperature range is the maximal possible operation temperature of coinjection, and the lower temperature limit the minimal possible coinjection temperature. As will be introduced later, the upper and lower temperature limit should be complete condensation temperature of water/bitumen and that of water/n-alkane respectively.

For a given solvent-containing reservoir fluid system, water/oil/solvent, theoretically two types of ternary phase behavior exist. Those two ternary types are classified based on the binary T-x phase behavior of oil/solvent. Usually, oil/solvent binary falls into Type II, III_m or IV of the K-S classification, which means phase boundaries between two-phase regions of oil/solvent binary is prone to disappear if pressure is increased. If within the steam-solvent coinjection operation temperature range, i.e. three-phase temperature of water/solvent and water/oil, there can be more than one oleic phases, the corresponding ternary system is classified as Ternary Type 1; if within

the temperature range, solvent is able to completely dilute into oil, the corresponding ternary system is classified as Ternary Type 2.

The dilution of bitumen with solvent is considered an important mechanism in steam-solvent coinjection. Properly implemented coinjection of steam-solvent enhances bitumen drainage and displacement efficiency as a result of sufficient solvent mixing with oil. Within the operation temperature range, oil/solvent binary temperature-compositional diagram may have several attached two-phase regions with the appearance of two oleic phases, oil-rich oleic phase (L1) and solvent-rich oleic phase (L2).

Later in this chapter, water/bitumen/n-alkane system is systematically studied based on the classification method proposed. Also in Chapter 4, the performance of DME, a solvent that has not been much studied in thermal recovery, is analyzed based on the classification method proposed in this chapter.

2.3 Case Study 1: Water/bitumen/n-Alkane Ternary System

This section provides a phase behavior study for water/bitumen/n-alkane ternary system with the consideration of water dissolution into oil by performing phase equilibrium calculation. The generic classification method mentioned in **§2.2** is applied here. Isobaric ternary phase behavior is then visualized in temperature-compositional space to show the differences between types.

2.3.1 EOS Model

The Peng-Robinson (PR) equation of state (1978) and the vdW mixing rules are coupled for phase equilibrium calculation. This model is used throughout this research. Details of the PR EOS and the vdW mixing rules can be found in **Appendix A**.

Only three components are considered in the model: water, single-component solvent and bitumen characterized as one pseudo component (1-PC). Critical properties for each component and binary interaction parameters (BIPs) are summarized in **Table 2.1** and **Table 2.2**.

The critical properties of water and n-alkanes were tabulated in the paper of Venkatramani and Okuno (2015) and were based on data from API technical data book and group-contribution method (Constantinou and Gani, 1994; Constantinou et al., 1995). A reliable BIP correlation by matching water/solvent three-phase behavior was developed by Venkatramani and Okuno (2015) for a better water dissolution prediction in oleic phase:

$$\mathrm{BIP}_{w/HC} = c_1[1 + \exp(c_2 - c_3 MW)]^{-1/c_4} \tag{2.3}$$

where c_1=0.24200, c_2=65.90912, c_3=0.18959, c_4=-56.81257 and *MW* is the molecular weight of n-alkane. For BIP between water and this particular bitumen, the correlation is scaled with a factor of 0.7 to account for the aromatics in the bitumen. This is because the affinity between water and bitumen is higher than that between water and n-alkane. This scaling factor 0.7 by Venkatramani and Okuno (2016) was matched upon experimental data of Amani et al. (2013a and b)

Bitumen is a JACOS of Athabasca bitumen characterized as Bitumen A in the study of Kumar and Okuno (2016). BIPs between bitumen and n-alkanes can be calculated by the following correlation (Kumar, 2016):

$$\mathrm{BIP}_{bit/sol} = 0.0349 \ln\left(\frac{V_{c-sol}}{V_{c-bit}}\right) + 0.1329 \tag{2.4}$$

where V_c is critical volume of bitumen or n-alkanes. $V_{c\text{-}sol}$s are standard experiment data and $V_{c\text{-}bit}$ can be calculated directly from Riazi and Daubert Correlation (1987). See **Table 2.1** for critical volumes.

2.3.2 Classification for Water/Bitumen/n-Alkane Ternary System

Water/oil/solvent ternary phase behavior can be deemed in the following way: water/bitumen binary reflects the phase behavior in steam-only injection; bitumen/solvent reflects phase

behavior of gas injection; and water/solvent reflects can be deemed as an extreme coinjection case where bitumen is completely displaced. **Figure 2.7** shows vapor pressure curves and three-phase curves for SAGD and coinjection. When no solvent is coinjected at all, the condensation temperature of steam is the T_{3p} of water/bitumen. Also, if bitumen is 100% displaced, the temperature of complete condensation of steam-solvent should be the T_{3p} of water/solvent. Therefore, the operation temperature range should start from the T_{3p} of water/n-alkane as the lower coinjection temperature limit, to the T_{3p} of water/bitumen as the upper coinjection temperature limit.

According to the generic classification method for ternary phase behavior in **§2.2**, oil/solvent is the pair that decides the water/bitumen/solvent ternary phase behavior classification. Within the steam injection operation temperature range, whether solvent can completely dilute oil decides the ternary classification.

P-T diagrams for pure component vapor pressure curves, three-phase curve of water/solvent and three-phase curves of bitumen/solvent are shown in **Figure 2.7**. Water/bitumen/n-C_4 and n-C_5 phase behaviors at 35 bars are selected as examples. Isobaric temperature-composition (T-x) diagrams for binaries are shown from **Figure 2.8** to **Figure 2.10**. Phase behavior study for all the pure components and binaries are done in a wide range of temperatures and pressures for water/bitumen/n-alkane systems. Water/bitumen and water/n-alkane are Type III systems (without a subscript m) and only bitumen/n-alkane is a Type III_m of the K-S classification. Also, the lower temperature boundary, which is three-phase temperature of water/n-alkane, is always on the higher temperature side of three-phase temperature of bitumen/n-alkane, if any. This means the lower temperature boundary always crosses either L1 one-phase region or L1-L2 two-phase region. Therefore, the classification method for water/bitumen/n-alkane would be: if in a bitumen/solvent isobaric T-x diagram, L1-L2 regions is connected to other two-phase region, the corresponding water/bitumen/n-alkane ternary system is classified as Ternary Type 1; otherwise, Ternary Type 2.

Figure 2.9 shows binary T-x diagrams for a Ternary Type 1 solvent, n-C_4. For bitumen/n-C_4 binary, within three-phase temperature of water/n-C_4 and water/bitumen, phase boundary exists between L1-L2 and L1-V, it is classified as Ternary Type 1. **Figure 2.10** shows binary T-x diagrams for a Ternary Type 2 solvent, n-C_5. However, for n-C_5, such boundary does not exist between three-phase temperatures of water/n-C_5 and water/bitumen, and therefore it is classified as Ternary Type 2. Follow this classification, at 35 bars, n-alkanes up to n-C_4 are classified as Ternary Type 1 solvents; n-C_5 and heavier are Ternary Type 2.

The binary phase behavior of bitumen/solvent results in significant three-phase region difference in corresponding water/bitumen/solvent ternary systems. Isobaric three-phase region transitions in temperature-compositional space are depicted in **Figure 2.11** and **Figure 2.12** for typical Ternary Type 1 and Ternary Type 2 respectively.

Figure 2.11 shows water/bitumen/n-C_4 the ternary diagrams at 35 bars**.** For n-C_4 (Ternary Type 1), when temperature is low, only W-L1-L2 three-phase region exists. In the vicinity of three-phase temperature of water/n-C_4, W-L2-V and W-L1-L2 coexist. As W-L2-V region expands with increasing temperature, W-L2-V and W-L1-L2 merge first, and then split into W-L1-V and V-L1-L2. As temperature is further increased, L1 vertex of W-L1-V swings towards water/bitumen binary edge. Between the three-phase temperature of water/n-C_4 and water/bitumen, L1 and L2 may coexist.

Figure 2.12 shows water/bitumen/n-C_5 ternary diagrams at 35 bars. Compared to n-C_4 case, ternary phase behavior is much simpler for n-C_5 case (Ternary Type 2). Only W-L1-L2 exists at low temperatures and gradually disappears as temperature increases. As temperatures continues increasing, no three-phase region exists for a narrow temperature range. Then, W-L1-V emerges from water/n-C_5 edge and L1 vertex swings towards water/bitumen edge. Between the three-phase temperature of water/n-C_5 and water/bitumen, only L1 exists, unlike Ternary Type 1 of which L1 and L2 may coexist.

The differences in the ternary phase behavior between two types resides in whether there can be coexistence of W, L1 and L2 within the three-phase temperature of water/solvent and water/bitumen. Ternary Type 1 may have W-L1-L2 region within the temperature range; Ternary Type 2 does not.

Three-phase region of water/bitumen/n-alkane system is shown in form of isobaric ternary prism in 3D. Complex phase transition, which discriminates Ternary Type 1 from Ternary Type 2, s shown through depiction of continuous three-phase region change with temperature in **Figure 2.13** and **Figure 2.14**.

2.3.3 Discussion on Classification

The water/bitumen/solvent classification method is based on binary phase behavior within the coinjection operation temperature range. Therefore, all the factors that affect phase behavior of bitumen/solvent behavior and T_{3p} should be discussed. The factors include the pressure, bitumen properties and solvent volatility.

Figure 2.15 shows bitumen/n-C_4 T-x diagrams at 60 bars. By comparison between **Figure 2.15** and **Figure 2.9**, increased pressure suppresses the existence of V phase and separate different two-phase regions. At 35 bars, n-C_4 is a Ternary Type 1 but is turned into Ternary Type 2 at 60 bars. Therefore, higher pressure can turn Ternary Type 1 solvent into Ternary Type 2 solvent by eliminating phase boundaries between two-phase regions. The pressure at which Ternary Type 1 turns into Ternary Type 2 is summarized for each n-alkane solvent in **Table 2.3**. This temperature is where different two-phase regions separate. This pressure is also compared with pressure at UCEP and CP related to the solvent. For the PR EOS and the specific bitumen used in this discussion, the pressure at which C_3 turns from Ternary Type 1 to Ternary Type 2 is over 100 bars. Also, the pressure at which C_6 is a Ternary Type 1 solvent should be lower than 1 bar.

Solvent volatility plays an important role in the classification, as is shown in **§2.3.2**. At 35 bars, C1 to n-C_4 are Ternary Type 1 and n-C_5 and heavier are Ternary Type 2. The temperature span of W-L-V region usually starts from the three-phase temperature of water/n-alkane to that of water/bitumen. Less volatile solvents have higher water/n-alkane three-phase temperature, and therefore smaller temperature range for W-L-V to happen.

At 35 bars, within Ternary Type 1 solvents, more volatile solvent has smaller temperature span for the complex three-phase transition to happen, i.e. W-L2-V and W-L1-L2 first merge and then split into W-L1-V and V-L1-L2 as in **Figure 2.11** (3) to (6). This transition happens between three-phase temperature of water/n-alkane and that of bitumen/n-alkane. The transition temperature span at 35 bars for Ternary Type 1 is summarized in **Table 2.4**. Also, ternary diagrams for an extreme Ternary Type 1 case, methane, are shown in **Figure 2.16** and **Figure 2.17**. “Merge and split” happen almost simultaneously at saturation temperature of methane.

As shown from **Figure 2.8** to **Figure 2.10**, phase boundaries do not disappear with changed pressure or solvent volatility between two-phase regions in the water/bitumen and water/n-alkane edge T-x diagram. It is the bitumen/solvent binary T-x phase behavior that is susceptible to pressure or solvent volatility. Within the chamber edge temperature range of steam/solvent coinjection, Ternary Type 1 solvents may have L1 and L2 simultaneously on, inside or outside the steam chamber, while Ternary Type 2 solvents only have L1. It is unfavorable to have two oleic phases outside steam chamber. A solvent-rich L2 phase indicates poor solvent dissolution into bitumen. Also, L2 phase shares limited oleic phase permeability with L1 phase and detriments mobility of L1 phase.

Since the miscibility between bitumen and solvent is a concern in the classification, the properties of bitumen also affect the ternary classification. However, this is not specifically studied in case study 1, because the critical properties of a different bitumen are not available in this research. Generally, ternary systems with lighter bitumen tends to be a Ternary Type 2.

2.4 Case Study 2: Water/Bitumen/n-Alkane Multicomponent System

In this section, a multicomponent EOS model based on latest experiment results is used to show the capability of the classification method beyond simplified ternary system shown in **§2.3**. Water/bitumen/n-alkane is studied to show how the classification method can be applied to complex reservoir fluid in reality.

2.4.1 EOS Model

A multicomponent system made of water, bitumen and n-alkane is studied. Same as the previous case study, the PR EOS with the vdW mixing rules is used. Critical properties of water and n-alkanes as well as BIPs between water/n-alkanes are the same as in 2.3.1.

Properties of a different Athabasca bitumen was characterized into 4 pseudo components (4-PC) in Gao et al.'s (2016) work. Its properties and BIPs were fine tuned to match latest PVT experiment data. Critical properties for each pseudo component can be found in **Table 2.5**. BIPs between 4-PC bitumen and n-alkanes are summarized in **Table 2.6**.

2.4.2 Classification and discussion

As mentioned earlier, bitumen/n-alkane is a Type III_m of the K-S classification that decides ternary phase behavior classification. For a multicomponent system with 4-PC bitumen, 4-PC/n-alkane pair should be examined to see how 4-PC/n-alkane affects water/4-PC/n-alkane multiphase phase behavior.

Figure 2.18 shows T-x diagrams at 35 bars for 4-PC/n-alkane mixtures. Overall composition is fixed here because degree of freedom for three-phase region is greater than 1 in multicomponent systems, i.e. phase behavior is changing with overall composition. Bitumen to solvent molar ratio is set to 0.1. L1-L2-V three-phase region exists for n-C_4 and n-C_6 cases, but not for n-C_8.

Accordingly, water/4-PC/n-alkane is examined at 35 bars, with 95 mol% water and 0.1 bitumen-solvent ratio. **Figure 2.19** shows T-x diagrams for systems including water. W-L1-L2-V 4-phase region exists for n-C_4 and n-C_6, but not for n-C_8.

In this case, n-C_4 and n-C_6 are classified as Ternary Type 1 while n-C_8 is classified as Ternary Type 2. It is the L1-L2-V three-phase behavior in bitumen/n-alkane mixture determines the W-L1-L2-V behavior in water/bitumen/n-alkane multicomponent system. The generic classification method still holds true for more complicated mixtures like in this case. This is due to the fact that, ideally, simplified ternary system water/bitumen/solvent is capable of capturing key multiphase behavior for more complicated reservoir fluids. Classification on simplified ternary systems is a good representation for reservoir fluids type in reality.

The case study 2 uses a different bitumen as in case study 1. That explains why C_6 is Ternary Type 1 in case study 2 but a Ternary Type 2 in case study 1. Generally, heavier oil turns Ternary Type 1 into Ternary Type 2.

The significance of the classification for ternary systems is to understand how the miscibility between solvent and bitumen can affect the bitumen dilution with water and solvent on the chamber edge. It has been shown through case study 1 and 2 that the separation of two different oleic phases is possible for Ternary Type 1 system. The existence of the Ternary Type 1 system of water/bitumen/n-C_4 has been observed by Gao et al. (2016) through experiment study. The EOS model in case study 2 is based on their experiment measurement of water/bitumen/solvent phase behavior. In their study, L1-L2-V was found coexisted for a bitumen/n-C_4 mixture with 97 mol% C4 around 413.25 K and 29.21 bars. In the corresponding ternary system with 62 mol% of water and 37 mol% of C4, the coexistence of W-L1-L2-V was observed around 433.05 K and 45.76 bars, which is in the vicinity of the complete condensation condition at this pressure. A separated oleic phase means poor bitumen dilution with solvent. Also, they found that lighter components in the bitumen was extracted to the L2 phases, and therefore the L1 phase becomes even more viscous and difficult to flow.

2.5 Conclusions

A generic classification method for phase behavior of water/oil/solvent ternary systems was developed in this chapter. This method classifies ternary systems based on three-phase behavior in temperature-composition space by investigation of phase behavior of bitumen/solvent, which falls into Type II, IV or III_m of the classification by van Konynenberg and Scott (1980).

- If the bitumen/solvent binary shows more than one oleic phases within the chamber edge temperature range, the corresponding water/bitumen/solvent ternary system is classified as Ternary Type 1; otherwise, it is classified as Ternary Type 2. Here, the chamber edge temperature range is defied by two extreme cases: the upper temperature bound is defined as the chamber edge temperature when solvent is not injected at all, i.e. the SAGD chamber edge temperature; the lower temperature bound is defined as the chamber edge temperature when bitumen is 100% displaced, i.e. the complete condensation temperature of water/solvent.
- For the specific n-alkane containing bitumen system studied in case study 1, n-alkanes up to n-C_4 are classified as Ternary Type 1, and n-alkanes heavier than n-C_4 are classified as Ternary Type 2. Ternary Type 1 has complex three-phase transitions among W, L1, L2 and V within the operation temperature range. However, only W, L1 and V exist for Ternary Type 2 phase behavior within coinjection operation temperature range, from T_{3p} of water/n-alkane to that of water/bitumen.
- The classification for case study 1 is subject to several conditions. Higher operation pressure will turn Ternary Type 1 into Ternary Type 2. Heavier bitumen will turn Ternary Type 2 into Ternary Type 1. Also, heavier solvents within the same family will turn Ternary Type 1 into Ternary Type 2.
- Case study 2 indicates the possibility of a second oleic phase L2 inside the steam chamber. The ternary classification method based on bitumen/solvent binary can be

applied to multicomponent systems. In the multicomponent system, n-C_4 and n-C_6 are Ternary Type 1 because L2 phase exists within the operation temperature range of steam-solvent coinjection. N-C_8 is classified as Ternary Type 2.

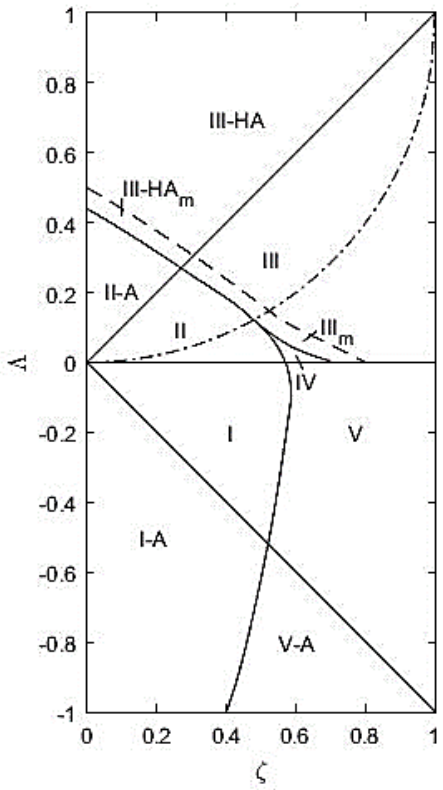

Figure 2.1 A reproduction of the binary classification method by van Konynenburg and Scott (1980). The vdW EOS was used in their classification method. Λ and ζ are only functions of a and b specific to the vdW EOS. Different regions are divided by enumerating all possible a and b values.

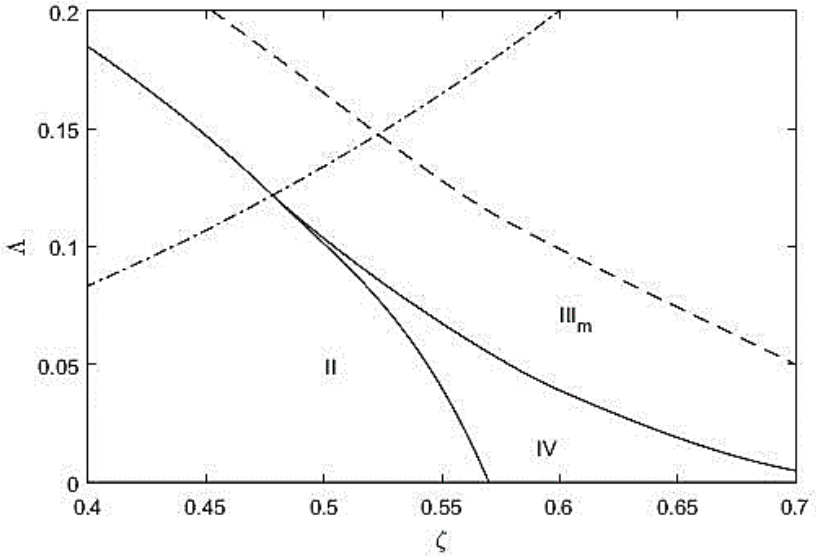

Figure 2.2 Boundaries between Type II, IV and III_m of the classification by van Konynenberg and Scott (1980). As will be shown in the subsequent figures, they share some common features. Transition from II to III_m may happen if the binary consists of a hydrocarbon and a non-water component. CO_2/n-C_{10} is Type II, while CO_2/n-C_{13} IV, and CO_2/n-C_{14} III_m.

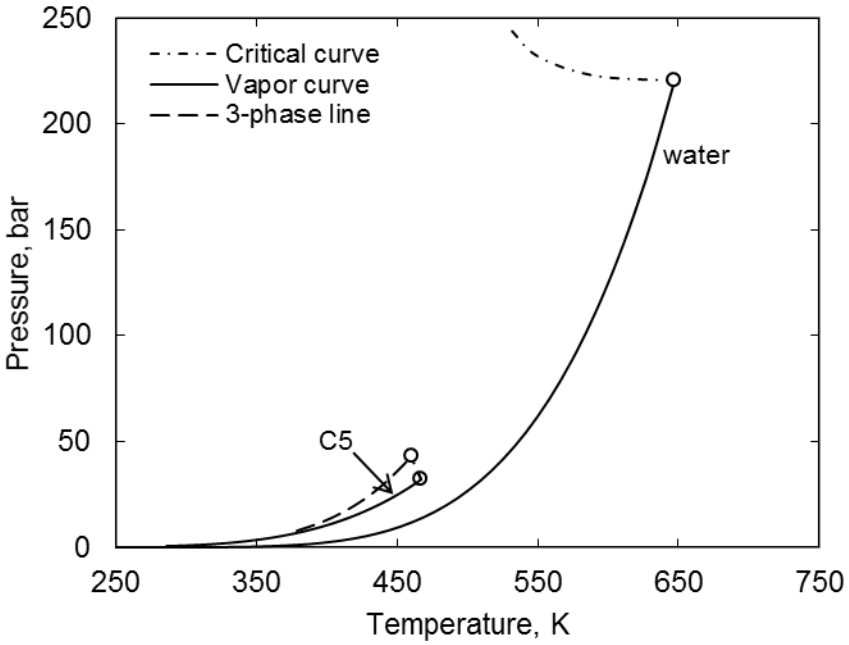

Figure 2.3 Schematic of typical Type III-HA binary P-T projections. Water/n-C_5 is taken as an example. three-phase line is to the left of both of the vapor pressure curves. One critical curve connects UCEP and CP n-C_5 and the other one connects CP water and infinity.

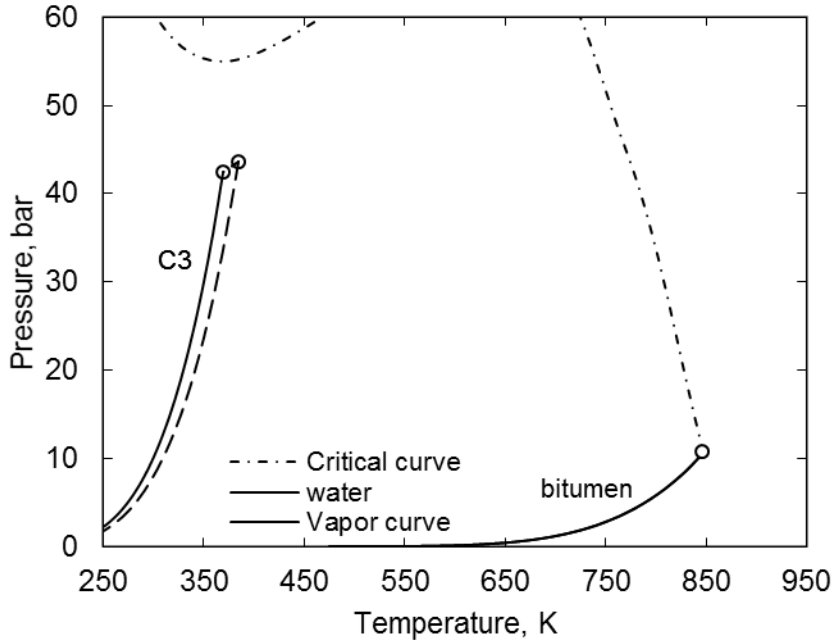

Figure 2.4 Schematic of typical Type III binary P-T projections. It is a Type III_m system to be specific. Bitumen/C_3 is taken as an example. three-phase line is between two vapor pressure curves. One critical curve connects UCEP and CP of C_3 and the other one connects CP of water and infinity.

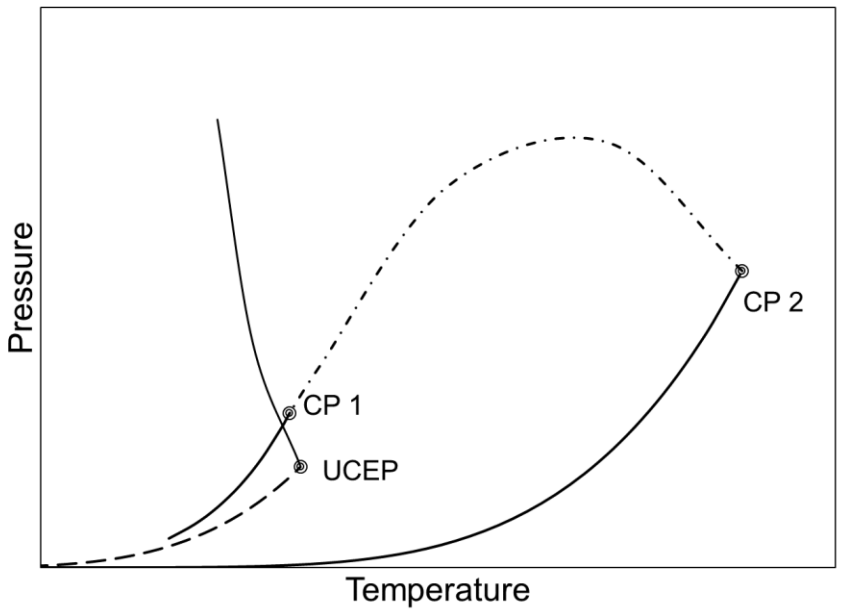

(1) Type II

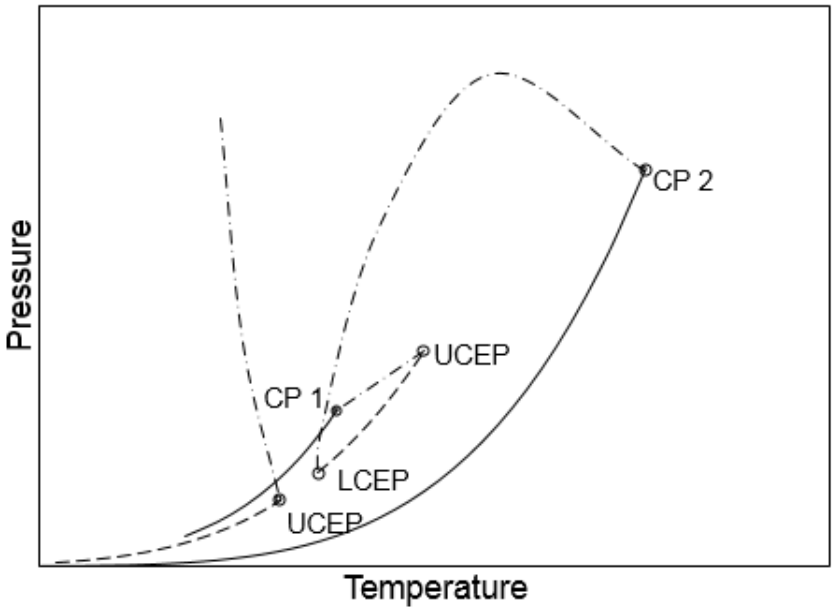

(2) Type IV

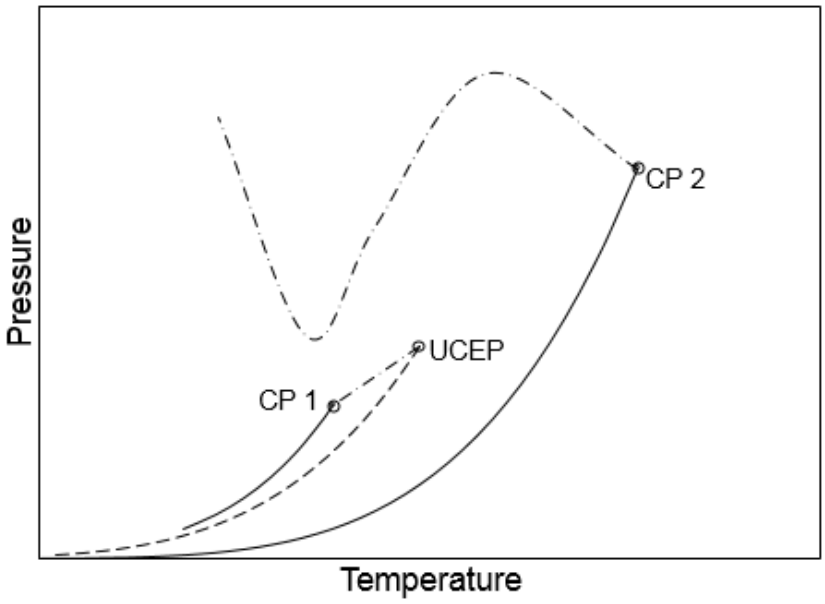

(3) Type III_m

Figure 2.5 Schematic to show the transition from Type II to III_m via IV in P-T diagram. Intersection of the S-shaped critical curve with three-phase line or vapor pressure curve results in three different types of phase behavior, and yet very similar.

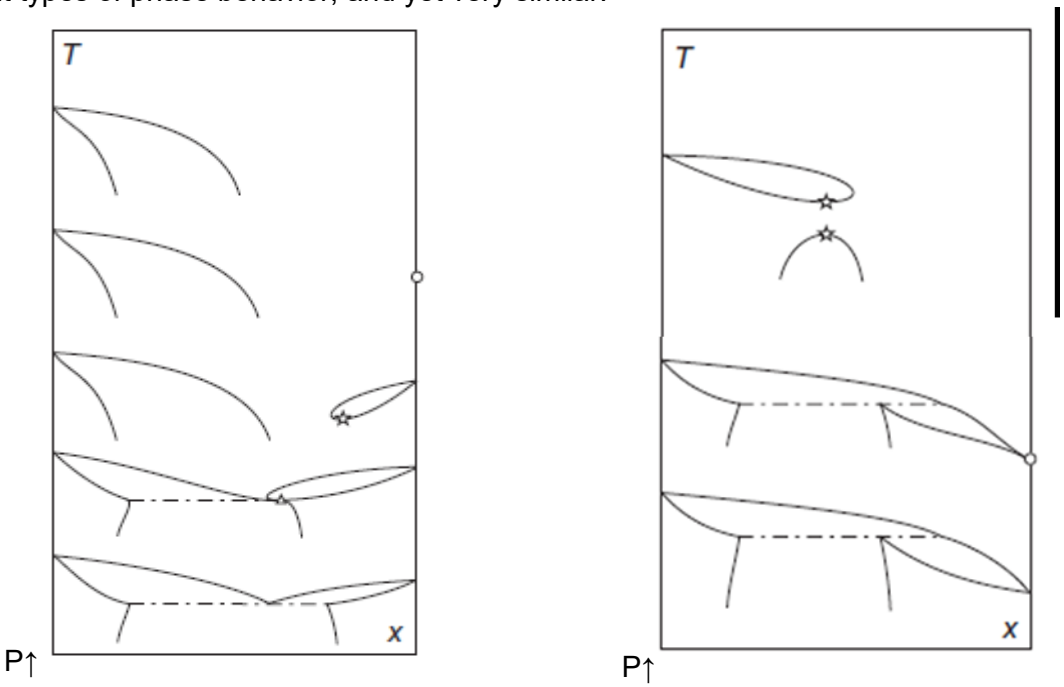

(1) Type III-HA (2) Type III_m

Figure 2.6 Schematic of van Konynenburg and Scott (1980) Type III-HA and Type III_m T-x diagrams with increased P (a figure from Deiter and Kraska, 2012). From the bottom to the top, pressure increases. The phase boundary is easy to disappear for III_m with increasing pressure.

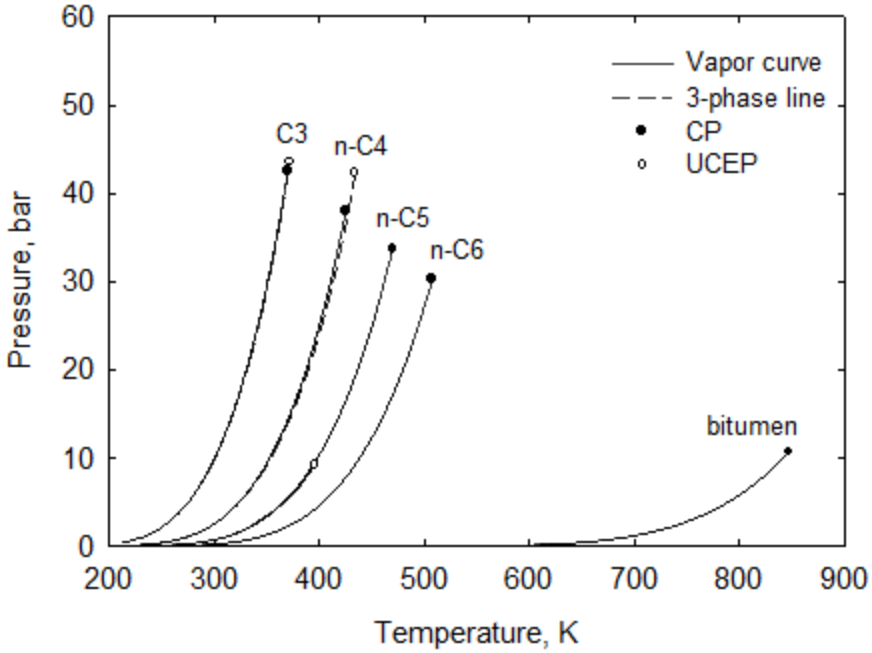

(1) Bitumen/n-alkane three-phase curves

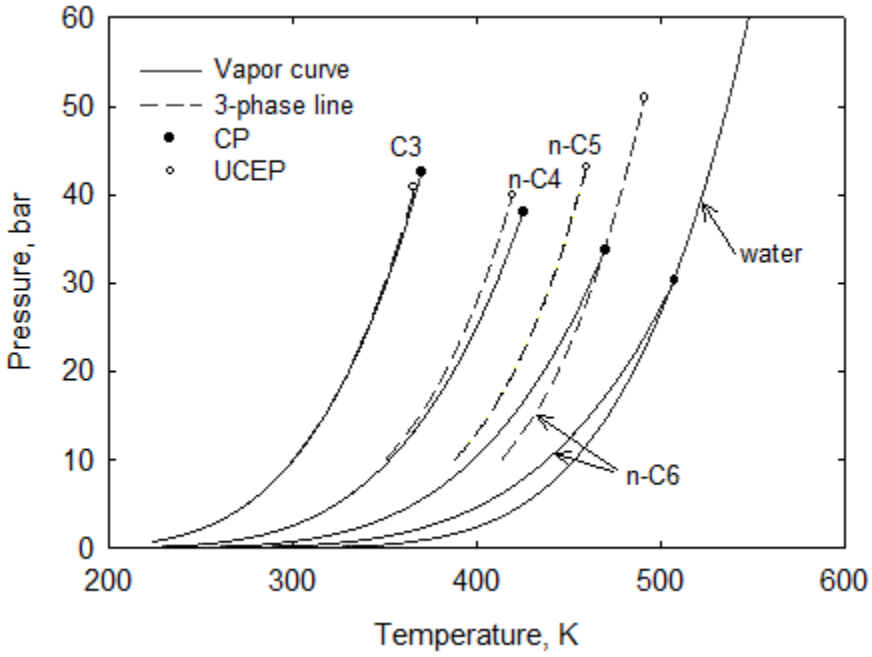

(2) Water/solvent three-phase curves

Figure 2.7 Vapor pressure curves and binary three-phase curves of water/bitumen/n-alkane system.

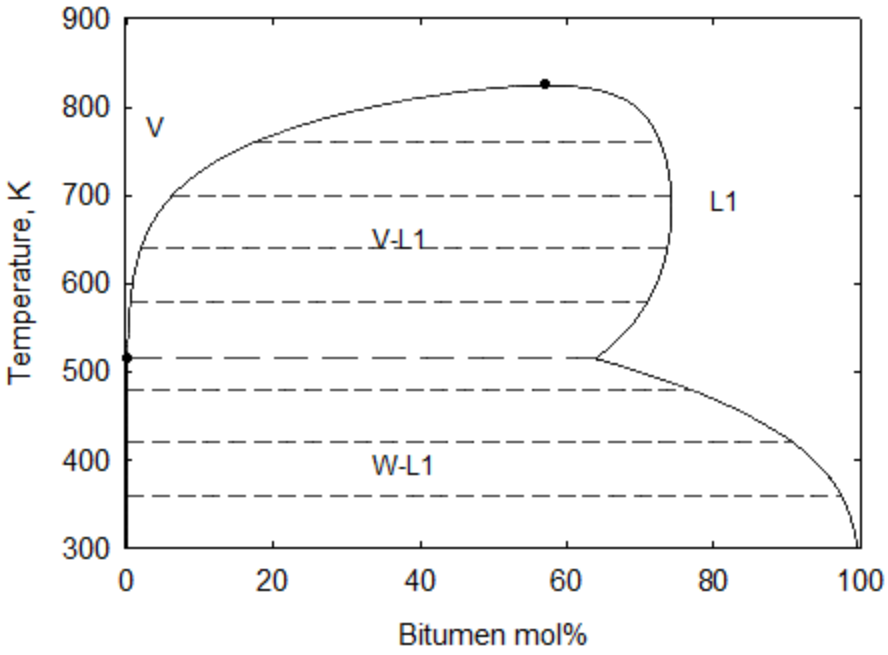

Figure 2.8 Water/bitumen T-x diagram at 35 bars. Long dashed line represents three-phase temperature of water/bitumen, which is 515 K. Short dashed lines are tie lines. Solid dots represent critical point or saturated point.

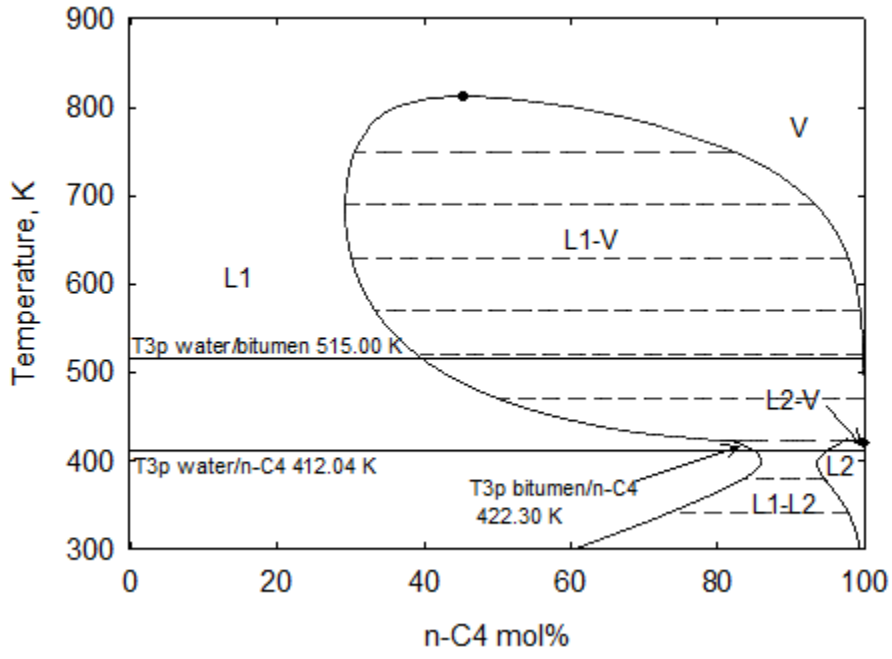

(1) Bitumen/n-C_4

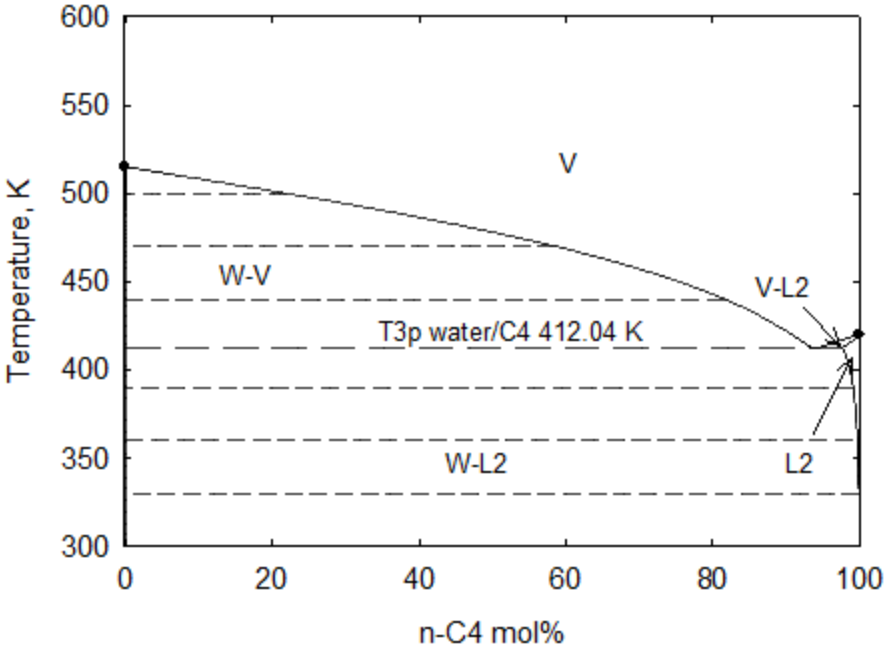

(2) Water/n-C_4

Figure 2.9 Ternary Type 1 solvent (n-C_4) binary T-x diagrams at 35 bars. Bitumen/n-C_4 is the Type III_m, of which the phase boundary between two-phase regions is prone to disappear with increased pressure. Phase boundary exists between L1-L2 and L1-V, thus this is classified as Ternary Type 1.

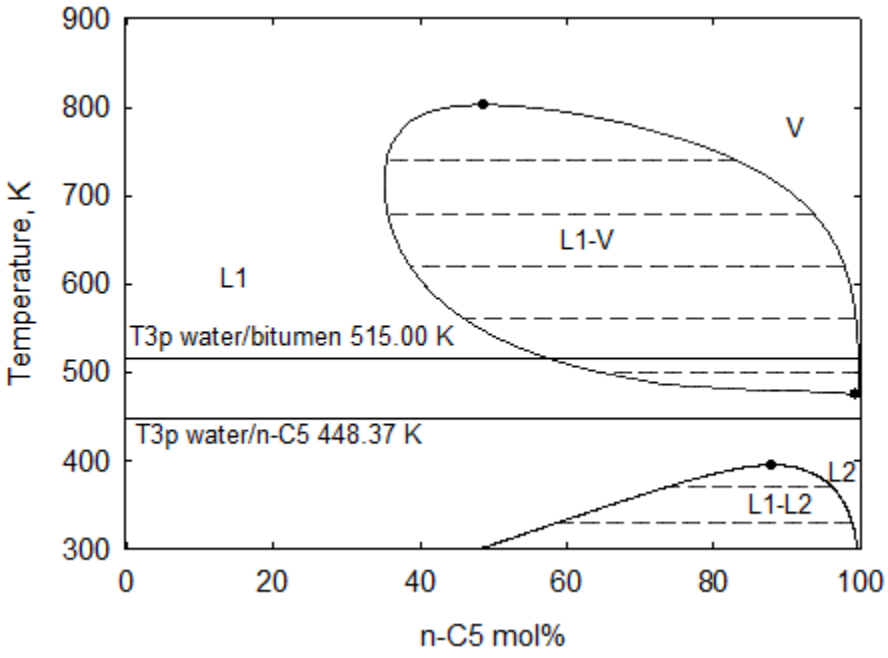

(1) Bitumen/n-C_5

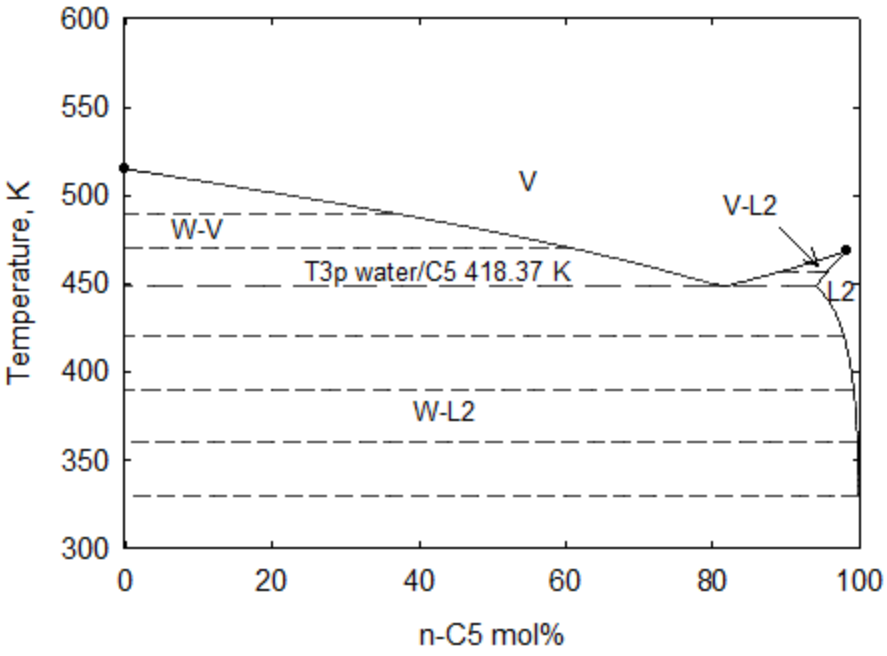

(2) Water/n-C_5

Figure 2.10 Ternary Type 2 solvent (n-C_5) binary T-x diagrams at 35 bars. Bitumen/n-C_5 is Type III_m, of which the phase boundary between two-phase regions is prone to disappear with increased pressure. L1-L2 and L1-V two-phase regions are separated without boundary in between, thus this is classified as Ternary Type 2.

P = 35 bars
T = 300 K

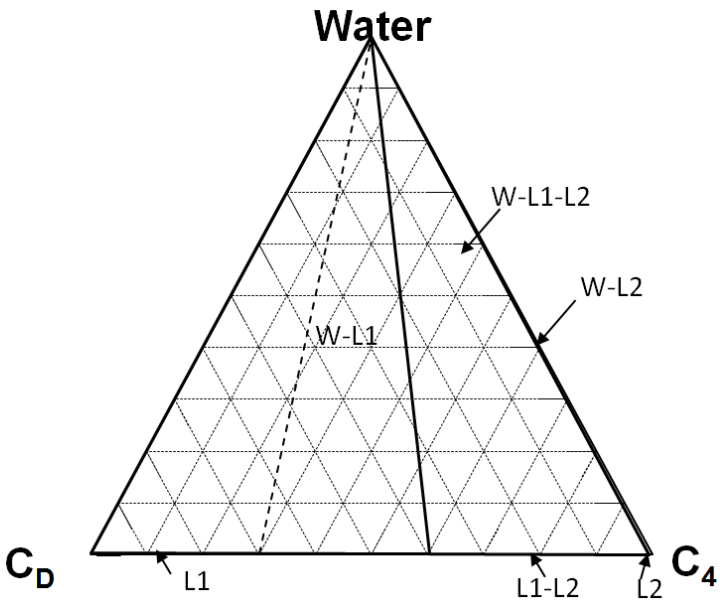

(1)

P = 35 bars
T = 400 K

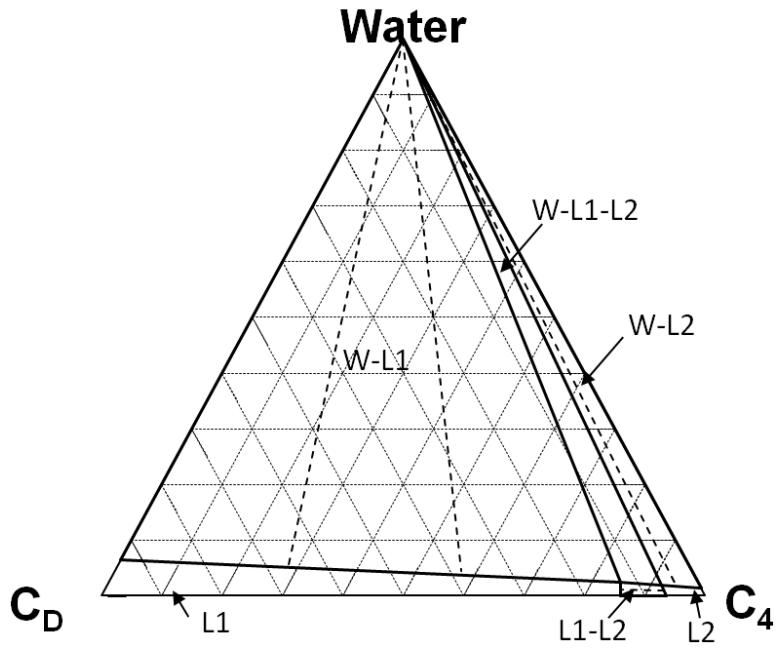

(2)

P = 35 bars
T = 412.04 K T3p of w-C4

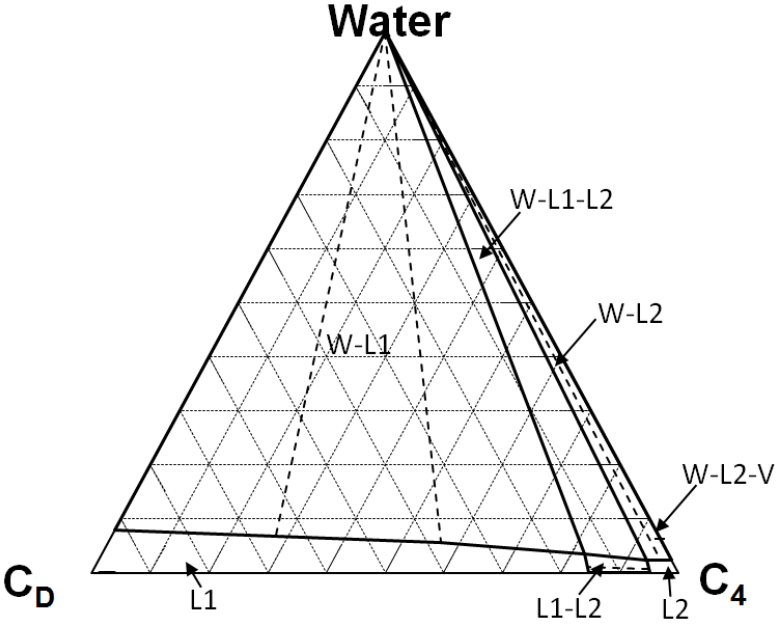

(3)

P = 35 bars
T = 414 K

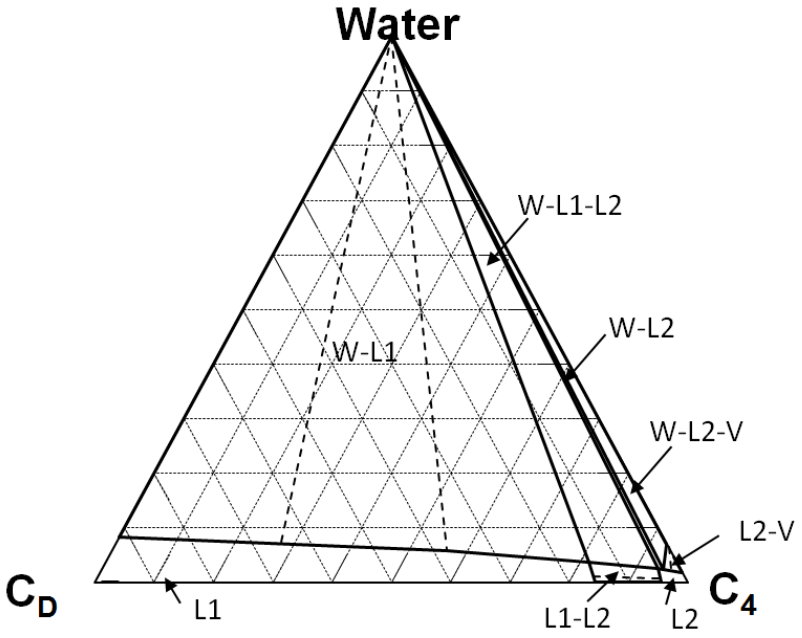

(4)

P = 35 bars
T = 417 K

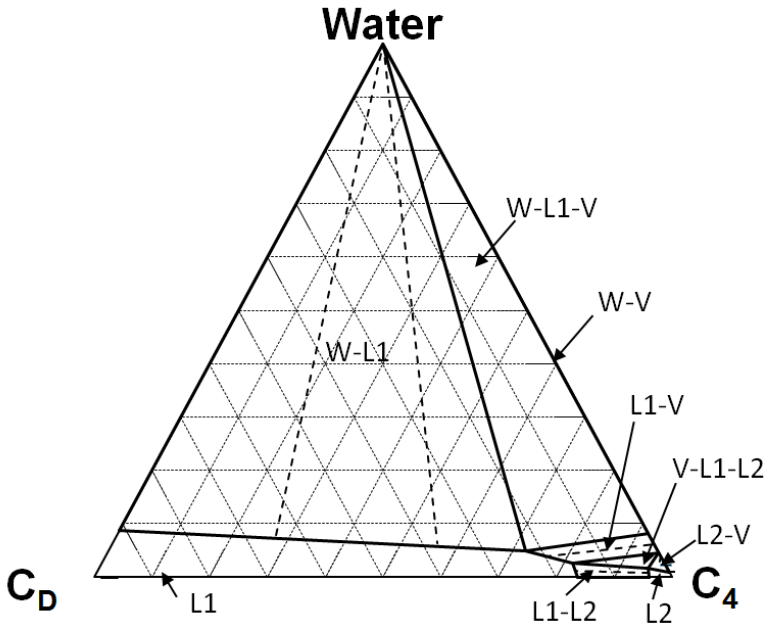

(5)

P = 35 bars
T = 422.3 K T3p of bit-C4

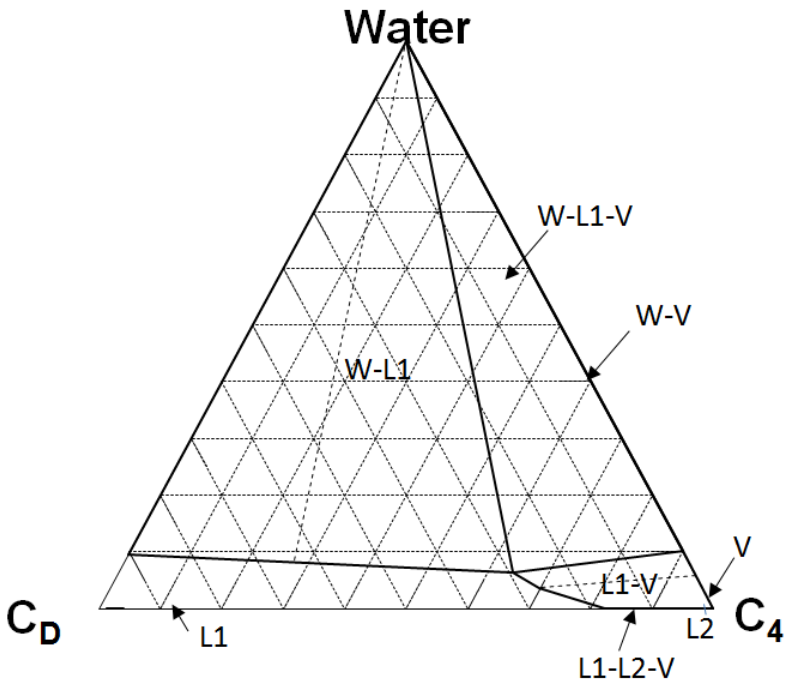

(6)

P = 35 bars
T = 475 K

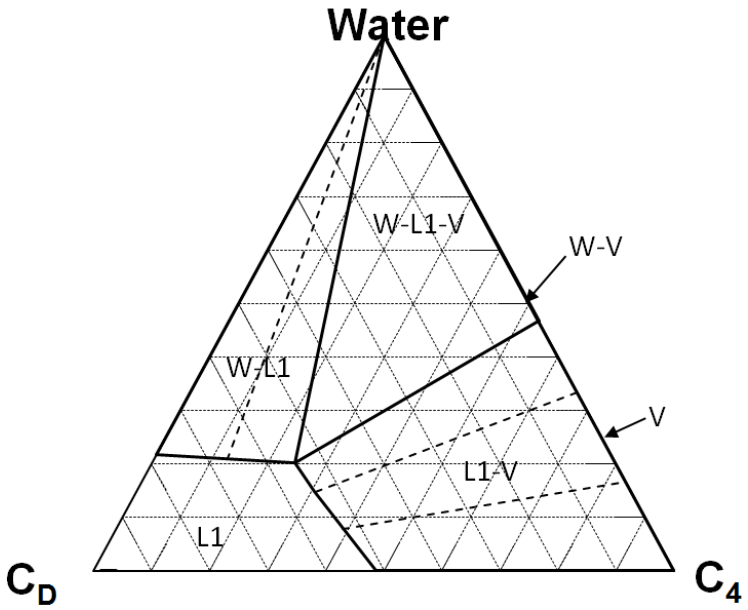

(7)

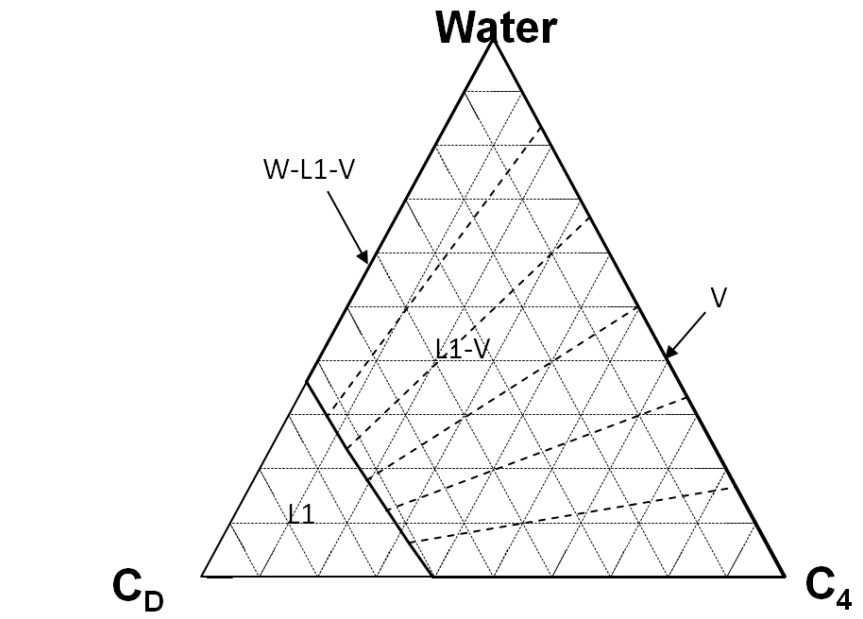

(8)

Figure 2.11 Ternary Type 1 ternary phase behavior at 35 bars. Water/bitumen/C_4 case is taken as an example. L1 represents bitumen-rich oleic phase, while L2 solvent-rich oleic phase. As temperature increases, complicated three phase region transition happens. (1) to (2): Only one three-phase region W-L1-L2 exists. (3) W-L2-V starts to emerge on the water/nC_4 edge at T3p of water/n-C_4. (4) to (6): First, W-L2-V gradually expands. Then, it merges with W-L1-L2 and immediately, W-L1-L2 and W-L2-V reform into W-L1-V and V-L1-L2. (7) to (8): L1 vertex swings towards water/bitumen edge and finally disappears onto water/bitumen edge.

P = 35 bars
T = 300 K

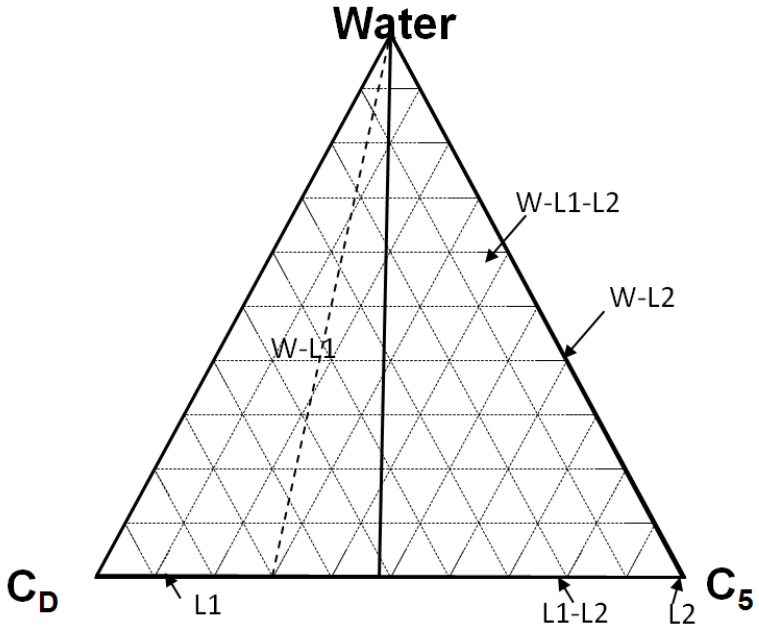

(1)

P = 35 bars
T = 385 K

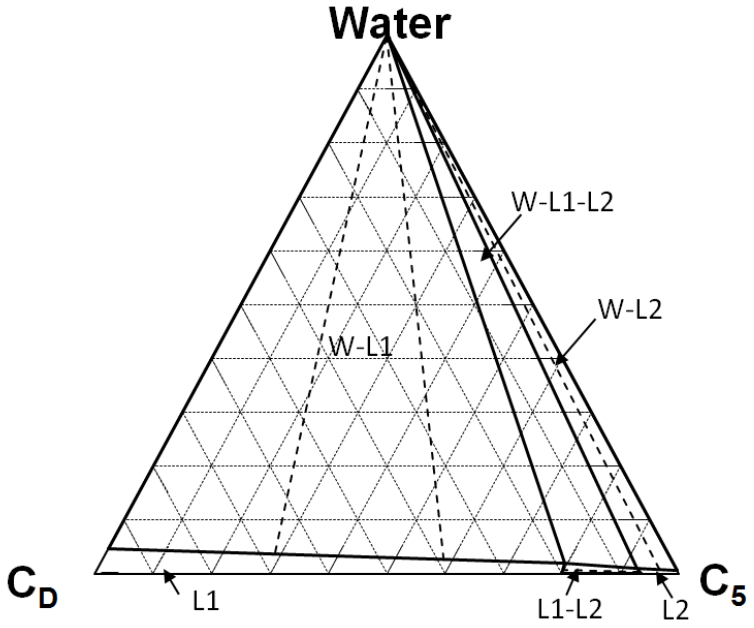

(2)

P = 35 bars
T = 392.7 K

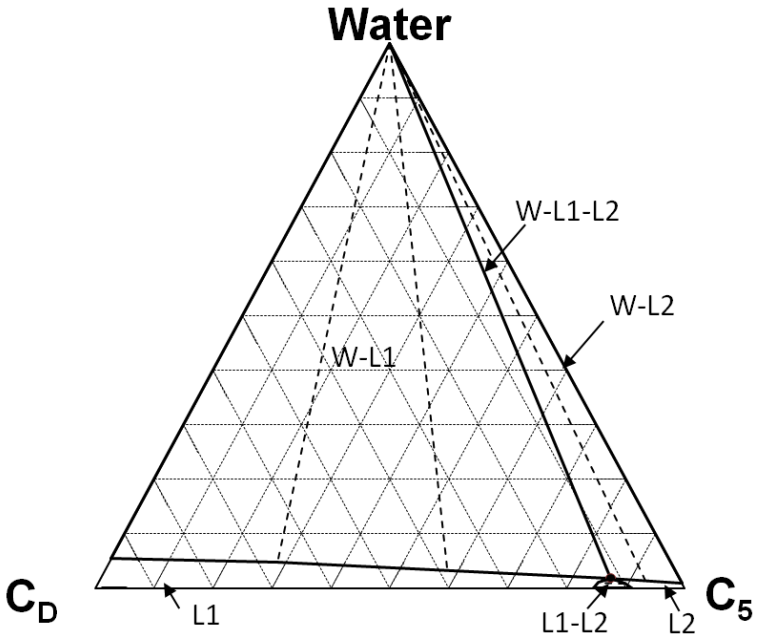

(3)

P = 35 bars
T = 448.37 K T3p of w-C5

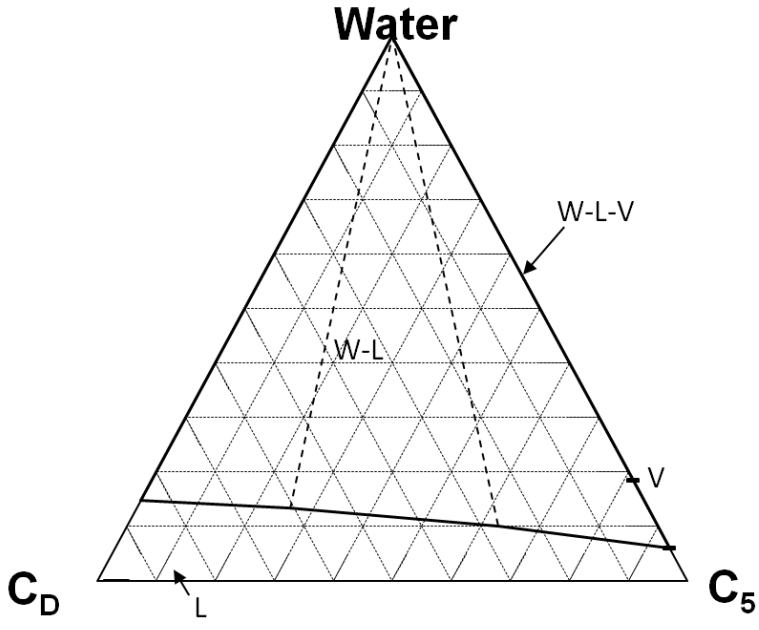

(4)

P = 35 bars
T = 465 K

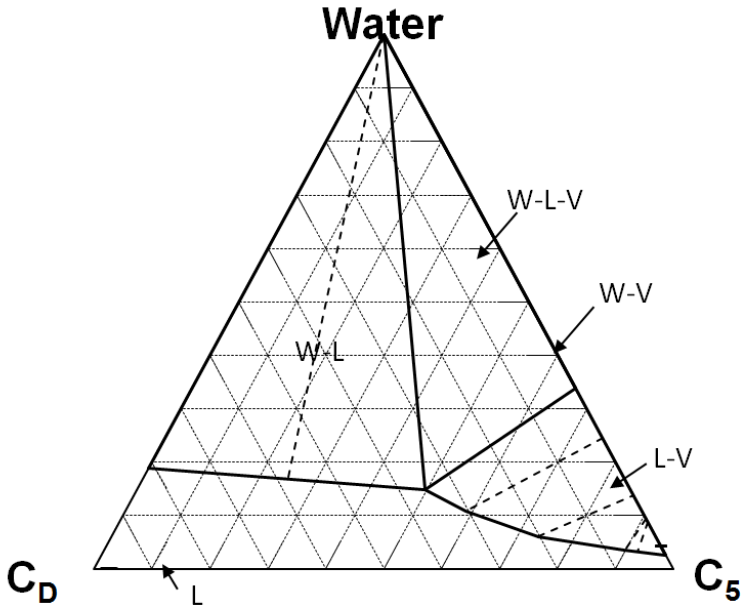

(5)

P = 35 bars
T = 495 K

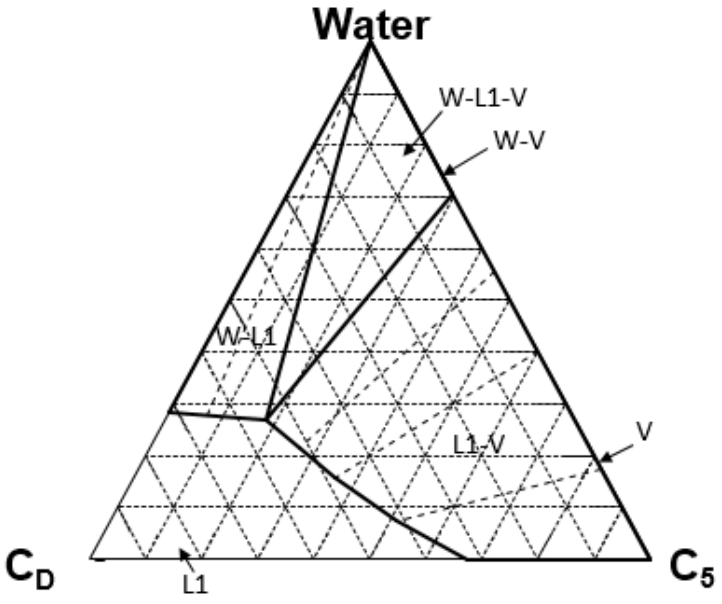

(6)

P = 35 bars
T = 515 K T3p of w-bit

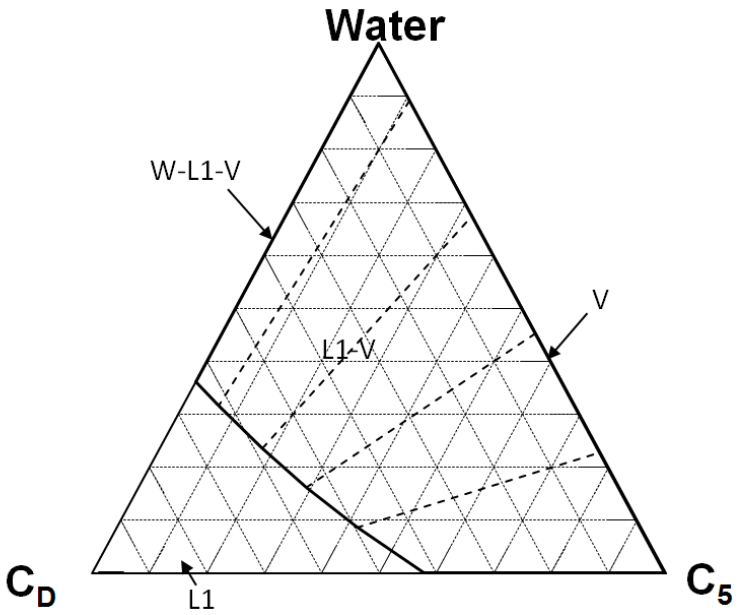

(7)

Figure 2.12 Ternary Type 2 ternary phase behavior at 35 bars. Water/bitumen/C_5 case is taken as an example.L1 represents bitumen-rich oleic phase, while L2 solvent-rich oleic phase. (1) to (3): Only one three-phase region W-L1-L2 exists. (4) No three-phase region exists. (5) to (7): W-L1-V emerges from water/n-C_5 edge at T3p of water/n-C_5. Then, L1 swings from water/n-C_5 edge towards water/bitumen edge. W-L1-V disappears at water/bitumen T_{3p}.

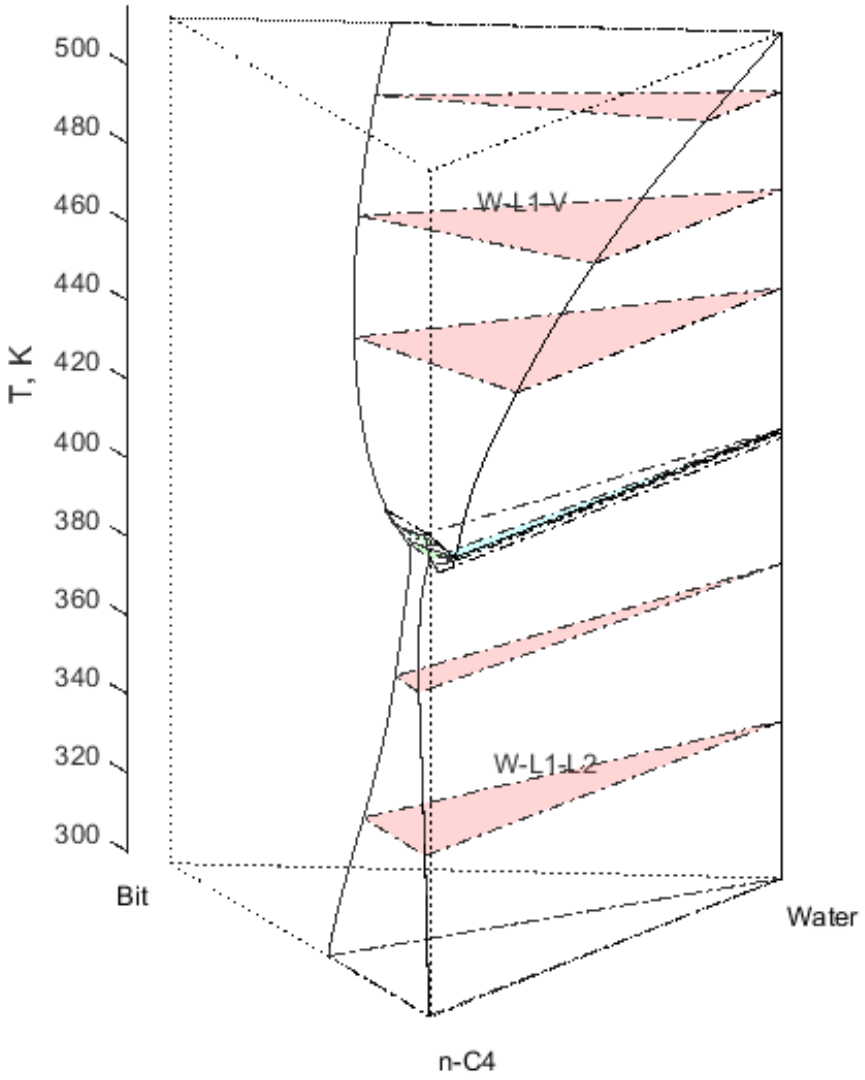
500
480
460
440
420
400
380
360
340
320
300
T, K
W-L1-V
W-L1-L2
Bit
Water
n-C4

(1)

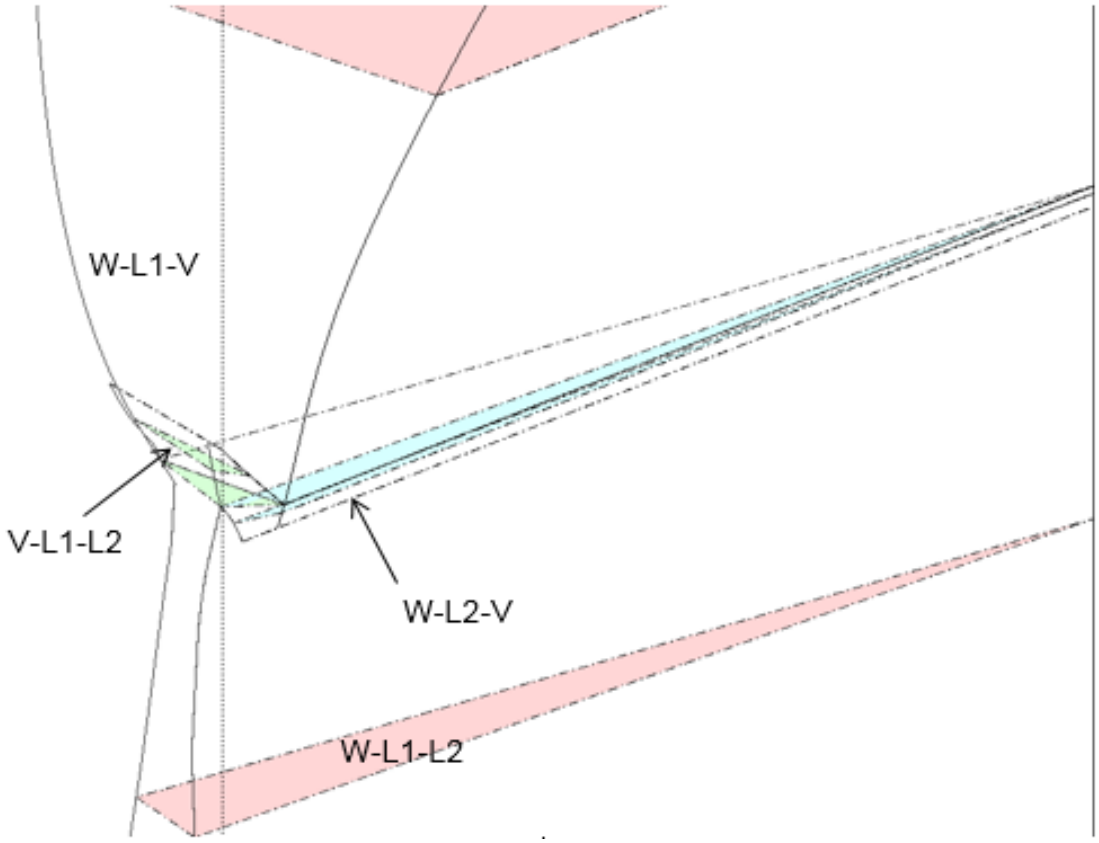

(2)

Figure 2.13 Typical Ternary Type 1 water/bitumen/n-alkane ternary phase behavior in 3D. Water/bitumen/n-C_4 is considered at 35 bars with temperature range from 300 K to 515 K. One continuous spatial solid geometry consists of four different kind of three-phase regions.

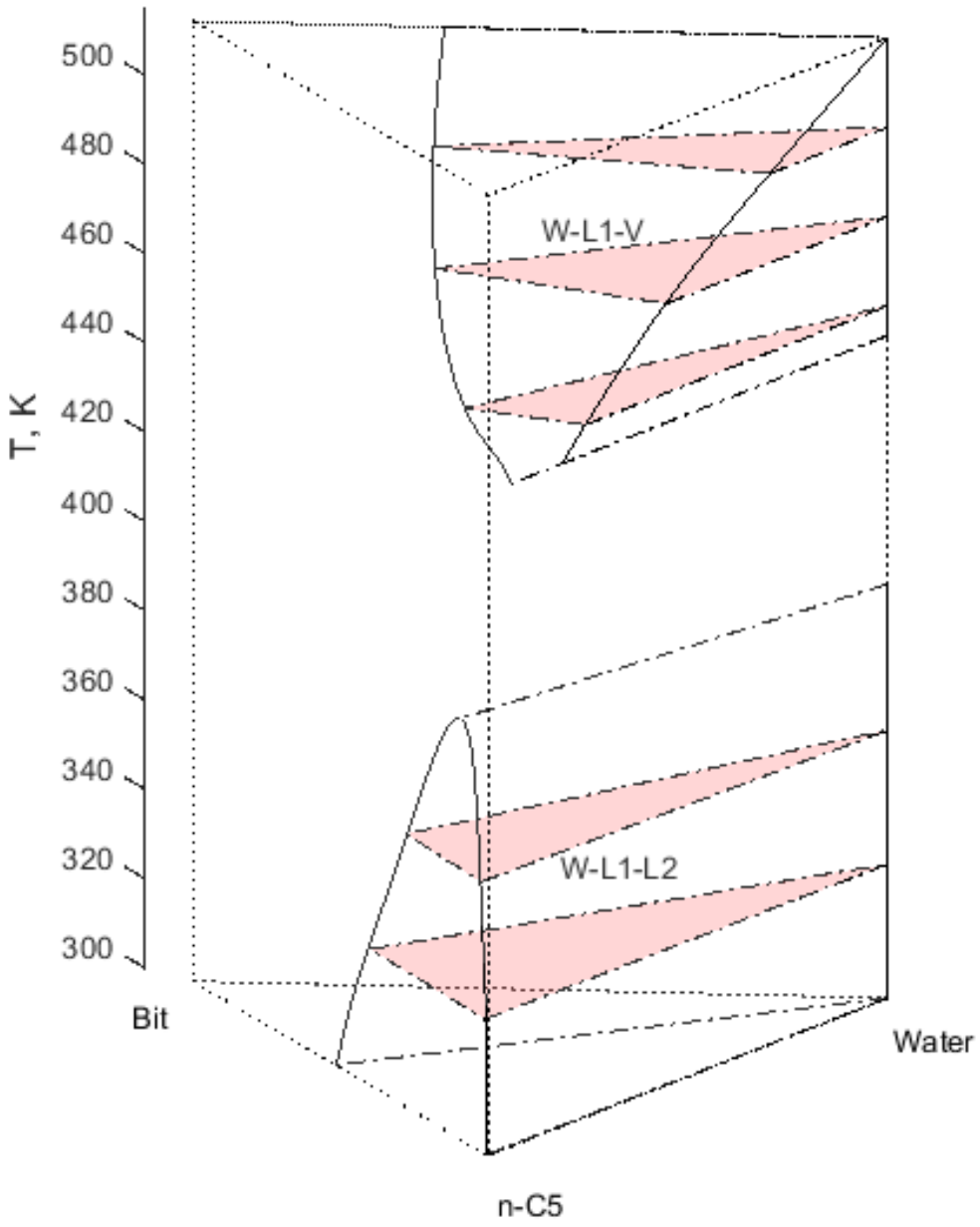

Figure 2.14 Typical Ternary Type 2 water/bitumen/n-alkane ternary phase behavior in 3D. Water/bitumen/n-C_5 is considered at 35 bars with temperature range from 300 K to 515 K. Two separate solid geometries are observed.

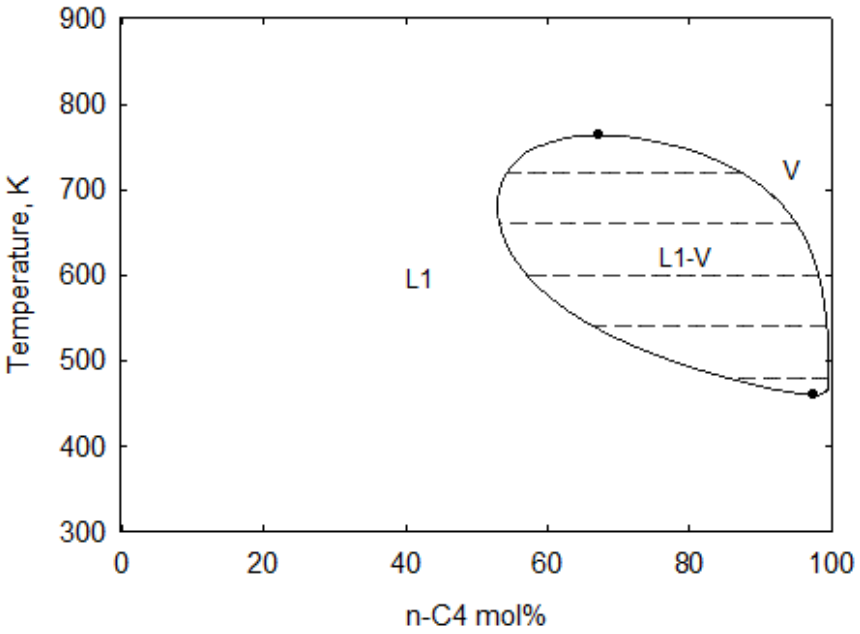

Figure 2.15 T-x diagram of bitumen/n-C_4 binary at 60 bars for case study 1. Increased pressure eliminates phase boundary between two-phase regions and turn n-C_4 into a Ternary Type 2 solvent at 70 bars.

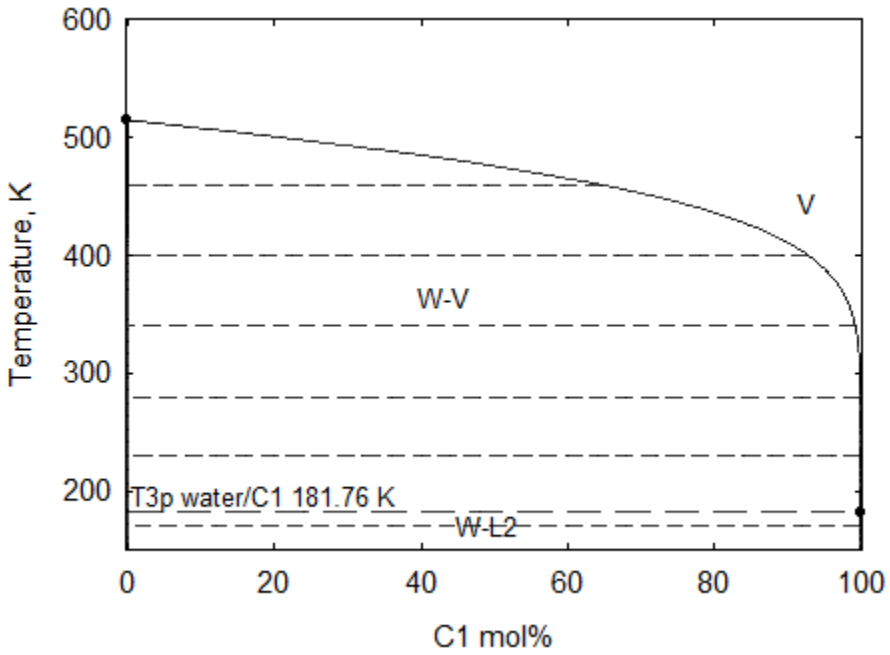

(1) Water/C1

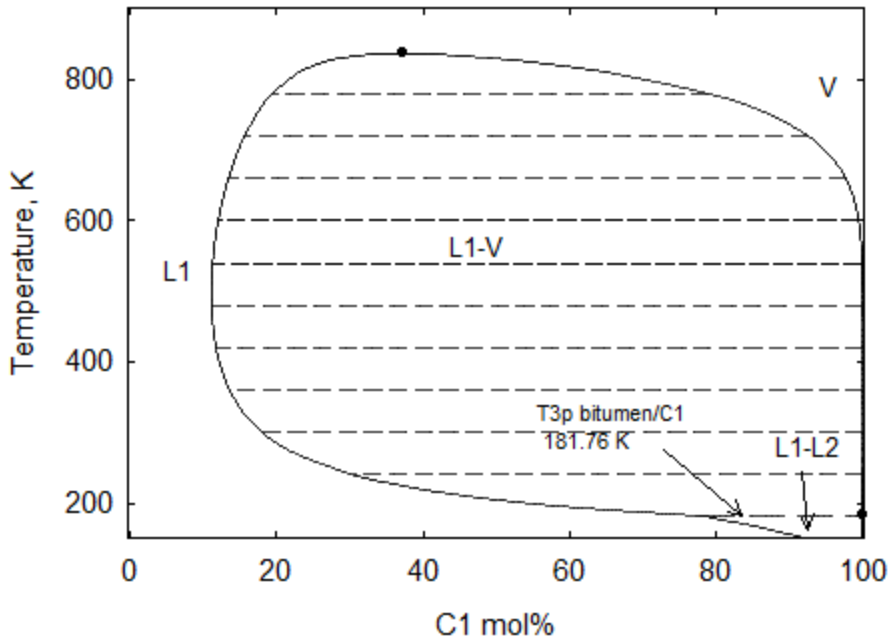

(2) Bitumen/C1

Figure 2.16 Binary phase behavior for extreme Ternary Type 1 case: methane. three-phase temperature of water/C1, bitumen/C1 and saturation temperature of methane are the same.

P = 35 bars
T = 150 K

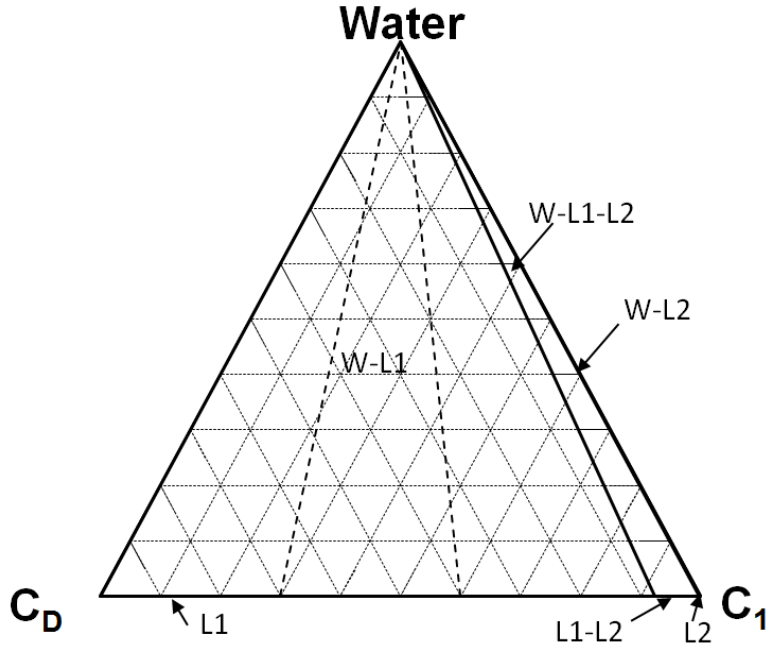

(1)

P = 35 bars
T = 181.76 K Tsat of C1

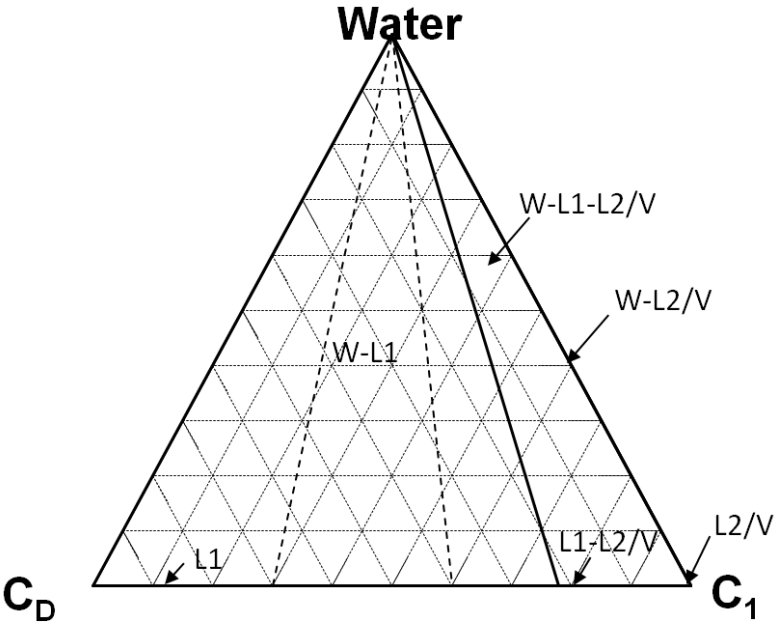

(2)

P = 35 bars
T = 300 K

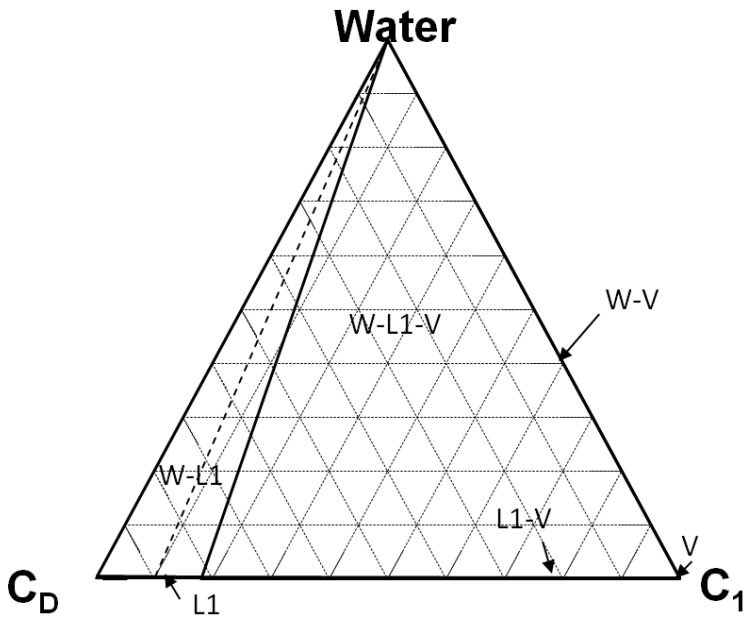

(3)

P = 35 bars
T = 400 K

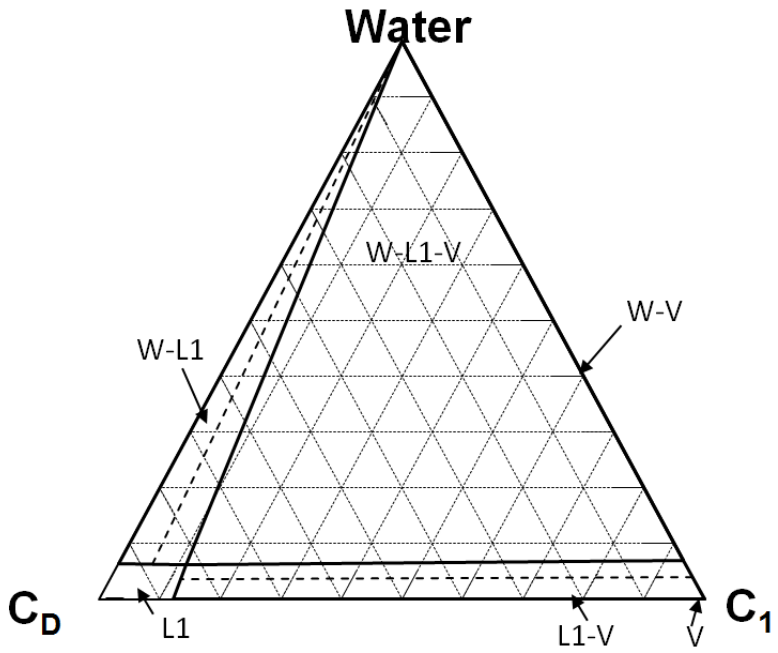

(4)

P = 35 bars
T = 515.0 K T3p of w-bit

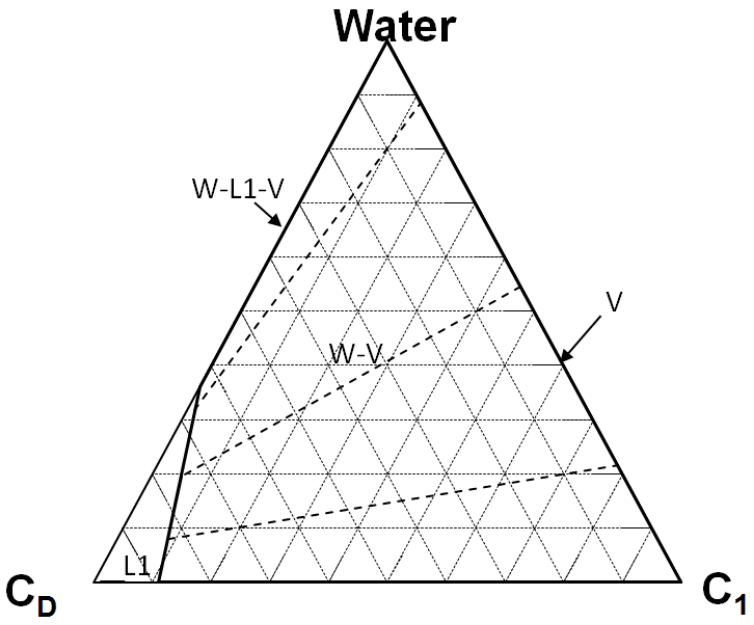

(5)

Figure 2.17 Ternary phase behavior of extreme Ternary Type 1 solvent: methane. Water/bitumen/C1 system under 35 bars is shown. Complex phase transition for Ternary Type 1 solvents happens simultaneously at saturation temperature of methane.

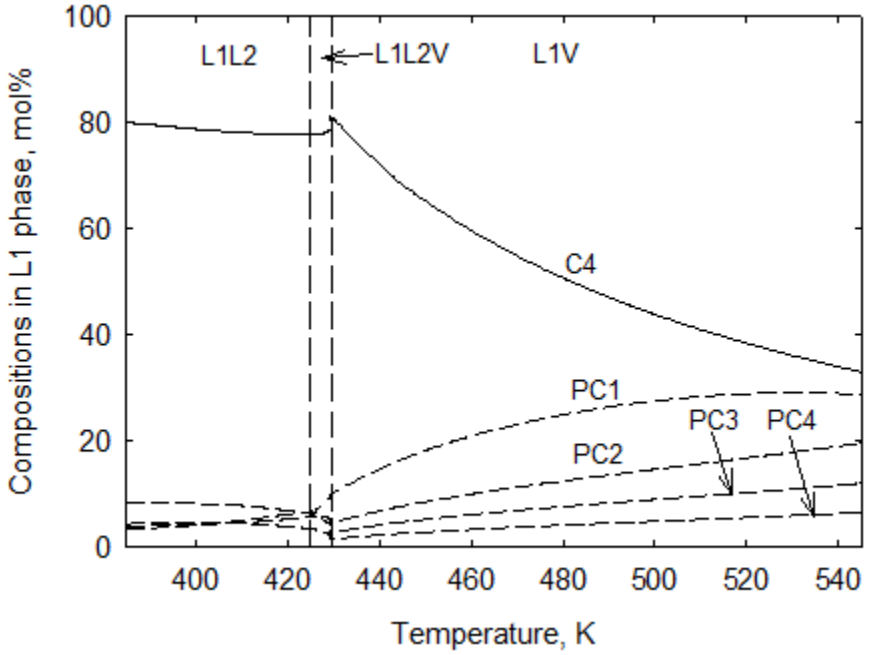

(1) Bitumen/C_4 L1 phase composition at 35 bars

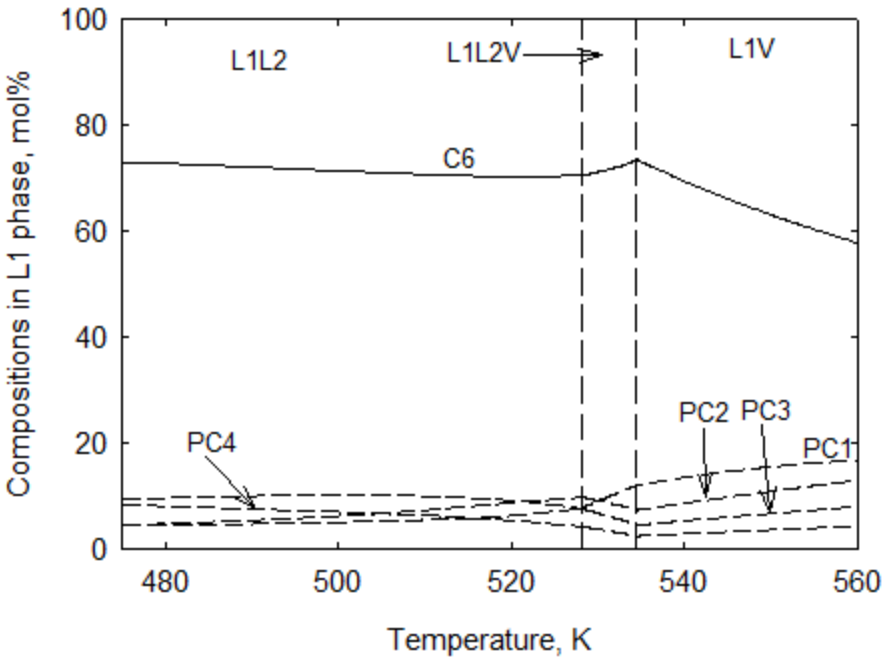

(2) Bitumen/C_6 L1 phase composition at 35 bars

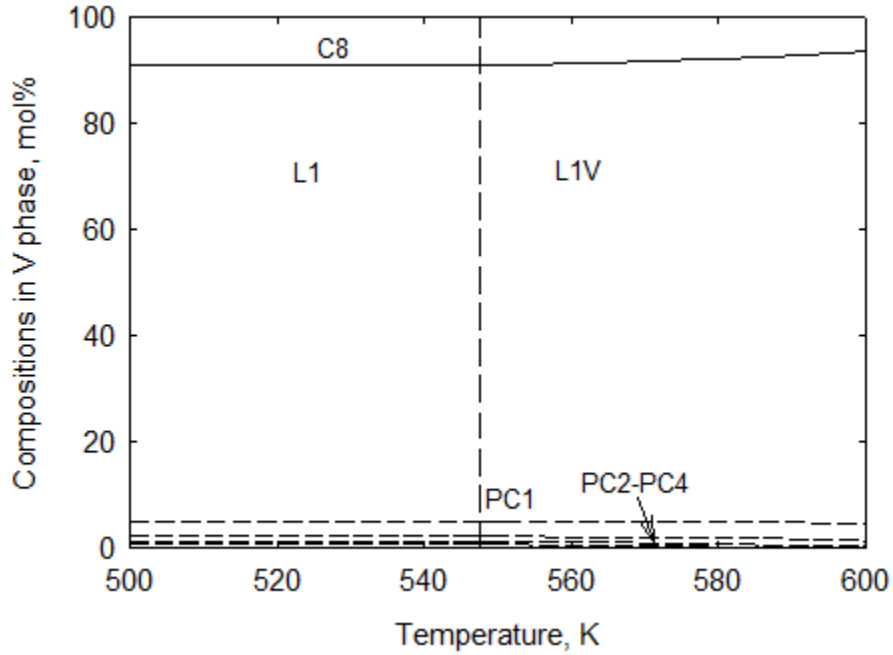

(3) Bitumen/C_8 V phase composition at 35 bars

Figure 2.18 Case study 2 isobaric phase behavior of 4-PC bitumen and n-alkane model at 35 bars. Bitumen-solvent ratio is 0.1. The existence of L1L2V of C_4 and C_6 explains why in Figure 2.17, WLLV exists for C_4 and C_6. The classification criterion still holds true for multicomponent systems like this.

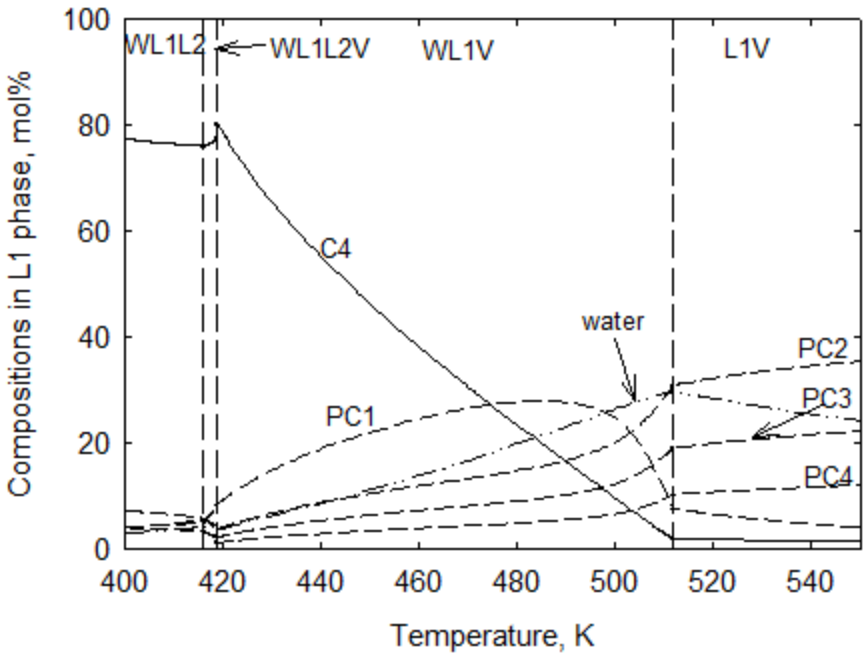

(1) Water/bitumen/C_4 L1 phase compositions at 35 bars

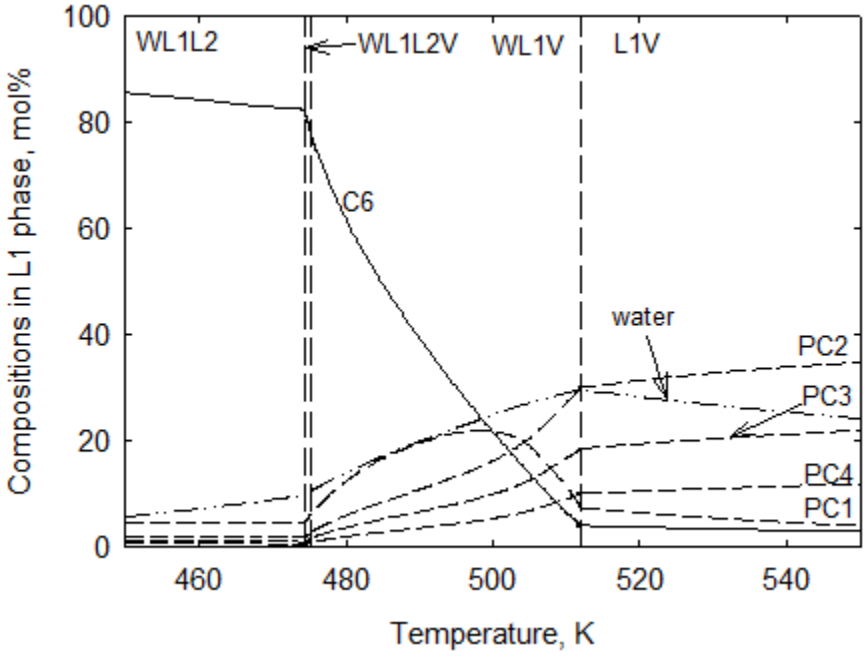

(2) Water/bitumen/C_6 L1 phase compositions at 35 bars

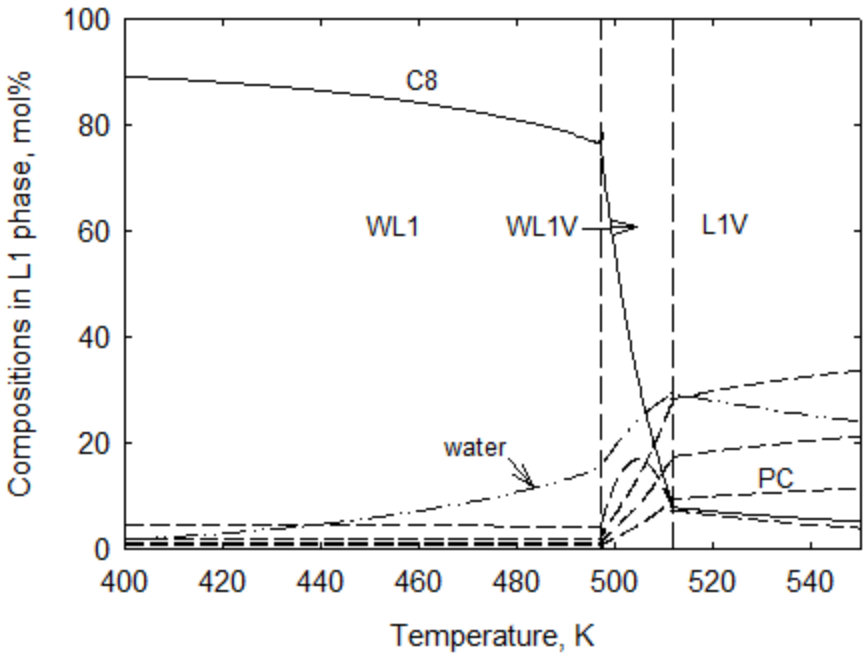

(3) Water/bitumen/C_8 L1 phase compositions at 35 bars

Figure 2.19 Case study 2 isobaric phase behavior of water/bitumen/n-alkane multicomponent model at 35 bars. 95 mol% overall water and 0.1 bitumen-solvent ratio are used. W-L1-L2-V 4-phase region exists for C_4 and C_6 case and they are classified as Ternary Type 1. C_8 is Ternary Type 2.

Table 2.1 Case study 1 critical properties and molecular weight for water/bitumen/n-alkane ternary EOS model. Bitumen is characterized as one pseudocomponent, symbolized as CD.

Comp	TC, K	PC, bar	ω	MW	Vc, cc/mol
C1	190.5611	45.9908	0.0157	16.0427	-
C_3	369.8278	42.4807	0.1543	44.0961	203
n-C_4	425.1222	37.9605	0.2014	58.1228	255
n-C_5	469.7000	33.7009	0.2511	72.1495	304
n-C_6	507.6000	30.2507	0.3010	86.1762	370
n-C_7	540.2000	27.4005	0.3505	100.2029	432
n-C_8	568.7000	24.9245	0.3980	114.2296	492
n-C_9	594.6000	22.9002	0.4459	128.2563	548
n-C_{10}	617.7000	21.1000	0.4898	142.2830	603
CD	847.1700	10.6381	1.0406	530.0000	1330
Water	647.0960	220.6400	0.3433	18.0100	-

Table 2.2 Case study 1 binary interaction parameters table for water/bitumen/n-alkane ternary system equilibrium calculation. The upper diagonal of the matrix is neglected because of symmetry.

BIP	C1	C_3	n-C_4	n-C_5	n-C_6	n-C_7	n-C_8	n-C_9	n-C_{10}	CD	Water
C1	0.000										
C_3	0.000	0.000									
n-C_4	0.000	0.000	0.000								
n-C_5	0.000	0.000	0.000	0.000							
n-C_6	0.000	0.000	0.000	0.000	0.000						
n-C_7	0.000	0.000	0.000	0.000	0.000	0.000					
n-C_8	0.000	0.000	0.000	0.000	0.000	0.000	0.000				
n-C_9	0.000	0.000	0.000	0.000	0.000	0.000	0.000	0.000			
n-C_{10}	0.000	0.000	0.000	0.000	0.000	0.000	0.000	0.000	0.000		
CD	0.000	0.067	0.075	0.081	0.088	0.094	0.098	0.102	0.105	0.000	
Water	0.732	0.666	0.636	0.607	0.579	0.553	0.527	0.503	0.480	0.169	0.000

Table 2.3 Case study 1 ternary classification sensitivity to pressure. Pressures at UCEP and CP as well as at which Ternary Type 1 turns into Ternary Type 2 (bifurcation) are summarized.

	P_c, bar	P_{UCEP}, bar	$P_{bifurcate}$, bar
C_3	42.48	43.58	143.95
n-C_4	37.96	42.26	43.24
n-C_5	33.70	9.20	9.20
n-C_6 and plus	-	<1	<1

Table 2.4 Case study 1 Ternary Type 1 system complex phase transition summary. At 35 bars, this starts from water/n-alkane three-phase temperature to that of bitumen/n-alkane.

	T_{sat}, K	$T_{3p\ w\text{-}sol}$, K	$T_{3p\ bit\text{-}sol}$, K	ΔT_{3p}, K
C1	181.76	181.76	181.76	0.00
C2	289.41	289.54	289.39	0.15
C_3	358.89	359.55	357.83	1.72
n-C_4	419.99	422.30	412.04	10.26

Table 2.5 Case study 2 bitumen critical properties, molecular weight and composition. Bitumen is characterized into 4 pseudo components by Kumar and Okuno (2016). Water and n-alkanes properties are the same as case study 1.

	TC, K	PC, bar	ω	MW	Mol% in bitumen
PC1	813.6410	18.9600	0.4393	296.9391	53.46
PC2	1066.1180	13.6800	0.8657	662.8018	23.95
PC_3	1244.3200	12.3200	1.0497	1082.6682	14.66
PC_4	1452.9860	11.6800	0.8947	2003.4936	7.92

Table 2.6 Case study 2 BIP table for the PR EOS.

	n-C_4	n-C_6	n-C_8	PC1	PC2	PC_3	PC_4	Water
n-C_4	0.000							
n-C_6	0.000	0.000						
n-C_8	0.000	0.000	0.000					
PC1	0.010	0.016	0.015	0.000				
PC2	0.015	0.028	0.031	0.050	0.000			
PC_3	0.028	0.035	0.041	0.050	0.040	0.000		
PC_4	0.030	0.046	0.055	0.050	0.040	0.030	0.000	
Water	0.636	0.579	0.527	0.200	0.200	0.200	0.200	0.000

Chapter 3 Analysis of Solvent Distillation

3.1 Introduction

In steam injection or steam/solvent coinjection, mobility of bitumen is enhanced because of the increased temperature and/or the dilution of bitumen with solvent. Besides, enhanced displacement efficiency that results in oil saturation that is lower than endpoint oil saturation is another important mechanism that makes steam-solvent coinjection superior to SAGD.

It was initially observed by Willman et al. (1961) through experiments that an almost zero residual oil saturation (S_{or}) was achieved in steam injection. Later, S_{or} lower than the endpoint oil saturation was reported in a number of field tests (Blevins et al., 1969; Volek and Pryor, 1972; Blevins and Billingsley, 1975). The low S_{or} is due to the distillation of solvent or light to medium components in the heavy oil. Solvent distillation is defined as the vaporization of distillable components in residual oil, leaving the heavy components in situ (Willman et al., 1961 and Prats, 1982). The distilled solvents would condense at steam front, dilute the bitumen and increase displacement efficiency. Condensation, dissolution into bitumen and vaporization of solvent, i.e. solvent distillation, result in volume shrink of residual oil, even lower than endpoint saturation.

Inside a steam chamber for steam-solvent coinjection, the steam and solvent first condenses on the edge of the steam chamber. Then the condensed water and solvent will mix with bitumen and therefore, bitumen is diluted. If temperature is increased, volatile components from the diluted bitumen may evaporate and therefore the volume of oleic phase shrinks.

Figure 3.1 explains the process of distillation through an imaginary PVT experiment. In a PVT cell at isobaric conditions, there are initially water phase that contains pure water or both water and dissolved solvent, and also oleic phase which is a bitumen diluted with solvent and water. If the pressure in the PVT cell keeps a constant and temperature is gradually increased, the light component from the liquid phases, i.e. water and solvent, will evaporate to the vapor phase. As a

result, the volume of the oleic and aqueous phases shrinks. The oleic phase becomes more viscous as water and solvent evaporated.

However, the solvent distillation is not yet analytically quantified so far. Willman et al. (1961) develops a mathematical description for steam drive performance. They measured S_{or} and incorporated the measurements into their calculation. Johnson et al. (1971) modeled volumetric change of oleic phase due to distillation as a function of solvent accumulation on chamber edge. However, the models mentioned above did not directly discuss residual oil saturation as a result of phase behavior.

Keshavarz et al. (2014) showed the mechanism of enhanced displacement efficiency by solvent distillation through ternary diagrams. In order to reduce the oil saturation to less than endpoint S_o, solvent should first accumulate on chamber edge, then phase splits and solvent evaporates as temperature increases. Following this explanation, Keshavarz and Chen (2014) modeled the average S_{or} inside the steam chamber mathematically, using Raoult's law and correlated temperature change during distillation. Raoult's law is only suitable for ideal solutions. Besides, they assumed only maximum one oleic phase and immiscibility between hydrocarbon and water. Therefore, accurately modeled phase behavior and reduced S_{or} as a result of phase behavior change were not an emphasis in their research.

In this chapter, the first thermodynamic tool is proposed to estimate displacement efficiency enhanced by solvent distillation. The algorithm solves analytical S_{or} with a few inputs compared to numerical simulation. The tool is based on the systematic phase behavior study including multiphase and multicomponent in **Chapter 2**. This model helps explain reduced S_{or} in steam or steam/solvent injection. Differences between two types of n-alkanes proposed in **Chapter 2** are discussed. Comparisons of Ternary Type 1 and 2 solvents are done through sensitivity analysis and numerical simulations.

3.2 Mechanistic Calculation of Distillation using an EOS

The solvent distillation in SAGD and steam-solvent coinjection begins with solvent and water mixing with bitumen on the edge of steam chamber. As described by Keshavarz et al. (2014), chamber edge is defined where the phase transition occurs between WL and WLV as shown in **Figure 3.2**. On the chamber edge, the overall composition is located on the WL edge of WLV tie triangle and vapor phase saturation is zero. The W phase contains 100% water, and the L phase contains water, bitumen and solvent. If temperature is increased from the one shown in **Figure 3.2 (1)**, distillable components will evaporate from the W and L phases. Distillable components may include water from the W and L phases and solvent from the L phase. These distillable components make up the V phase inside the chamber, in which W-L-V coexist. **Figure 3.2 (2)** shows the chamber edge condition in a reservoir. The overall composition is resided on the boundary between W-L and W-L-V.

Based on the systematic phase behavior study in Chapter 2, another situation of chamber edge condition specific to Ternary Type 1 n-alkanes is also possible, which is shown in **Figure 3.3**. If the chamber edge temperature is low, W-L1-L2 coexists on the chamber edge. L1 is the bitumen-rich oleic phase and L2 the solvent-rich oleic phase. In this chamber edge condition, overall composition can be located on or inside W-L1-L2 tie triangle. If temperature is increased from **Figure 3.3 (1)**, W, L1 and L2 will evaporate simultaneously. **Figure 3.3 (2)** shows a schematic of chamber edge for this situation. W-L-L is outside the chamber and W-L-V inside the chamber. The overall composition resides within the W-L1-L2 in the ternary diagram.

One special case in Ternary Type 1 solvent is methane (C_1). The live bitumen contains mainly C_1 as the solution gas. Bitumen has limited capacity to maintain solution gas such as C_1. Usually, live bitumen has a gas-oil ratio (GOR) somewhere between 0 to 5 m^3/m^3. If the Athabasca bitumen in case study 1 of Chapter 2 is considered, a GOR of 5 m^3/m^3 is corresponding to 10 mol% of C_1 in the Athabasca bitumen. If only steam is injected in to the bitumen reservoir, C_1 will evaporate from the live bitumen. Therefore, the chamber edge temperature will be affected by the

evaporated C_1. **Figure 3.4** shows the ternary phase behavior on chamber edge at 35 bars when the Athabasca bitumen described in case study 1 of Chapter 2 is considered. The GOR of the live bitumen is 5 m^3/m^3 (or 10 mol% C_1 in bitumen). If a zero GOR is considered, the chamber edge temperature will be the same as three-phase temperature of water/bitumen at 35 bars, i.e. 515.00 K. The chamber edge temperature is lowered from 515.00 K to 442.76 K if a 10 mol% C_1 is dissolved in bitumen. Under this condition, only one oleic phase, L1, exists on the chamber edge.

In the mechanistic study in this section, the bitumen is assumed to be a dead bitumen, i.e. no solution gas is considered in the bitumen. Later on in this thesis, the effect of non-zero GOR on the chamber edge condition and displacement efficiency will be revisited.

Distillation of water is assumed to be constrained by endpoint water saturation (S_{wr}) inside the steam chamber. Endpoint water saturation is the irreducible water saturation. The irreducible water cannot be taken away by flow, usually because the water is stuck in the pores or is attached to the surface of rock. The irreducible water saturation is affected by the porosity, pore structures, rock compositions and wettability on the rock surface. The tighter the pore, or the more heterogeneous the porosity, the greater the irreducible water saturation is. Also, the more hydrophilic the rock surface, the greater the irreducible water saturation. It is assumed that the distillation ends when water saturation reaches irreducible level, because wet steam is injected in SAGD or coinjection, and heat losses always exist. This means water in the state of liquid always exists. The water condensate occupies the pore space and is a source of the water saturation inside a chamber. The part of water that is in the excess of the residual water saturation flows, and leaving the residual amount inside the chamber. In the end of distillation, the evaporation and condensation of water will reach a dynamic balance. This chapter is to quantify how much solvent is distilled from L phase if water saturation is reduced to a given S_{wr}.

Resulting S_{or} depends on many factors, such as operation pressure, bitumen properties, volatility of solvent, accumulation of solvents and water on the chamber edge, and endpoint phase

saturations decided by rock properties. Due to the complexity, simplifying assumptions are made and sensitivities of each affecting factors are analyzed.

Assumptions for simplification are listed below.

- Isobaric condition during the distillation process. During steam injection, the pressure inside and outside the steam chamber is assumed to be the same as injector bottomhole pressure. Since the oil saturation and water saturation are no more than the endpoint saturations, liquid phases cannot flow. The flowing vapor phase has very high mobility so that it does not require high pressure difference to flow inside a steam chamber. This justifies the isobaric assumption. In reality, the pressure is the highest near the injector, and gradually decreases as it becomes distant from the injector. However, the difference in pressure of near wellbore area and area far from wellbore is negligible. This is because the propagation of pressure wave is faster than the propagation of steam chamber.
- Chamber edge is defined where phase transition happens between WL (or WLL) and WLV. Take water/bitumen/n-alkane ternary system as an example, two types of chamber edge conditions are possible. For Ternary Type 1 solvents (as C_3 in), W-L1-L2 or simply W-L1 appears on chamber edge. For Ternary Type 2 solvents, only W-L1 on chamber edge is possible.
- Fixed overall composition is assumed during distillation of water and solvent. In reality, overall composition on the chamber edge cannot be controlled directly. This is done by manipulation of the injection strategy, i.e. the injection pressure, the injection rate, and/or the injection ratio of steam and solvent. Also, from the chamber edge to inside the chamber edge, flow always exists. This unavoidably results in a change in overall composition during the distillation. However, without a fixed overall composition, it is impossible to define the beginning and the end of the distillation, as will be shown soon in this section. This assumption will give the most conservative estimation for analytical

S_{or}. This quantification method only provides a simplified way to explain distillation, without consideration of mass balance or energy transfer as in numerical simulation.

- Water saturation cannot be lower than irreducible water saturation S_{wr}. As aforementioned reason in this section, water always exists in the reservoir.

Saturations can be calculated in the following way,

$$S_j = \frac{\beta_j \rho_j}{\sum_{k=1}^{Np} \beta_k \rho_k} \tag{3.1}$$

where j is the phase, which can be W, L or V phase, S_j is the saturation of phase j, β_j the mole fraction of phase j, ρ_j is the density of phase j, and N_p is the number of phases. β_j can be either analytically determined by the Rachford-Rice algorithm, or geometrically determined by the material balance or the so-called lever rule. An example using the lever rule is given in **Figure 3.5**. The phase mole fractions of W, L and V phases can be determined by the geometric relations below,

$$\beta_w = \frac{l_b}{l_a + l_b}, \qquad \beta_o = \frac{l_d}{l_c + l_d}, \qquad \beta_g = \frac{l_f}{l_e + l_f} \tag{3.2}$$

where w, o and g represents the W, L and V phase respectively, and l represents the length of each section indicated in **Figure 3.5**.

The algorithm for analytical S_{or} for solvent distillation is presented as follows:

Step 1 Make a phase behavior model at pressure P with an EOS and proper mixing rules.

If a cubic EOS with the vdW mixing rules is considered, basic EOS inputs include the operation pressure, critical properties and binary interaction parameters, and volume shift parameters.

Step 2 Define chamber edge conditions. Set $T=T_{edge}$.

Chamber edge temperature (T_{edge}) can be uniquely determined with the overall composition based on assumption 2. For an example, if at most three phases coexist, T_{edge} can be determined via simple geometric relationship using the lever rule. (1) If W-L exists on chamber edge, $\beta_g = 0$, i.e. $l_f = 0$. (2) If W-L1-L2 exist on chamber edge, T_{edge} would be the unique temperature where W-L1-L2 turns into W-L1-V for Ternary Type 1 (**Figure 2.13**). In general, a Rachford-Rice algorithm capable of negative flash can be used to determine the temperature at which vapor phase mole fraction is zero.

Step 3 Calculate phase mole composition β_j.

β_j can be calculated using the robust multiphase Rachford-Rice algorithm of Okuno et al. (2010) with K-values based on the EOS at z, P, and T.

Step 4 Calculate phase molar density and phase saturation.

One of the convenient methods to calculate saturations is described in **Appendix B**.

Step 5 Check if $S_w > S_{wr}$.

- If so, increase T by 0.01 K and go back to Step 3.
- If not, continue to the next step.

Step 6 Output residual saturations at upper T bound (T_{Swr}) at which S_w is S_{wr}.

The distillation is considered come to an end when S_w reaches S_{wr} in the analytical solution. The corresponding temperature T_{Swr} can be found by both Equation 3.1 and 3.2, when S_w=S_{wr}.

A flowchart for this algorithm is shown in **Figure 3.6**. To sum up, inputs of the analytical S_{or} requires EOS and mixing rules, critical properties, BIPs, overall composition and endpoint saturations. Outputs include saturation change with temperature during distillation.

3.3 Case Study 1: Water/Bitumen/n-Alkane Ternary System

The algorithm presented in **§3.2** are applied to water/bitumen/n-alkane ternary system described in **§2.3.1**. Bitumen is characterized as one pseudo component in the EOS model. An example calculation for n-C_5 is first given to show how the algorithm work to solve analytical S_{or}. Then, sensitivity analysis is done regarding solvent volatility of n-alkanes, chamber edge solvent accumulation, chamber edge water concentration (z_w), irreducible water saturation (S_{wr}) and endpoint oil saturations of reservoir rock.

3.3.1 Example Calculation

Analytical S_{or} for n-C_5 distillation is shown as an example. The operation pressure is set to 35 bars, which makes n-C_5 a Ternary Type 2 solvent. The overall composition at the chamber edge is assumed to be 98 mol% water and 1.2 mol% n-C_5. S_{wr} is set to 0.25. Conditions for this example are summarized in **Table 3.1**.

Figure 3.7 (1) visualizes the whole process of distillation through ternary prism. It is assumed that the overall composition is constant throughout the distillation. Chamber edge can be found when overall composition is located on the W-L1 edge of W-L1-V tie triangle. This is when n-C_5 and water starts to evaporate from liquid phases, and when vapor phase starts to emerge. As temperature increases, the L1 vertex of the tie triangle swings towards the water/bitumen edge in composition space due to solvent evaporation from L1 phase until S_{wr} is reached. Analytical S_{or} can be calculated at T_{Swr}.

Figure 3.7 (2) shows mass transfer from liquid phases to vapor phase during distillation process. On the chamber edge, overall composition is located on the W-L1 edge of W-L1-V and S_g is zero. As temperature increases, due to the evaporation of solvent and water from L1 phase, L1 contains a higher molar fraction of bitumen and a smaller fraction of solvent. This makes L1 vertex of W-L1-V getting closer to the water-bitumen edge and therefore S_o is reduced. Besides,

increased temperature result in V vertex of W-L1-V getting closer to the water vertex of composition space. As a result, S_g is increased.

Figure 3.8 shows how S_w, S_o and S_g change with temperature increase during distillation. As solvent from L phase and water from W and L phases evaporate, volumes of W and L shrink and volume of V expands. As in **Figure 3.7 (2)**, the distilled solvent from L phase and evaporated water from both W and L phases account for the volume change. The distillation is considered come to an end when the amount of water evaporated is equal to that of water condensed. In the end of distillation, water cannot further transfer from liquid phases to the vapor phase, and therefore as the assumption 4, saturation of water and oil cannot be further reduced. Analytical T_{edge}, T_{Swr} and residual saturations are summarized in **Table 3.2**. With a temperature increase from T_{edge} 463.73 K to T_{Swr} 500.32 K, residual oil saturation is reduced to 0.0595.

3.3.2 Sensitivity Analysis

Solvent Volatility

As shown in Chapter 1, steam coinjected with different n-alkanes has shown varied capability of enhancing displacement efficiency. A thermodynamic reason behind this has to be examined to understand why a specific solvent is reported to be the optimum. The algorithm was performed to show how relative solvent volatility to water affects analytical S_{or}.

Conditions to calculate analytical S_{or} are as follows: The operation pressure is 35 bars. C_3, n-C_5, n-C_7 and n-C_{10} are selected for demonstration. The overall composition at the chamber edge is assumed to be 1.2 mol% solvent and 98 mol% water. The endpoint water and oil saturations are 0.25 and 0.13, respectively. Conditions are summarized in **Table 3.1** for volatility sensitivity analysis and the subsequent analysis.

Figure 3.9 shows analytical S_{or} for different n-alkanes. **Table 3.3** shows the analytical residual saturations, T_{edge} and T_{Swr} for each n-alkane. Under the same conditions, C_3 has the lowest chamber edge temperature, but achieves lowest S_{or}. A heavier solvent yields a higher chamber

edge temperature, but also higher S_{or}. However, from C_3 to C_7, the differences in terms of analytically calculated S_{or} is less than 1% under the conditions examined.

Ternary diagrams at T_{edge} and T_{Swr} are shown in **Figure 3.10**. With a fixed overall composition, bitumen-solvent ratio on the chamber edge is set to be the same for each solvent. What makes each solvent different is the water content in oleic phase. The heavier the solvent, more water is dissolved in L phase on the chamber edge because T_{edge} is higher. At the end of distillation where S_{wr} is about 0.25, L phase of lighter solvents contains a smaller proportion of solvent.

The incremental temperature (ΔT) during distillation, i.e. the difference between T_{Swr} and T_{edge}, is summarized in **Figure 3.11**. Also, the amount of solvent and water distilled from liquid phases throughout the distillation process is shown in **Figure 3.12**. The ratio of evaporated water to solvent for each volatility case is shown in **Figure 3.13**. Lighter solvents can achieve greater temperature increase during distillation as a result of lower chamber edge temperature. Besides, lighter solvent allows relatively less water evaporation and more solvent distillation from liquid phases. Relative volatility of water to solvent is smaller for lighter solvents. Analytical solution shows water component transfers only from the W phase to the V phase, and n-alkane only transfers from the L phase. The total water content in the L phase remains almost a constant. More C_3 distilled from the L phase into the V phase, and less water transferred from the W phase to the V phase. Therefore, more oil saturation reduction is achieved by C_3. Both higher temperature increase and lower relative volatility between water and solvent for lighter solvents explains why lighter solvents achieves lower S_{or} during distillation.

If a live bitumen is used with C_1 as the solution gas, the displacement efficiency can be further improved for steam-solvent coinjection, because C_1 is more volatile than any other n-alkanes. However, the appearance of C_1 in the bitumen may detriment chamber edge temperature for steam-solvent coinjection as C_1 evaporates into the V phase.

Pressure

Operation pressures can significantly affect phase behavior. As described in **Chapter 2**, n-C_4 can be converted from Ternary Type 1 to Ternary Type 2 if operation pressure is increased from 35 to 60 bars. It is important to discuss analytical S_{or} sensitivity to pressure due to distillation.

Overall composition is set to 98 mol% water and 1.2 mol% solvent. Endpoint saturations are 0.25 and 0.13 for aqueous and oleic phase respectively. 3 different pressures are used to perform analytical S_{or}, 15, 35 and 60 bars (**Table 3.1**).

Figure 3.14 shows analytical S_{or} sensitivity to pressure for n-alkane solvents. **Table 3.4** summarizes analytical residual saturations. Increased operation pressure improves displacement efficiency for all the volatility cases. At high pressures such as 35 and 60 bars, differences in terms of displacement efficiency of Ternary Type 1 and light Ternary Type 2 solvents are less than 0.5%. Generally, lighter solvents are less affected by pressure increase than heavier ones. By further increase pressures from 35 bars, limited S_{or} reduction can be achieved for Ternary Type 1 and light Ternary Type 2 solvents.

Figure 3.15 shows the ΔT during distillation for each volatility cases at three different pressures. Mole fraction of water and solvent evaporated from liquid phases during distillation is summarized in **Figure 3.16**. The relative amount of evaporated water to solvent is shown in **Figure 3.17**. Generally, increased pressure results in increased ΔT; however, there are a few exceptions mainly because of differences between T_{3p} of water/bitumen and water/solvent is not monotonically changing with pressure. The increased ΔT allows more solvent to evaporate. With increased pressure, C_3 (Ternary Type 1) is limited to let more solvent to evaporate from L phase because the solvent in residual oil is already too low at low pressures. Analytical S_{or} of C_{10} (Ternary Type 2) is more sensitive to pressure increase than lighter solvents. This is because of the existence of enough distillable solvent in residual oil and therefore increased ΔT allows more solvent to evaporate.

Solvent Accumulation

Solvent dissolution in L phase in the vicinity of chamber edge is an important mechanism that results in enhanced displacement efficiency and drainage rate. Effective solvent dissolution through convection improves bitumen recovery and oleic phase mobility. Recall the differences between two types of n-alkanes ternary phase behavior. A solvent-rich oleic phase may exist other than the bitumen-rich oleic phase for Ternary Type 1. Two types of solvents may have very different chamber edge conditions.

Two types of chamber edge condition exist for Ternary Type 1: when solvent concentration is low, overall composition sits on the W-L1 edge of W-L1-V; when solvent concentration is high, overall composition is inside the W-L1-L2 region. The latter situation has separated oleic phases on the chamber edge, which indicates poor solvent dissolution into bitumen.

Here, a series of solvent concentration is plotted against analytical S_{or} for selected n-alkanes. Operation pressure is set to 35 bars. Water concentration, Swr and endpoint So are 98 mol%, 0.25 and 0.13 respectively (**Table 3.1**).

Table 3.5 summarizes the analytical S_{or} and **Figure 3.18** shows S_{or} sensitivity to solvent concentration for selected n-alkanes. In general, S_{or} for all solvents are sensitive to solvent concentration change. Lighter solvents are more sensitive to solvent concentrations than heavier ones although C_3 to n-C_7 shows very similar sensitivity to solvent concentration change. S_{or} is almost halved if solvent dissolution in bitumen is doubled for C_3 to n-C_7. Also, there should be a threshold solvent accumulation to cause oil saturation lower than 0.13, the endpoint oil saturation. Heavier solvents need more solvent accumulation to result in similar S_{or} as lighter solvents do. If the curves of the analytical solutions are extrapolated from the left-hand side, they will intersect with the endpoint S_o line. The corresponding solvent concentration of the intersects represent the minimum solvent concentration to result in reduced S_{or} lower than S_o. When the solvent concentration is 2 mol% on the chamber edge, the analytical S_{or} should be theoretically zero.

Figure 3.19 shows ΔT during distillation under three selected solvent concentrations. **Figure 3.20** shows the amount of water and solvent evaporated from liquid phases during distillation. **Figure 3.21** shows the relative amount of water distilled to that of solvent. One of the reasons is the increased ΔT due to lowered chamber edge temperature as a result of increased solvent concentration, which allows more solvent to evaporate. Besides, volatile solvent has more incremental solvent evaporation due to increased solvent dissolution in bitumen. For heavier solvent like C_{10}, increased solvent concentration may even result in more water evaporation than that of lower solvent concentration case. This is correspondent with the sensitivity of analytical S_{or} to solvent concentration in **Figure 3.18**. In the competition of solvent and water evaporation, lighter solvent is superior to heavier solvents in distillation capability.

Water Concentration in overall composition

As the lever rule indicates, relative position of overall composition inside a tie triangle together decide the saturation of each phase. Besides bitumen-solvent ratio, sensitivity analysis for water concentration should also be conducted. Conditions are 35 bars, 1:4 bitumen-solvent ratio, 0.25 S_{wr} and 0.13 S_{or}, which are summarized in **Table 3.1**.

Figure 3.22 and **Table 3.6** show analytical S_{or} for a series of water concentration. With 1 mol% of water concentration increase, an estimated 1.5% of oil saturation can be reduced for C_3 and 3% for C_{10}. Therefore, if water concentration is increased, the S_{or} of heavier solvents is more affected than lighter ones. Also, for 1:4 bitumen-solvent ratio, each solvent has a threshold water concentration to result in reduced S_{or}.

Figure 3.23 shows ΔT during distillation for selected water concentration cases. Also, water and solvent evaporated from liquid phases during distillation are summarized in **Figure 3.24**. Relative volatility of water to solvent is shown in **Figure 3.25**. Increased global water accumulation increases ΔT for all the cases. This allows more water and less solvent to transfer from liquid

phases to vapor phase. Another observation is that the trend of mole fraction of distilled solvent is not monotonically changing with CN for C_3 case, because the overall composition resides in W-L1-L2 tie-triangle on the chamber edge of C_3 case. The degree of freedom does not allow for the coexistence of four phases (W-L1-L2-V) inside a chamber. As a result, the evaporation of L2 phase cannot be counted into the solvent evaporation. Despite that, the increased water concentration correspondingly reduces solvent overall concentration and oil saturation on the chamber edge. Improved S_{or} by increased water concentration is a combined result of increased ΔT and less solvent content to evaporate.

Endpoint Saturation

As mentioned earlier, competition between water and solvent evaporation explains lower S_{or} achieved by lighter solvents as a result of greater temperature increase. S_{wr} as an important constraint in the algorithms of analytical S_{or} should be examined. However, in reality, S_{wr} may not affect phase behavior in reservoir as much direct as in the analytical solution, because change in S_{wr} results in very different relative permeability curves, and therefore alters the flow inside the reservoir. Therefore, the consequence of changed S_{wr} may be hard to quantify in simulation study.

Conditions are 35 bars, 98 mol% water concentration, 1.2 mol% solvent, 0.13 S_{or}. Three different S_{wr}s, 0.10, 0.25 and 0.40, are examined (**Table 3.1**).

Figure 3.26 and **Table 3.7** show the analytical solutions of S_{or} under different S_{wr}. Lowered S_{wr} significantly reduces S_{or} for all n-alkanes. Heavier solvents are more affected by S_{wr} reduction. At 0.10 S_{wr}, all the n-alkanes results in very similar S_{or}.

Figure 3.27 shows increased ΔT because of lowered S_{wr} for all the cases. In **Figure 3.28**, the amount of solvent and water evaporated from liquid phases are summarized. More solvent is allowed to evaporate with increased ΔT as a result of lowered S_{wr}. **Figure 3.29** shows the relative volatility of all the n-alkane cases compared to water under different S_{wr} conditions. From those figures, the S_{or} is closely related to whether temperature can be further increased and whether

more solvent can be distilled from L phase, as a result of solvent competition with water. C_{10} case has the greatest incremental water and solvent evaporation compared to lighter solvents, it is the most sensitive solvent to S_{wr}.

As mentioned earlier, threshold water or solvent concentration exists so that oil saturation can be reduced to lower than endpoint S_o. Lower endpoint S_o requires more solvent accumulation to result in reduced S_{or}.

3.4 Case Study 2: Water/Bitumen/n-Alkane Multicomponent System

The algorithm is not limited to ternary systems with up to three phases such as case study 1 in **§3.3**. In this section, the algorithm is applied to a multicomponent EOS model described in **§2.4.1** with up to four phases. The system contains water, bitumen characterized as four pseudo components and n-alkane solvent. Descriptions of holistic EOS model can be found in **§2.4.1**.

What makes case studies 1 and 2 different from each other is the additional degrees of freedom because more components are used in case study 2. The Ternary Type 1 n-alkanes in a ternary system cannot have L2 and V phase at the same time inside steam chamber, i.e., L2 on the chamber edge, if exists, will disappear the instant solvent starts to evaporate. However, in a multicomponent system like in case study 2, W-L1-L2-V coexist inside the chamber before L2 totally disappears. This characteristic of multicomponent systems makes it possible to probe into the differences between two types of n-alkanes in distillation process.

The conditions for the algorithm performances are, 35 bars pressure, 1:10 bitumen-solvent ratio, 95 mol% global water concentration, 0.25 S_{wr} and 0.13 endpoint S_o. The analytical S_o is plotted against total molar enthalpy ($\underline{H}^t$), which can be calculated by equations below,

$$\underline{H}^t = \sum_{j=1}^{Np} \beta_j \underline{H}_j \tag{3.3}$$

$$\underline{H_j} = \sum_{i=1}^{Nc} x_{ij}\underline{H_i^{IG}} + \underline{H}^{excess} \tag{3.4}$$

where $\underline{H}^t$ is the total molar enthalpy, Np total phase number, Nc total component number, β_j phase j mole fraction, $\underline{H_j}$ molar enthalpy of phase j, $\underline{H_i^{IG}}$ molar enthalpy of ideal gas for component i, x_{ij} mole fraction of component i in phase j, and $\underline{H}^{excess}$ excess molar enthalpy between real and ideal fluid mixtures.

Table 3.8 shows analytical residual saturations for n-C_4, n-C_6 and n-C_8 cases. More volatile solvents need greater temperature increase to achieve lower S_{or}. **Figure 3.30** shows $\underline{H^t}$ changes with temperature. The temperature range where distillation happens is labeled out. The mixture containing n-C_8 requires more energy than lighter solvents to increase temperature by 1 K. However, n-C_8 needs less ΔT to achieve S_{or} than lighter ones. Therefore, as a whole, lower S_{or} achieved by volatile solvents is a result of larger energy requirements due to larger temperature increase.

Figure 3.31 shows analytical S_o changing with $\underline{H^t}$. Lighter solvents need more energy injected to achieve better S_{or}. As in **§2.4** , n-C_4 and n-C_6 are classified as Ternary Type 1 and n-C_8 Ternary Type 2. On chamber edge, W-L1-L2 may coexist for Ternary Type 1 solvents while only W-L1 is possible for Ternary Type 2 solvents. When Ternary Type 1 solvent starts to evaporate on the chamber edge, L1 and L2 evaporates together with W, however, L2 evaporates much faster than L1, since L2 is a separated phase with much more volatile contents than L1. This results in rapid reduction in oil phase saturation in the beginning of distillation for Ternary Type 1 when L2 is not totally gone. **Table 3.9** shows average $\triangle \underline{H^t}$ per unit S_o reduction calculated for both W-L1-L2-V and W-L1-V regions of Ternary Type 1. The existence of the solvent-rich oleic phase L2 is beneficial in terms of S_o reduction because much less energy is required for W-L1-L2-V region to reduce S_o than W-L1-V region. Since n-C_6 has a larger temperature range for W-L1-L2-V

compared to n-C_4, n-C_6 is on average more energy efficient to reduce oil saturation, even slightly greater than n-C_8.

3.5 Simulation Case Study

The CMG STARS (Computer Modelling Group, 2013) is used for simulation study of steam/n-alkane coinjection. Half of a reservoir with dimensions of 70×37.5×20 (m) is divided into 70×1×20 gridblocks. A pair of horizontal well with length of 37.5 m is placed at the left end of the reservoir. See **Table 3.10** for summary of reservoir properties and other simulation parameters. The relative permeability for each phase is shown in **Figure 3.32**.

1 mol% of methane is considered as the solution gas in initial bitumen. This is corresponding to a GOR of 0.44 m^3/m^3. Altogether, four components exist throughout the simulation: water, bitumen as one pseudo component, single-component n-alkane and methane. K-values are tabulated based on the EOS model described in **Chapter 2** using WINPROP (2013). WINPROP performs phase equilibrium calculations to obtain K-values using the PR EOS and the vdW mixing rules if solvent is insoluble in the aqueous phase. When solvent is soluble in aqueous phase, the Henry's law is initiated for aqueous phase fugacity calculation (Nghiem and Li, 1984). However, the way of WINPROP using Henry's law heavily relies on correlations regressed upon commonly seen soluble molecules such as n-alkanes, CO_2 and SO_2. It may have limited accuracy for solvents that behaves very different from n-alkanes, CO_2 and SO_2. Besides, K-values are tabulated in the WINPROP with a constant overall composition. That is, K values from the WINPROP are only dependent on temperature and pressure. Here, a rough estimation of chamber edge overall composition, 90 mol% water and 10 mol% hydrocarbon, is used to tabulate K-value tables. Since STARS allows only one oleic phase and up to three phases, K-values tabulated ignore the existence of solvent-rich oleic phase (L2).

Reliable viscosity and density models from Venkatramani and Okuno (2016) are used. In STARS, non-linear mixing of liquid phase viscosity is used. A detailed description of how the non-linear viscosity models were obtained can be found in there paper. A linear mixing of pure component densities is used for liquid phases density. Densities are summarized in **Table 3.11** and **Table 3.12**. The vapor phase is modeled as ideal gas and its density follows ideal gas EOS prediction in STARS.

The injection well operates at a constant 35 bars and the production well at a constant 15 bars. The whole simulation project lasts for 10 years. A 6-month reservoir preheating is considered at the beginning of simulation. Two injection strategies are considered here: first, solvent is coinjected with steam at a constant concentration of 2 mol% throughout the simulation; second, same strategy is used as the first one initially, and then stop injecting solvent immediately the steam chamber reaches the outer reservoir boundary. The second strategy is used because the bitumen drainage rate slows down in the late stage of bitumen recovery. It would be economically beneficial to stop injecting solvent and recovery the retained solvent. Here, C_3, n-C_5, n-C_7 and n-C_{10} are selected as pure solvents to be coinjected with steam. C_3 is a Ternary Type 1 solvent at 35 bars, while the rest are Ternary Type 2. Recovery factor, cumulative steam-oil ratio (CSOR) and solvent recovery are shown in **Figure 3.33** to **Figure 3.38** for two different strategies.

In general, Type 2 solvents (C_5, C_7 and C_{10}) are more efficient than Type 1 (C_3) in terms of bitumen recovery, SOR and solvent recovery. In **Figure 3.33** and **Figure 3.36**, Type 2 solvents are able to recovery more bitumen faster. Type 2 higher chamber edge temperature and efficient mixing of solvent with bitumen account for Type 2 efficiency of bitumen recovery.

In **Figure 3.34**, CSOR is plotted against bitumen recovery factor for the first strategy. For same amount of bitumen recovered, lower SOR is desired because it indicates less steam amount required. All n-alkane solvents show improvement in CSOR compared to steam-only injection case; however, Ternary Type 2 solvents demand less steam injection to produce same amount

of bitumen as Ternary Type 1 solvents. Each Ternary Type 2 solvent shows very similar SOR to produce same amount of bitumen. In contrast, **Figure 3.36** shows CSOR against bitumen recovery factor for second strategy. Steam-only injection at later simulation stage results in increase of CSOR compared to that of **Figure 3.34**. However, Ternary Type 2 solvents are still better than Ternary Type 1 in terms of CSOR.

In **Figure 3.35**, solvent recovery is plotted against bitumen recovery factor. Ternary Type 1 solvent needs more barrels of solvent retention to achieve the same amount of bitumen recovery as Ternary Type 2. **Figure 3.38** shows solvent retention after switching to the second operation strategy. By switching to the second strategy, steam-only injection at later simulation stage, Type 2 solvents can be more efficiently recycled. Because Ternary Type 2 solvents are more narrow-boiled in the whole W-L1-V region than Ternary Type 1 solvents, as is shown in **§3.4** case study 2. With little temperature increase, L1 phase composition is able to change more rapidly for Ternary Type 2 than Type 1. Besides, steam-only injection increases water concentration in the whole reservoir. L1 phase saturation of Ternary Type 2 is more sensitive to global water concentration as is shown in **§3.3**, case study 1. Therefore, Ternary Type 2 solvents can be more efficiently recycled than Type 1.

It is not possible to quantitatively validate the result of analytical S_{or} through simulation study for the following reason. For one thing, the simulated reservoir is not a closed system. Overall composition is changing from the chamber edge to inside the chamber. For another thing, in order to compare the S_{or} between the two methods, same P, T and overall composition should be used. The distillation analysis on S_{or} is performed upon phase equilibrium calculation of the PR EOS. STARS performs phase equilibrium calculation using K-value tables generated by the PR EOS, and the lowest S_w achieved in simulation is always about S_{wr}. Therefore, predictions from simulation and analytical solution would be undoubtedly consistent. Validation of analytical S_{or} using simulation would simply be a comparison of phase behavior predictions between PR EOS and K-values generated by PR EOS.

Here, analytical S_{or} is only qualitatively validated through numerical simulation. C_5, C_6, C_7 and C_8 are considered here. First, they are all Ternary Type 2 solvents at 35 bars. C_3 and C_4 are not considered in the qualitative validation because of incapability of STARS to model more than one oleic phase. Phase behavior in the simulation for Ternary Type 1 is bounded by L1, the only oleic phase that is modeled in STARS. Second, C_5 to C_8 cases use non-linear logarithmic mixing rules for L phase viscosity calculation. C_{10} case uses linear logarithmic mixing for the L phase viscosity because available experiment data indicates the L viscosity is almost linear to C_{10} content in the L phase. Without more data to justify C_{10} using linear logarithmic mixing for L phase viscosity, it is safe to avoid discussion on C_{10} case for now.

Since residual oil contains both bitumen and solvent, average oil saturation in reservoir in the end of simulation is considered. 2 mol% of solvent is coinjected with steam throughout the simulation without injection strategy manipulation.

Since the overall composition on the chamber edge in a simulated reservoir is not something that can be directly controlled. Rather, it is the injection strategy, e.g. the operation pressure, the injection rate and the steam to solvent ratio. When 2 mol% of solvent are injected with 98 mol% of steam at 35 bars, the chamber edge bitumen to solvent ratio when chamber edge temperature becomes steady is about 1:30. The overall water concentration on the chamber edge is about 80 mol%. In contrast to the analytical solution studies, take the sensitivity analysis of the analytical solutions to pressure, the chamber edge water concentration is set to 98 mol% and the bitumen to solvent ratio on the chamber edge is 2:3. Again, in an actual reservoir, the chamber edge overall composition can be changed by manipulation of injection strategy. However, the relationship between the injection strategy and material accumulation on the chamber edge is not a concern of this research. Only qualitative validation is shown below.

Figure 3.39 shows average S_{or} in reservoir at 35 bars and 60 bars. At 35 bars, lighter solvent shows lower S_{or} with distinct trend with respect to carbon number, which is consistent with the analytical solution prediction. However, at 60 bars, the trend becomes not obvious and average

S_{or} crosses each other with very little differences between each case. Analytical solutions indicate almost the same S_{or} at 60 bars from C_3 to C_{10}. Differences of average S_{or} in each volatility case at 35 bars and 60 bars are also shown in **Figure 3.40**. Generally, average S_{or} of lighter solvent shows lower sensitivity to pressure increase. This is also consistent with analytical solution predictions. Therefore, the simulation result is consistent with that of analytical solution in terms of volatility and pressure sensitivity.

Also, how the residual oil saturation is affected by chamber edge overall composition is shown in **Figure 3.41 (1)**. Steam-C_7 coinjection is taken as an example at 35 bars. **Figure 3.41 (2)** shows the overall composition on the chamber edge for the 12^{th} row. From the well pair to deep inside the reservoir, the chamber edge water concentration is dropping, however, the chamber edge solvent concentration is increasing. In the vicinity of the well pair, the solvent concentration is almost zero and water concentration is high. Correspondingly, the S_{or} is around endpoint oil saturation in the vicinity of well pair. However, solvent gradually accumulates on the chamber edge and water concentration drops as the chamber sweeps into the reservoir. Therefore, the S_{or} deep inside the reservoir is lower than the endpoint S_o. The reduction of oil saturation deep inside the reservoir is clearly a result of solvent accumulation.

Figure 3.42 shows simulated average S_{or} for C_6 case when 0.10 S_{wr} and 0.25 S_{wr} are examined. Analytical solution suggested lower S_{wr} results in lower S_{or}. However, S_{wr} affect simulation more than just phase behavior. In reality, change in endpoint saturations alters the relative permeability curves. This substantially affects flow and displacement in the simulations. It is understandable that the S_{wr} sensitivity of analytical solutions does not necessarily reflect that of the simulation results.

As a qualitative tool for distillation explanation, it is important that it shows the general trend consistently with the simulation. It can be seen from the validation that, the algorithm for analytical solutions can qualitatively predict the general trend in the simulation. For the solvent volatility, the lighter solvent predicts lower S_{or} in the simulation, which is the same as the analytical solutions.

Also, the higher the pressure, the more sensitive of heavier solvent in terms of displacement efficiency. Also, in the simulation, more solvent accumulation results in lower residual oil saturation despite the decreasing water.

3.6 Conclusions

In this chapter, a thermodynamic tool was developed to analytically explain residual oil saturation due to distillation. The tool was developed by use of the PR EOS with the vdW mixing rules. Water dissolution in the oleic phases and solvent partitioning in the aqueous phase are possible in the model. This tool can estimate S_{or} with a few inputs, unlike reservoir flow simulation.

Also, two ternary types of water/bitumen/n-alkane were revisited in this chapter using numerical simulations. Efficiency of solvent usage, i.e. the bitumen recovery, steam-oil ratio and solvent retention by using the solvent, was compared for coinjection cases with Ternary Type 1 and 2 solvents.

The following conclusions are drawn based on the analytical S_{or} study:

- Ternary Type 1 can achieve lower S_{or} than Ternary Type 2 based on the analytical solutions study. First, this is because of a volatile solvent can achieve greater incremental temperature during solvent distillation process. It requires more energy input for a ternary system of water, bitumen and heavier solvent to increase 1 K. Also, more solvent can be evaporated during distillation for lighter solvents than heavier ones as a result of competition between solvent and water evaporation from liquid phases. Finally, the existence of L2 in Ternary Type 1 is rich in volatile components, which makes the distillation of L2 much easier than that of L1.
- Sensitivity analysis shows that more volatile solvents, higher operation pressure, higher solvent accumulation, higher water concentration and lower endpoint water saturation are beneficial for displacement efficiency. Uncertainties in terms of all these

factors influence the analytical S_{or} in a unified way: that is, lower S_{or} can be achieved if incremental temperature is higher and/or more solvent can be distilled from liquid phases compared to water.

- Ternary Type 1 may not be better than Ternary Type 2 in terms of drainage rate. Chamber edge conditions can be different for Ternary Type 1 and Ternary Type 2 n-alkane solvents. For Ternary Type 1, aqueous phase and only a bitumen-rich oleic phase L1 exist when solvent concentration is low on chamber edge. However, when chamber edge temperature is low, an additional solvent-rich oleic phase L2 exists. For Ternary Type 2 solvents, only W and L1 appear ahead of a chamber edge. The separation of liquid hydrocarbons into two oleic phases in the vicinity of chamber edge may occur with Ternary Type 1 solvents which results in low solvent solubilities in bitumen compared to Type 2 solvents.
- Analysis of solvent performances in terms bitumen recovery, steam-oil ratio and solvent retention indicates that Ternary Type 2 solvents are more efficient. For Ternary Type 2, a faster drainage rate, lower steam-oil ratio and lower solvent retention can be achieved by injection of steam only after a period of coinjection.
- The analytical S_{or} was validated using numerical simulations. Coinjection of a more volatile solvent with steam tends to result in a lower S_{or}. A higher operating pressure also increases displacement efficiency. S_{or} decreases with increasing level of solvent accumulation near a chamber edge. However, S_{wr} impacts on simulation results in a more complicated way than just the change in phase behavior. Endpoint saturation affects relative permeability and, therefore, has a great impact on the flow in simulation.

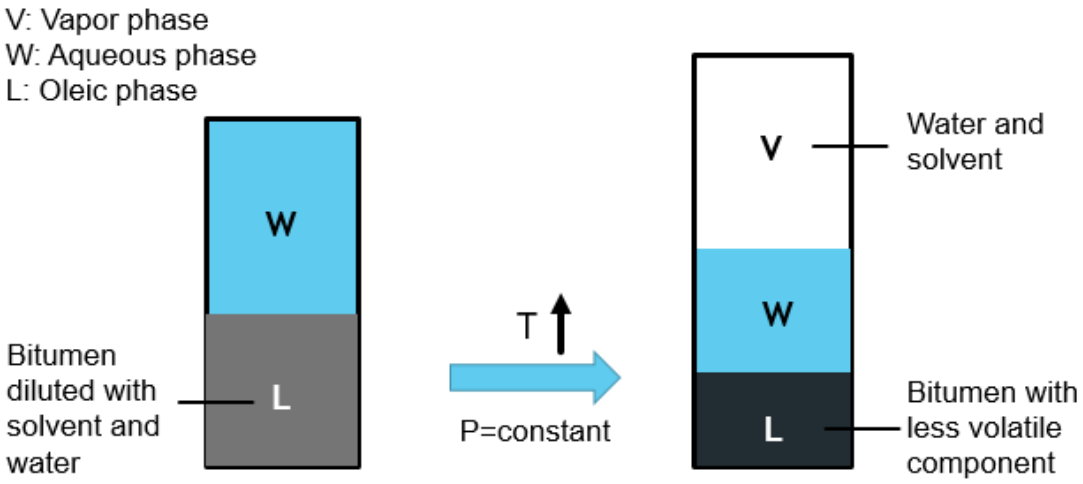

Figure 3.1 An explanation of the distillation mechanism. Initially, there are water phase and a oleic phase of a bitumen diluted with solvent and water. If pressure keeps constant and temperature is increased, solvent and water may transfer from water and oleic phases to the vapor phase, and therefore, the volume of oleic phase shrinks.

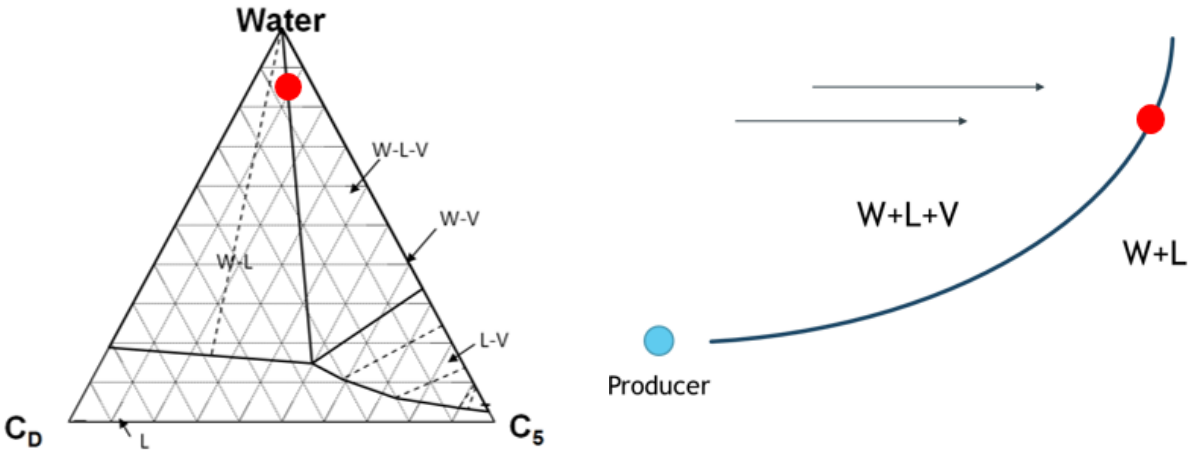

(1) Ternary diagram (2) Schematic of chamber edge

Figure 3.2 The first situation of chamber edge. Single-phase and two-phase regions are associated with three-phase regions, but are not shown here deliberately for clarity. C_5 is taken as example at 35 bars based on 1-PC EOS model of case study 1 in Chapter 2. Outside the steam chamber, there is W and L phase, while inside the chamber there is W-L-V. The overall composition on the chamber edge is located on the edge of W-L and W-L-V boundary.

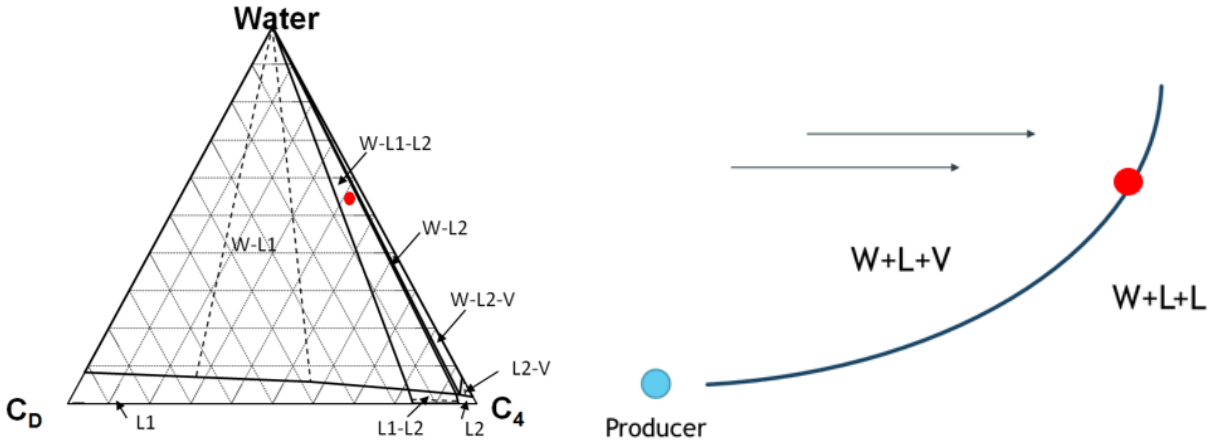

(1) Bitumen-solvent ratio = 1:4 (2) Schematic of chamber edge

Figure 3.3 The second situation of chamber edge. C_4 is taken as example at 35 bars based on 1-PC EOS model of case study 1 in Chapter 2. Outside the steam chamber, there is W-L-L, while inside the chamber there is W-L-V. The overall composition on the chamber edge is located within the W-L1-L2 region in the ternary diagram. Chamber edge temperature should be the 4-phase temperature at this pressure.

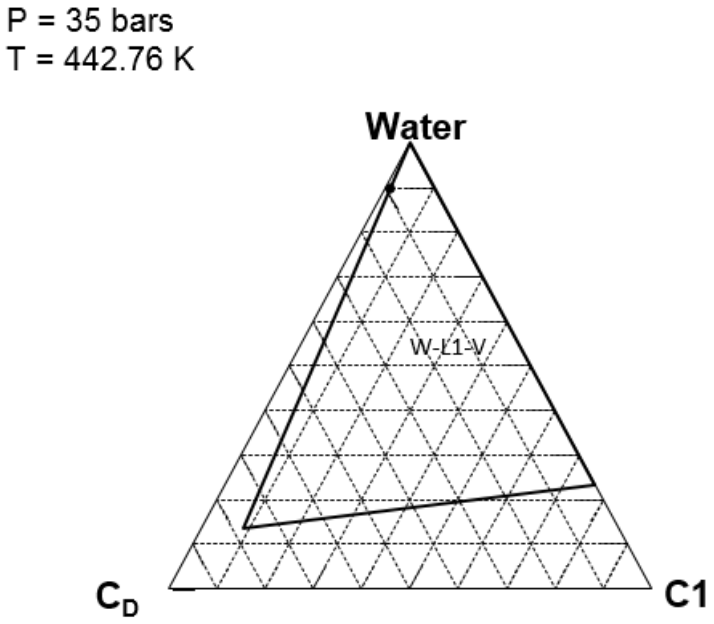

Figure 3.4 Ternary phase behavior on the chamber edge for SAGD. A GOR of 5 m3/m3 (or 10 mol% C1 in the bitumen) is considered. If a zero GOR is considered, the chamber edge temperature should be 515.0 K, the same as T_{3p} of water/bitumen at 35 bars. Solution gas such as C_1 lowers chamber edge temperature for SAGD.

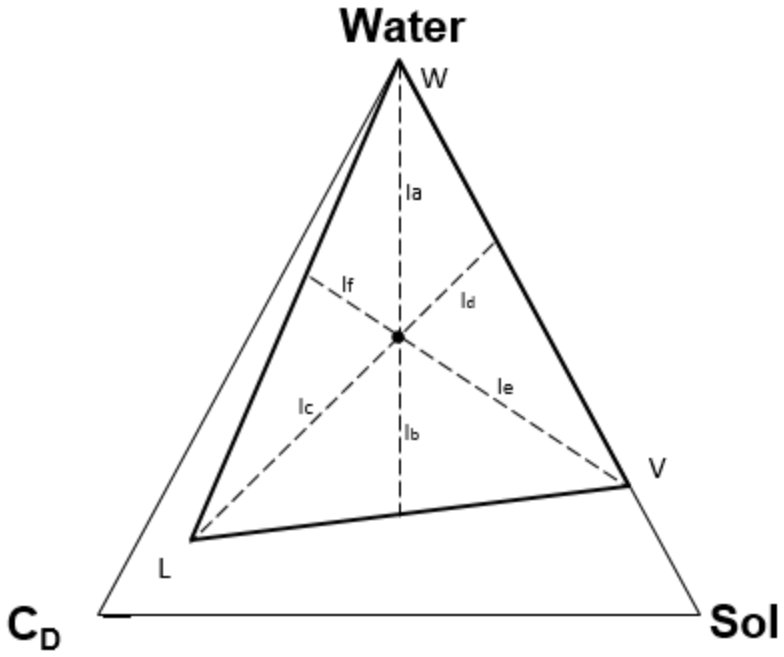

Figure 3.5 Example calculation of phase mole fraction using the lever rule. Solid dot represents overall composition. The lower case “l” represents the length of each dashed section.

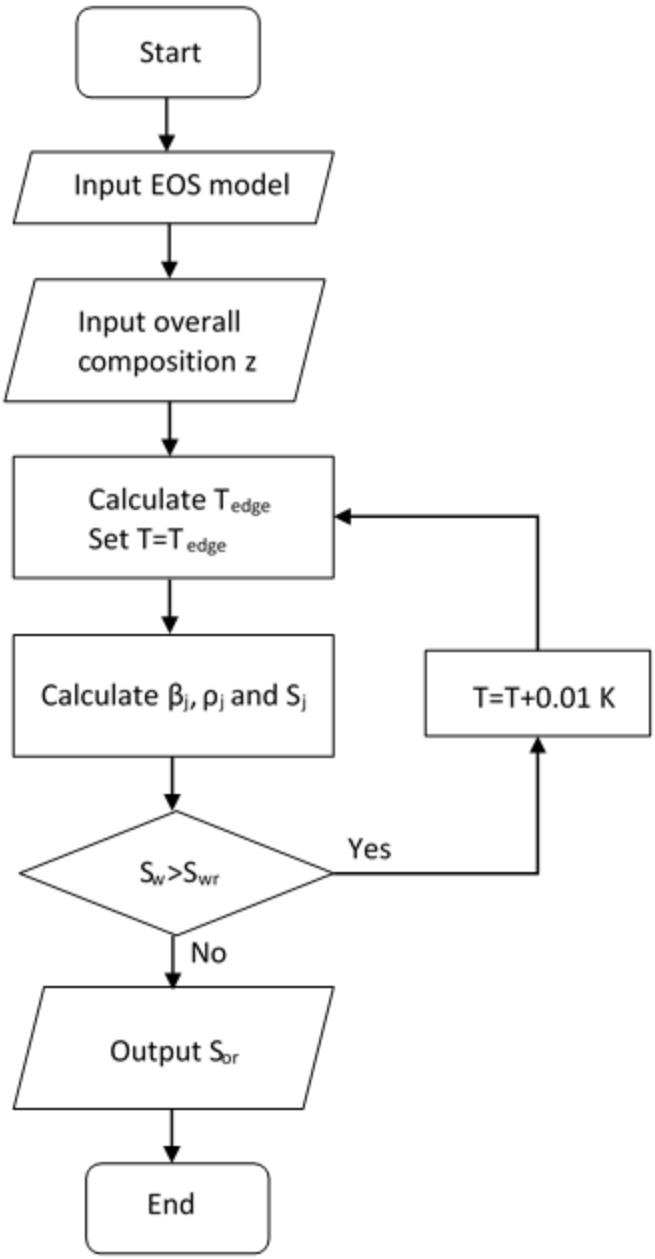

Figure 3.6 A flowchart of the algorithm for analytical residual oil saturation calculation.

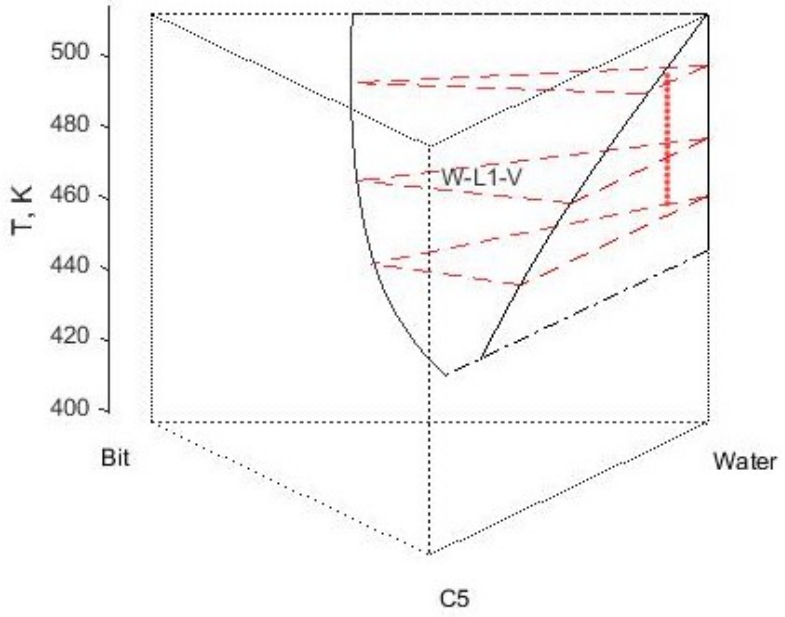

(1) 3D

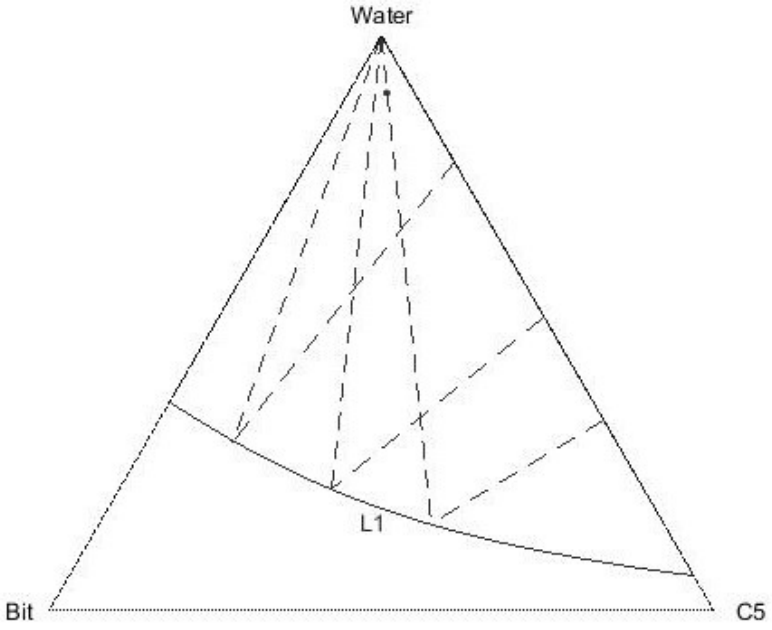

(2) Projections from the vertical view

Figure 3.7 Case study 1 example calculation of analytical Sor due to distillation. (1) The whole distillation process is visualized in 3D. (2) Mass transfer from liquid phases to vapor phases is shown in 2D. Dots are overall compositions, which has been exaggerated for demonstration purpose. L1 trajectory in temperature-composition space is shown in solid curve. Overall composition initially locates on the W-L1 edge of W-L1-V. L1 then swings towards water/bitumen edge as temperature goes up as a result of solvent distillation.

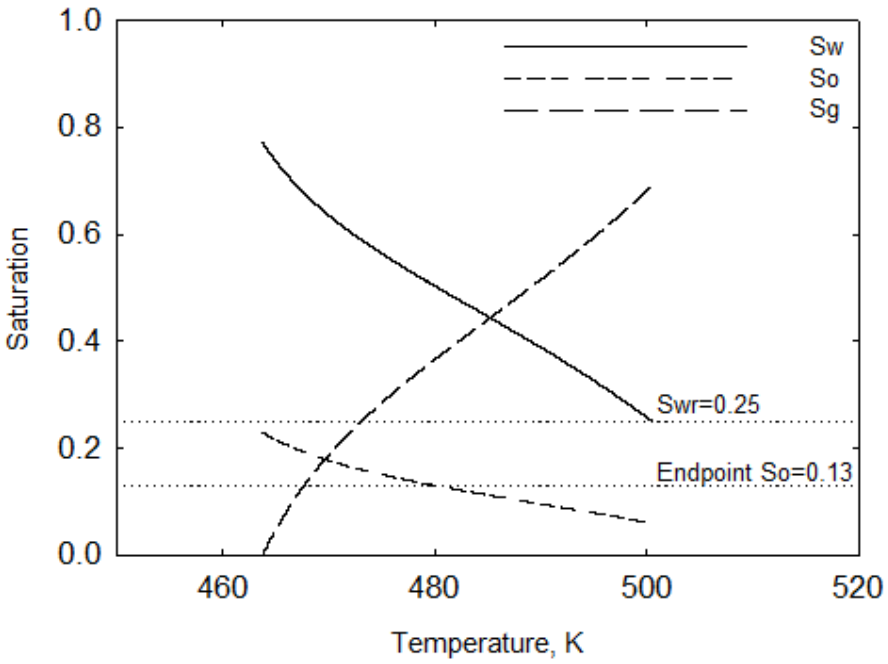

Figure 3.8 Case study 1 example calculation using n-C_5. Saturation changes with temperature during distillation process.

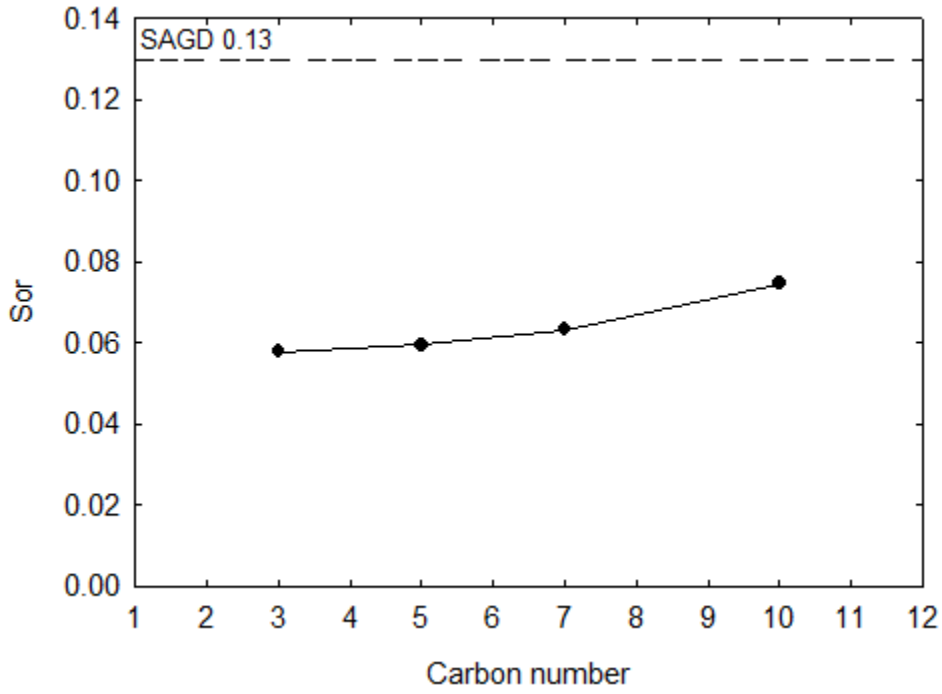

Figure 3.9 Case study 1 analytical S_{or} sensitivity to solvent volatility.

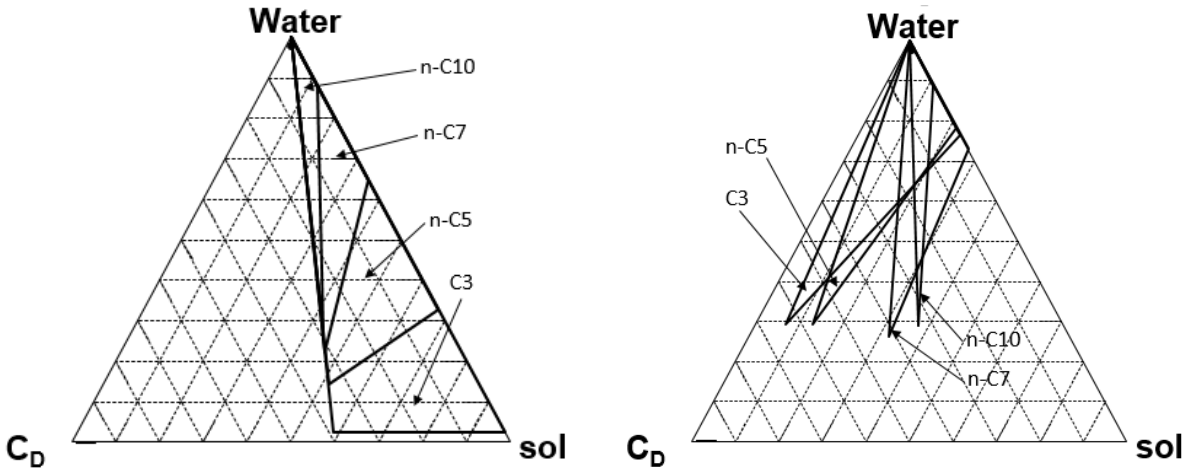

(1) T_{edge} (2) T_{Swr}

Figure 3.10 Case study 1 solvent volatility sensitivity analysis. Phase behavior at the beginning and ending of solvent distillation process.

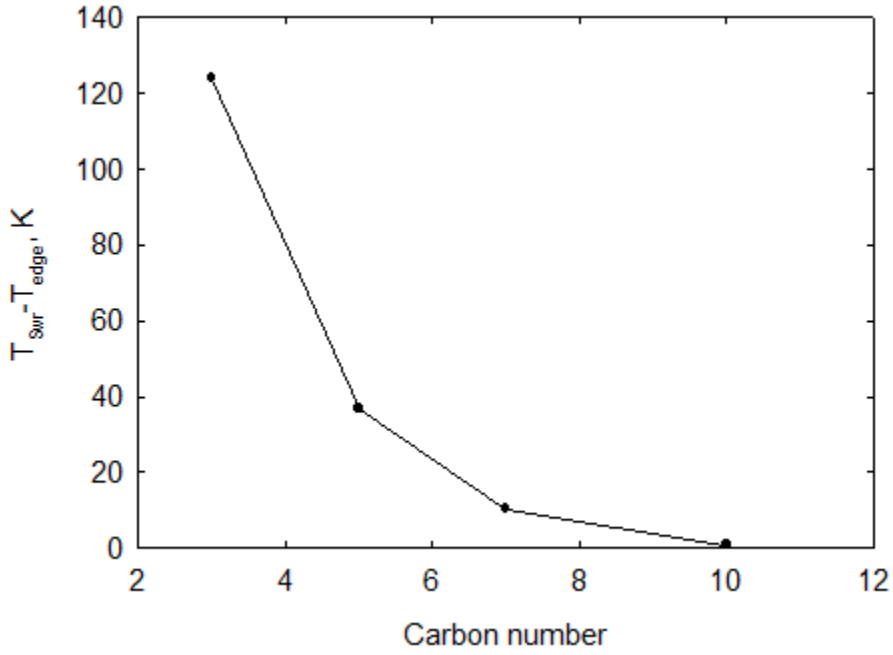

Figure 3.11 Case study 1 solvent volatility sensitivity analysis. Increased temperature during distillation is summarized.

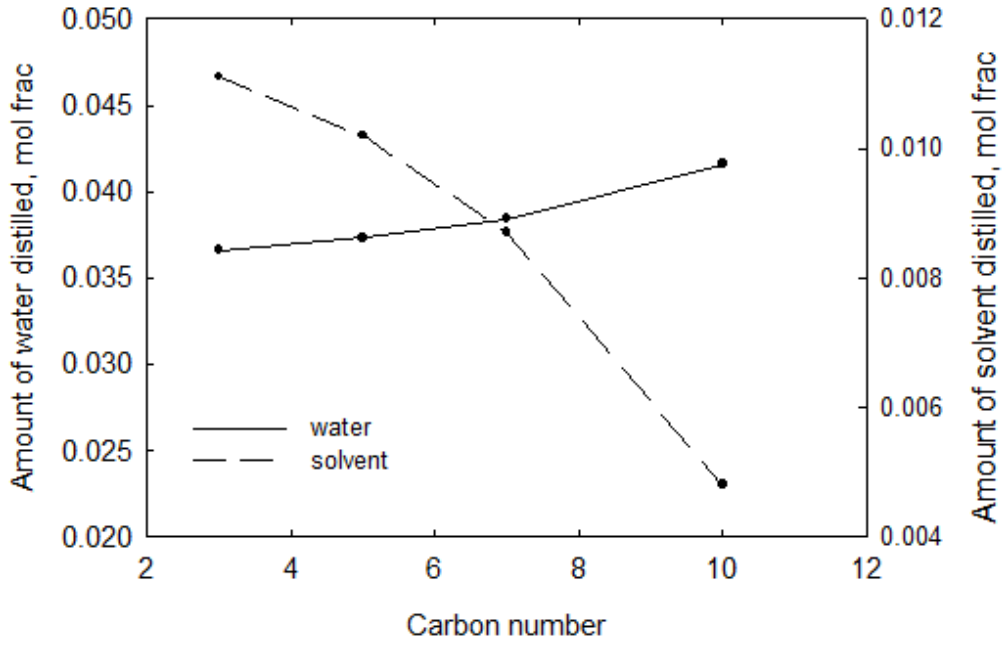

Figure 3.12 Case study 1 solvent volatility sensitivity analysis. Mole fraction of water evaporated from W and L phase and mole fraction of solvent distilled from L phase are summarized.

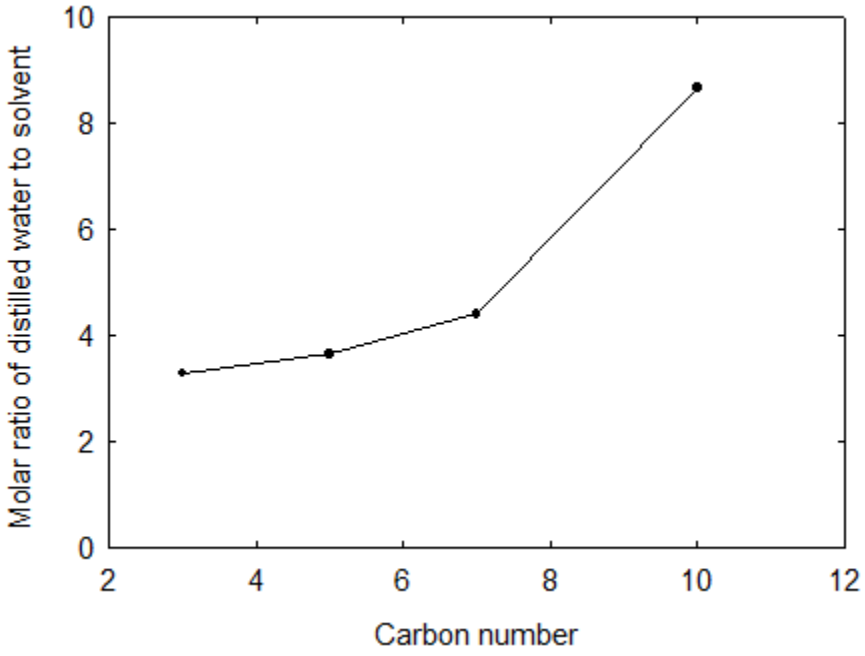

Figure 3.13 Case study 1 solvent volatility sensitivity analysis. The mole fraction ratio of evaporated water to evaporated solvent from liquid phases.

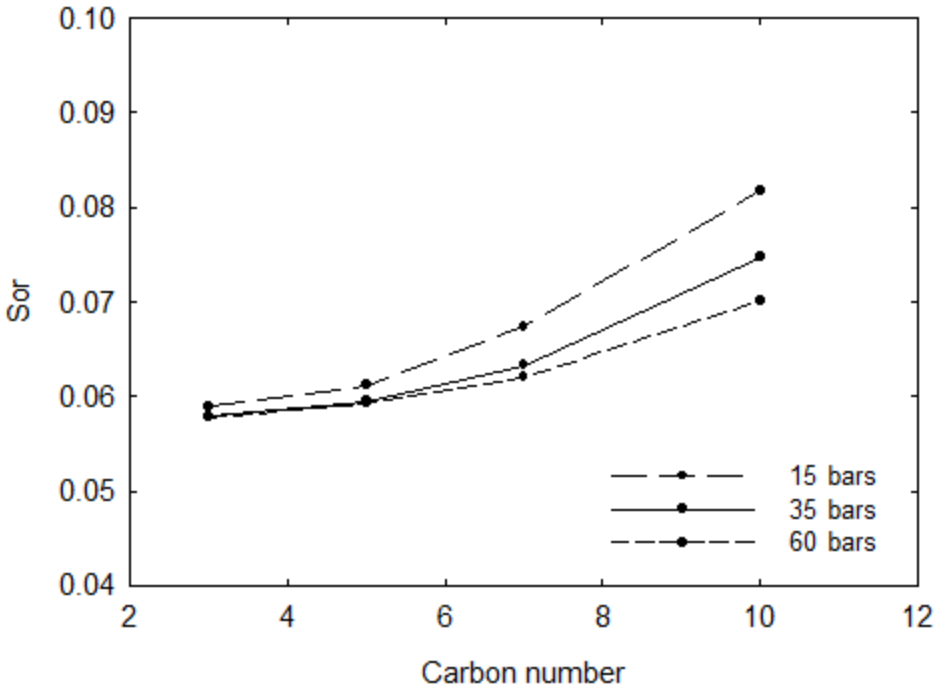

Figure 3.14 Case study 1 analytical S_{or} sensitivity to operation pressure.

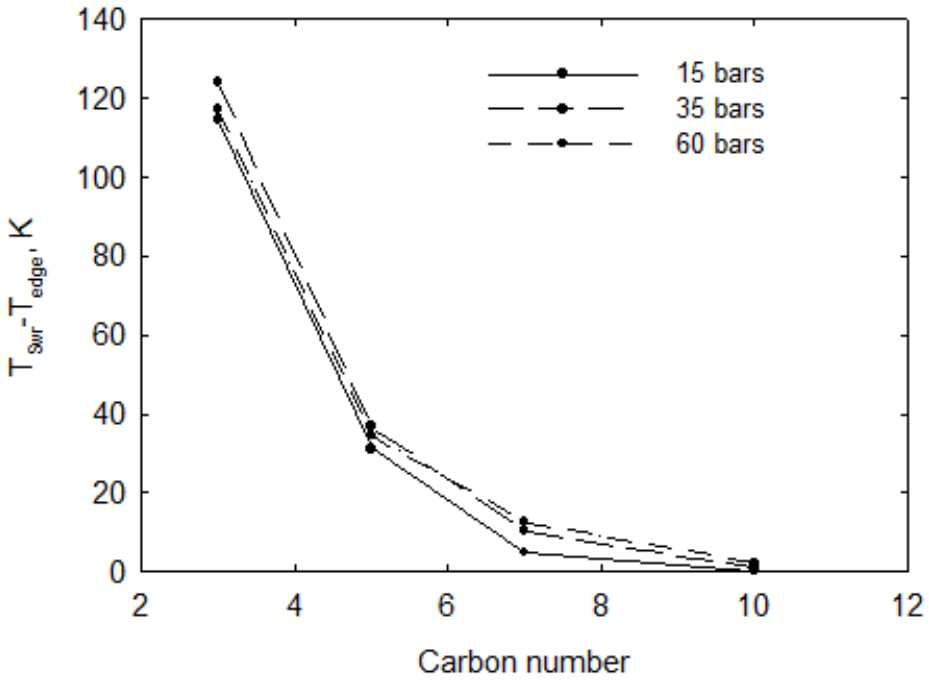

Figure 3.15 Case study 1 operation pressure sensitivity analysis. Increased temperature during distillation is summarized.

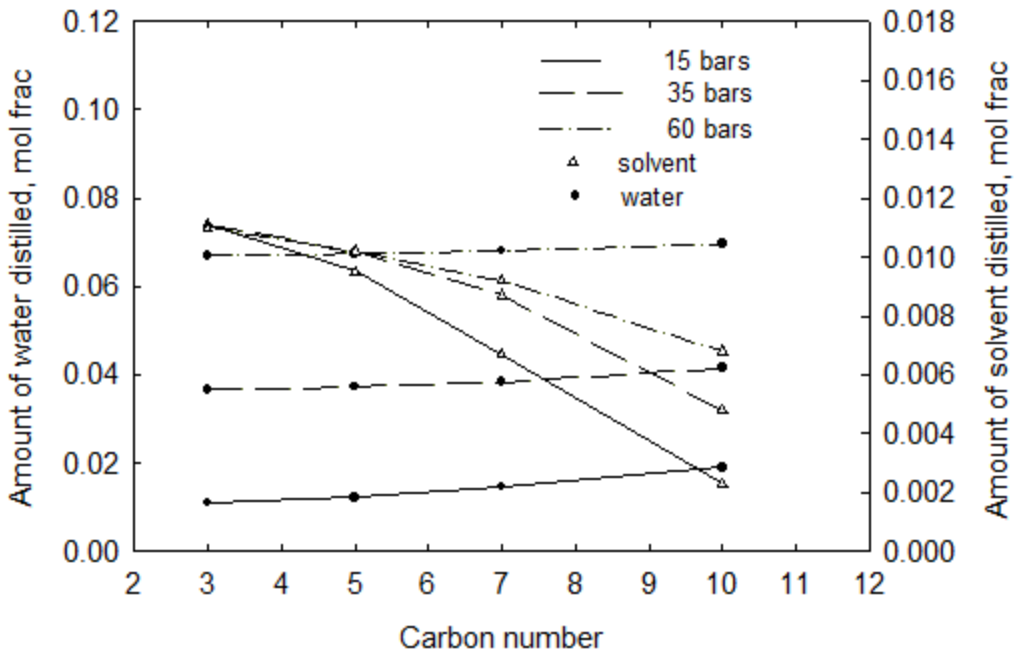

Figure 3.16 Case study 1 operation pressure sensitivity analysis. Mole fraction of water evaporated from W and L phase and mole fraction of solvent distilled from L phase are summarized.

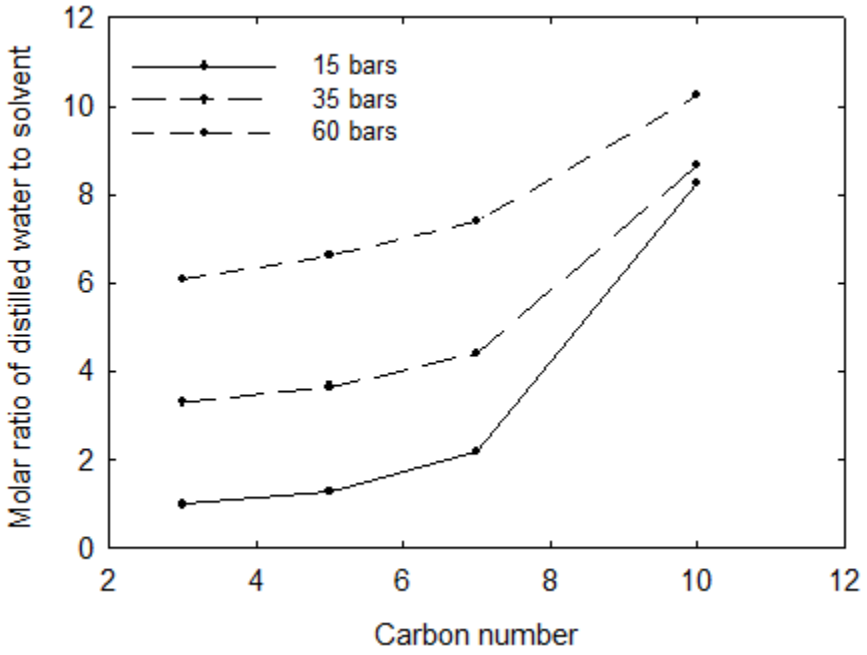

Figure 3.17 Case study 1 operation sensitivity analysis. The mole fraction ratio of evaporated water to evaporated solvent from liquid phases is summarized with respect to carbon number.

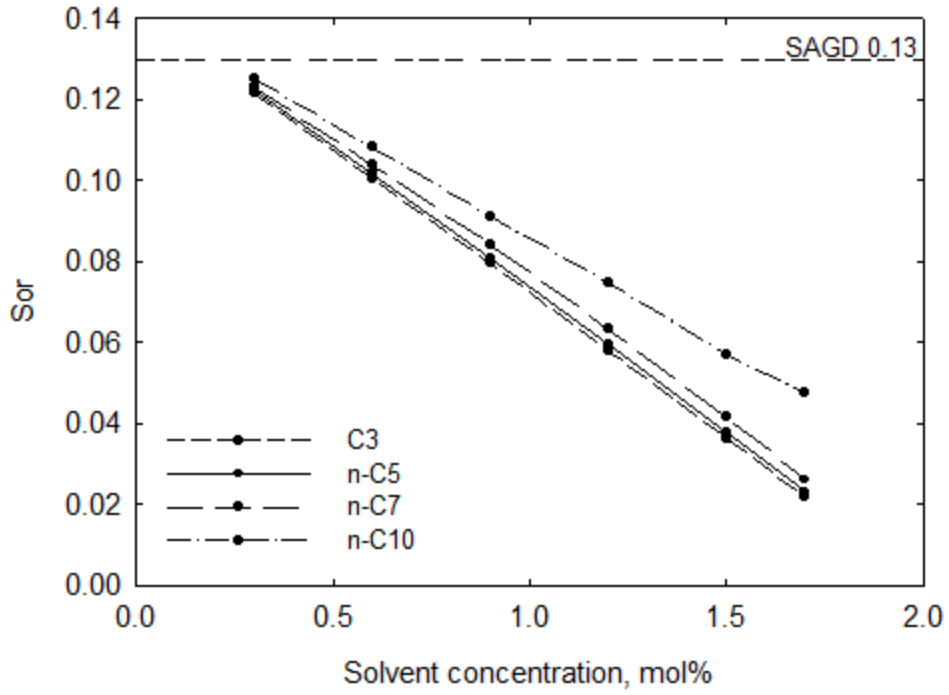

Figure 3.18 Case study 1 analytical S_{or} sensitivity to solvent accumulation on chamber edge. The water concentration in this figure is 98 mol%. If the curves of the analytical solutions are extrapolated from the left-hand side, they will intersect with the endpoint S_o line. The corresponding solvent concentration of the intersects represent the minimum solvent concentration to result in reduced S_{or} lower than S_o.

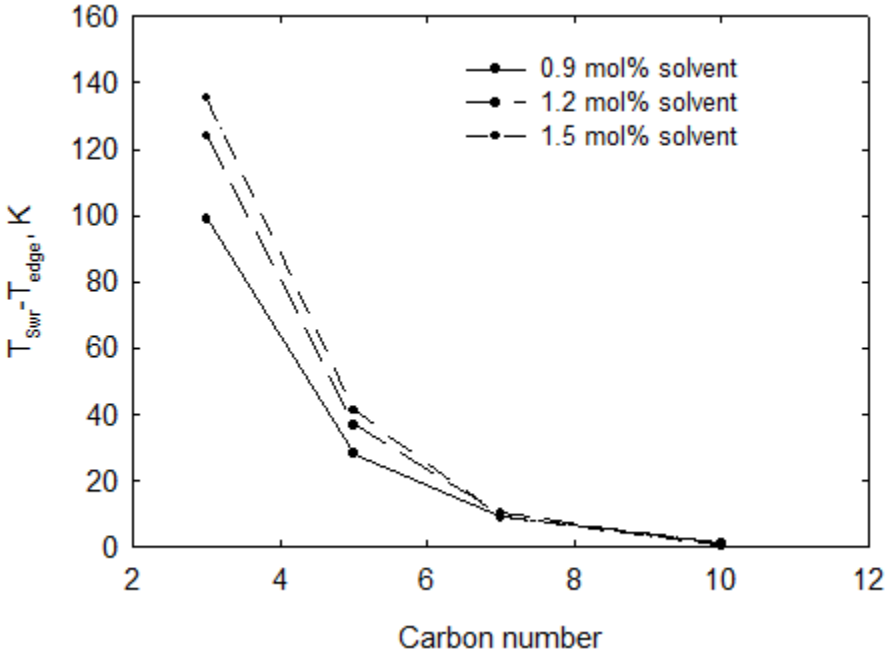

Figure 3.19 Case study 1 solvent accumulation sensitivity analysis. Increased temperature during distillation is summarized.

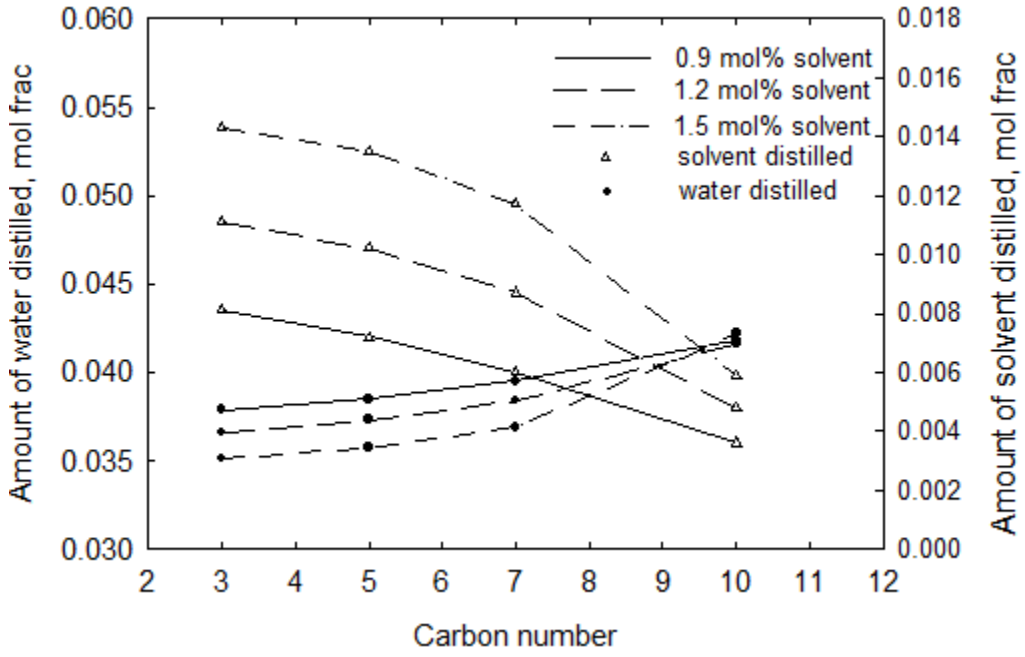

Figure 3.20 Case study 1 solvent accumulation sensitivity analysis. Mole fraction of water evaporated from W and L phase and mole fraction of solvent distilled from L phase are summarized.

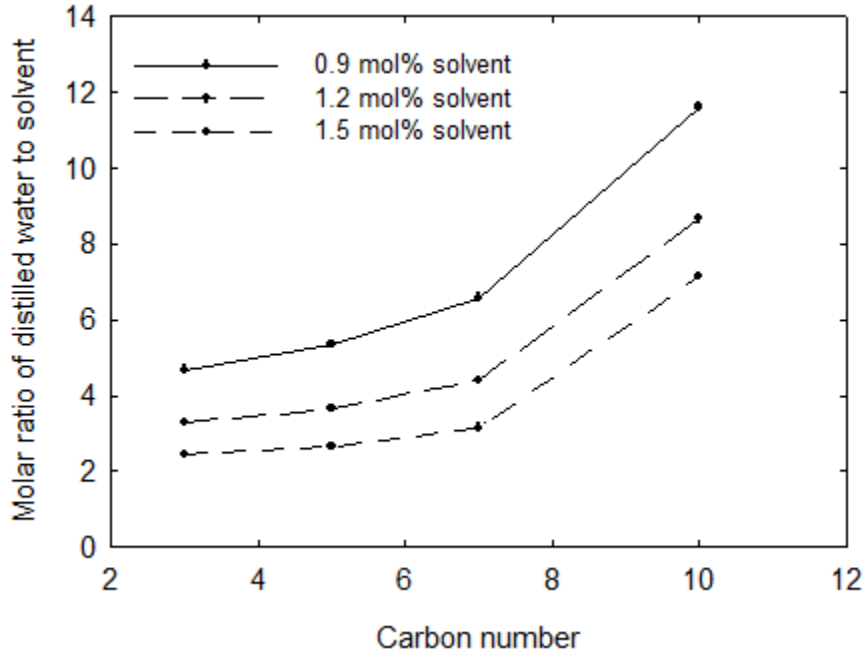

Figure 3.21 Case study 1 solvent accumulation analysis. The mole fraction ratio of evaporated water to evaporated solvent from liquid phases is summarized with respect to carbon number.

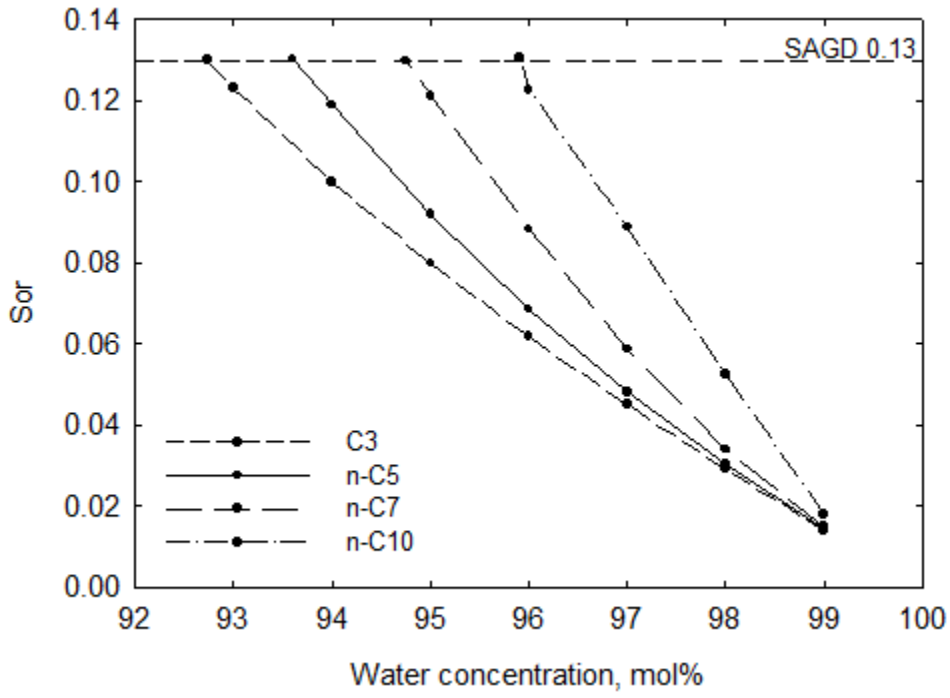

Figure 3.22 Case study 1 analytical S_{or} sensitivity to water accumulation on chamber edge.

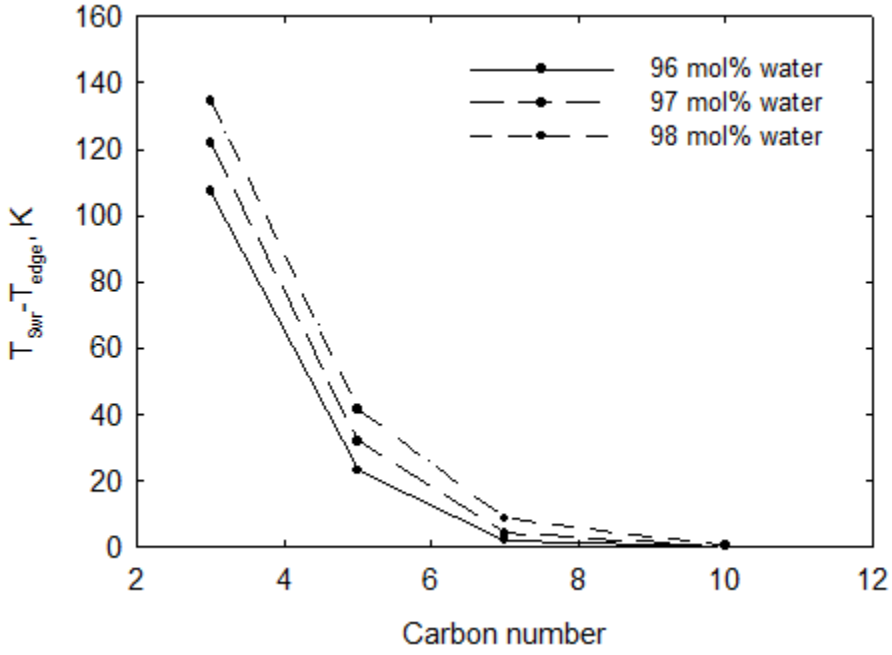

Figure 3.23 Case study 1 overall water concentration sensitivity analysis. Increased temperature during distillation is summarized.

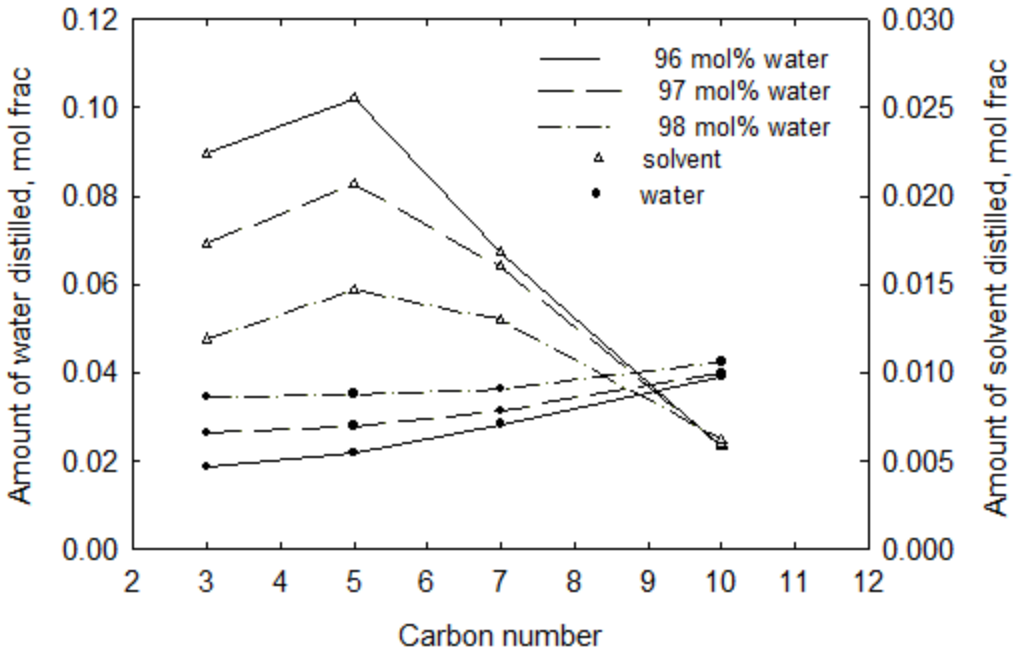

Figure 3.24 Case study 1 overall water concentration sensitivity analysis. Mole fraction of water evaporated from W and L phase and mole fraction of solvent distilled from L phase are summarized.

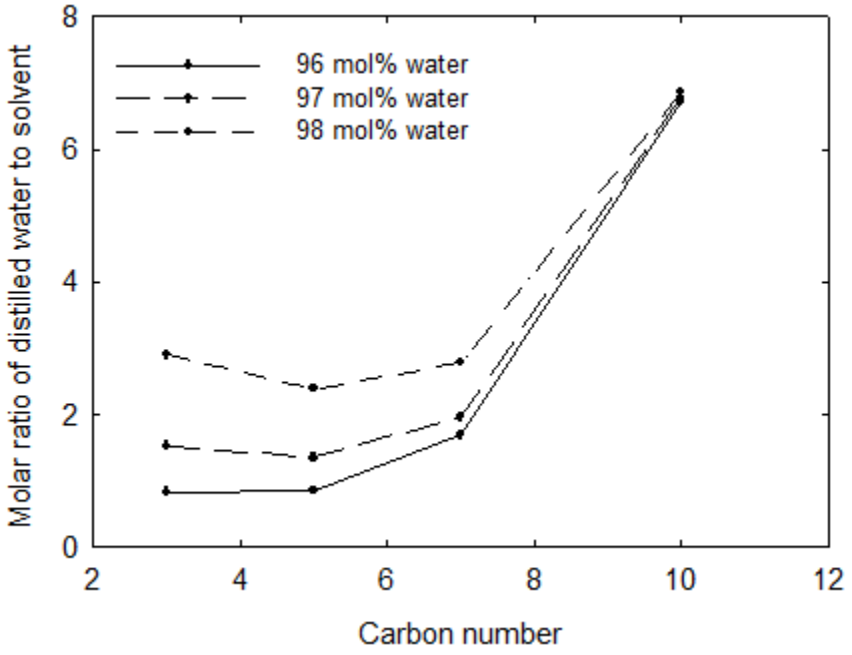

Figure 3.25 Case study 1 overall water concentration analysis. The mole fraction ratio of evaporated water to evaporated solvent from liquid phases is summarized with respect to carbon number.

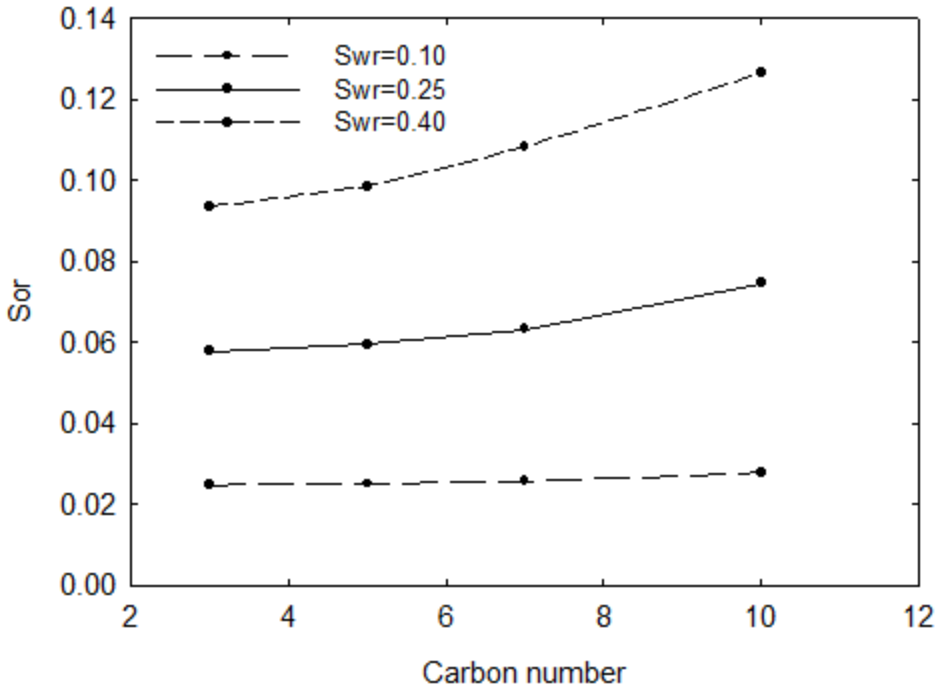

Figure 3.26 Case study 1 analytical S_{or} sensitivity to irreducible water saturation (S_{wr}).

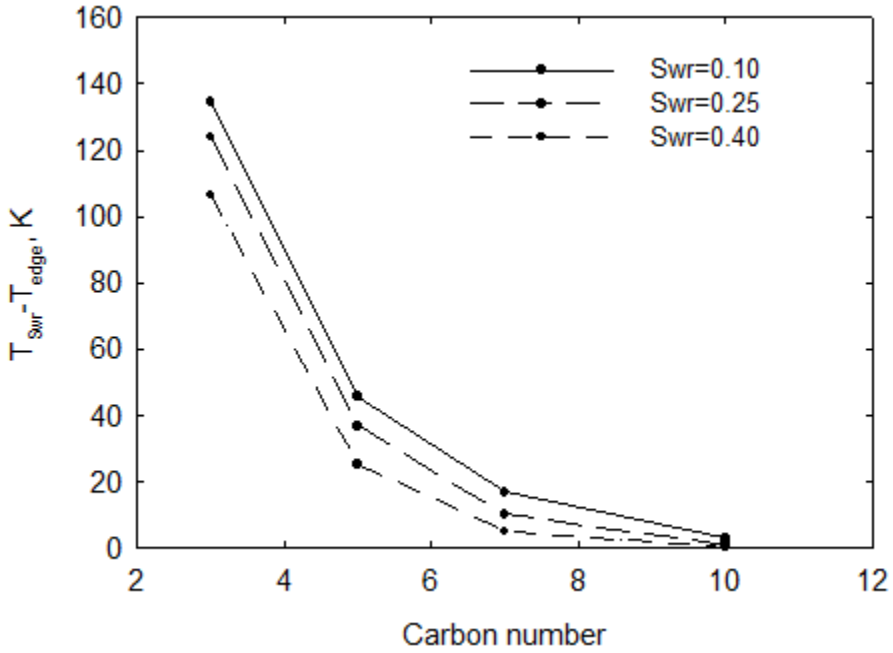

Figure 3.27 Case study 1 analytical S_{or} sensitivity to irreducible water saturation (S_{wr}). Increased temperature during distillation is summarized.

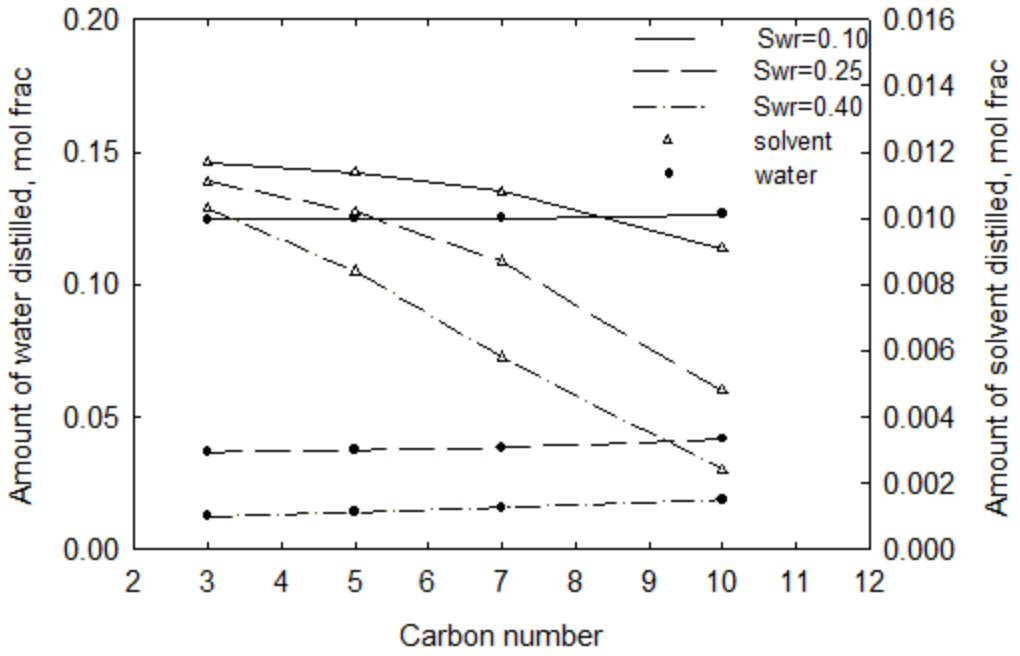

Figure 3.28 Case study 1 analytical S_{or} sensitivity to irreducible water saturation (S_{wr}). Mole fraction of water evaporated from W and L phase and mole fraction of solvent distilled from L phase are summarized.

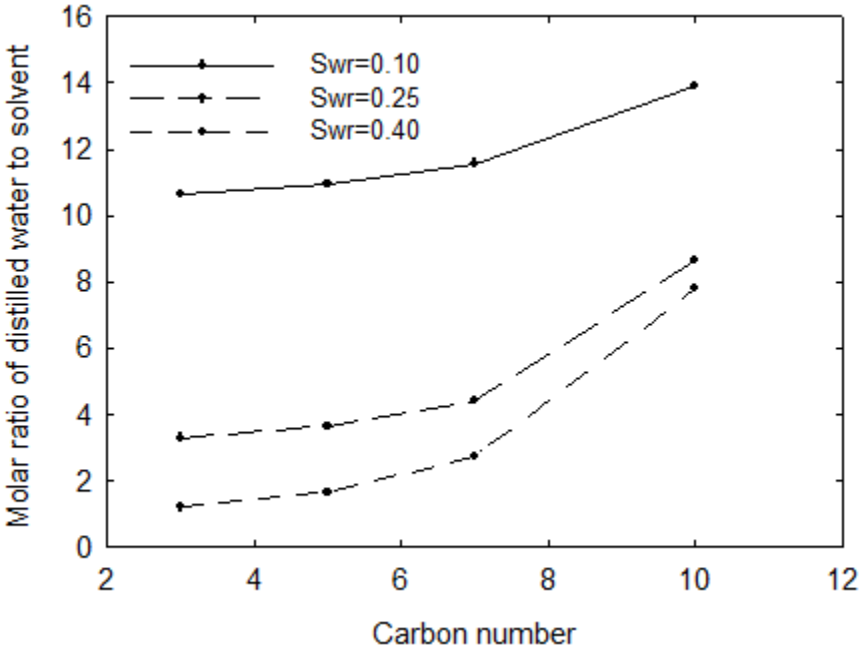

Figure 3.29 Case study 1 analytical S_{or} sensitivity to irreducible water saturation (S_{wr}). The mole fraction ratio of evaporated water to evaporated solvent from liquid phases is summarized with respect to carbon number.

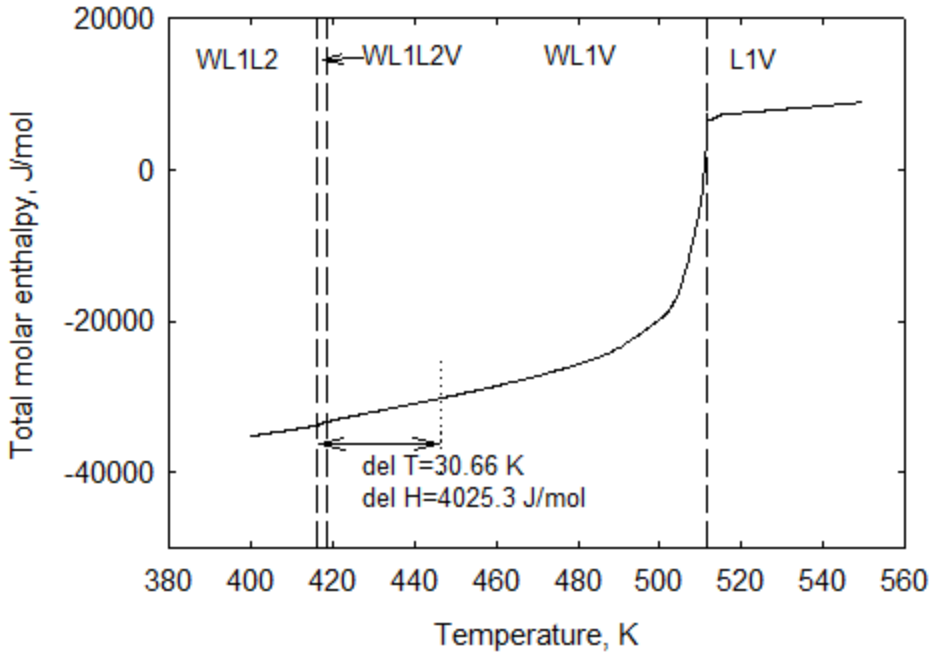
20000
0
-20000
-40000
WL1L2
WL1L2V
WL1V
L1V
del T=30.66 K
del H=4025.3 J/mol
380
400
420
440
460
480
500
520
540
560
Total molar enthalpy, J/mol
Temperature, K

(1) n-C_4

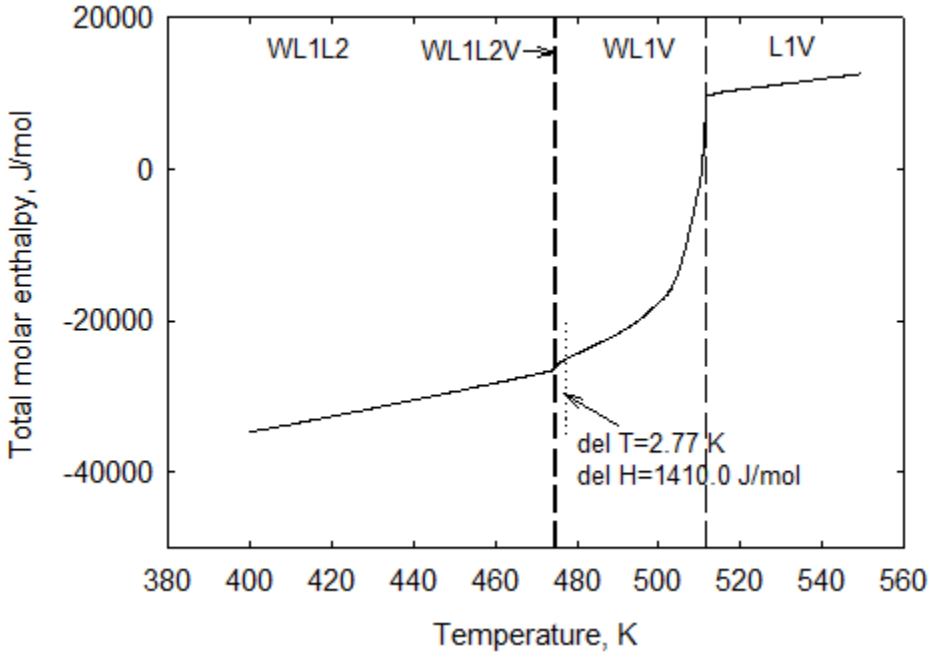
20000
0
-20000
-40000
WL1L2
WL1L2V
WL1V
L1V
del T=2.77 K
del H=1410.0 J/mol
380
400
420
440
460
480
500
520
540
560
Total molar enthalpy, J/mol
Temperature, K

(2) n-C_6

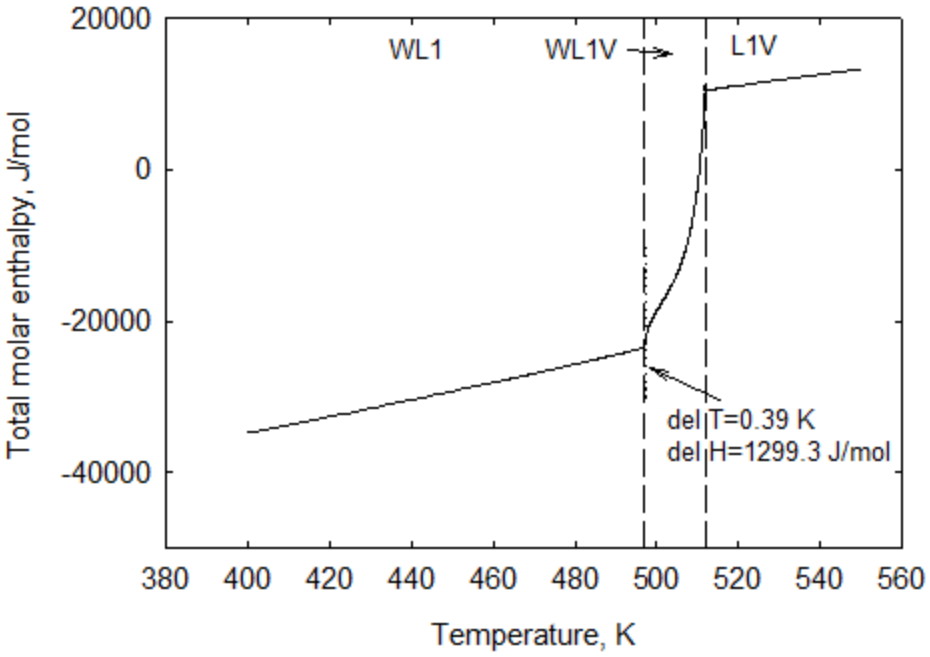

(3) n-C_8

Figure 3.30 Case study 2 total molar enthalpy change with temperature. ΔT indicates temperature range of solvent distillation. Ligter solvent has much larger temperature range.

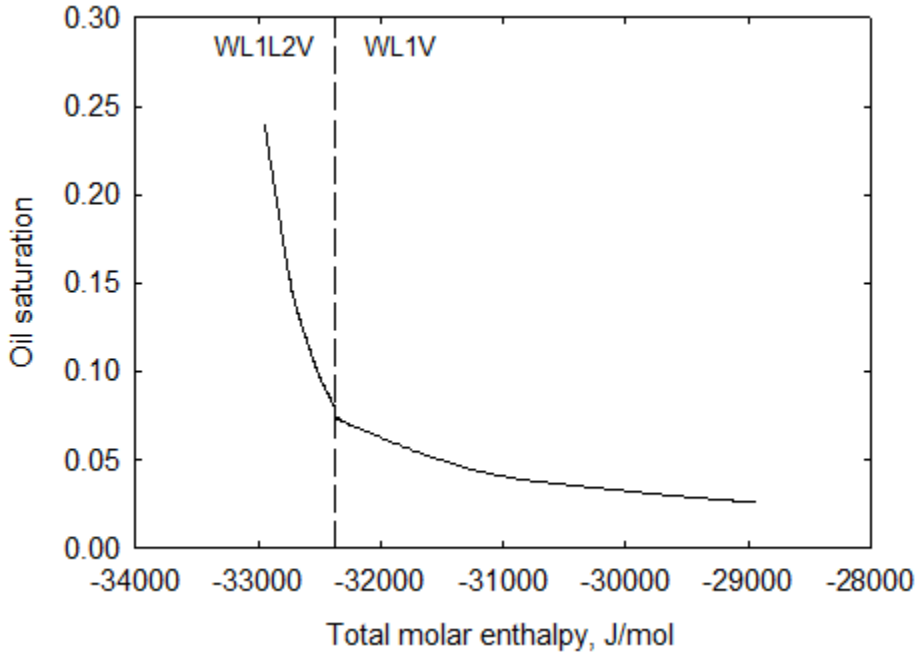

(1) n-C_4

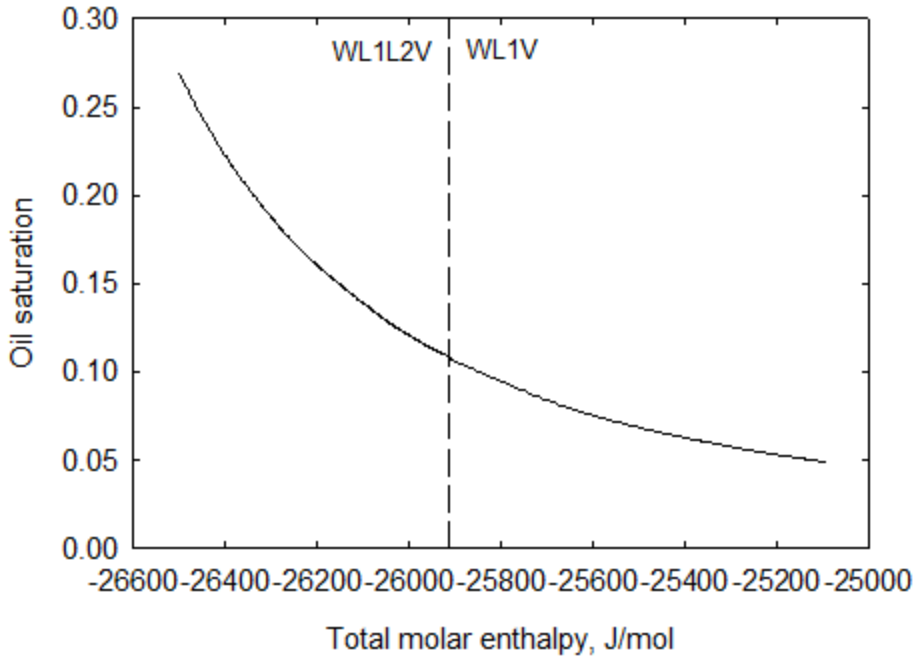

(2) n-C_6

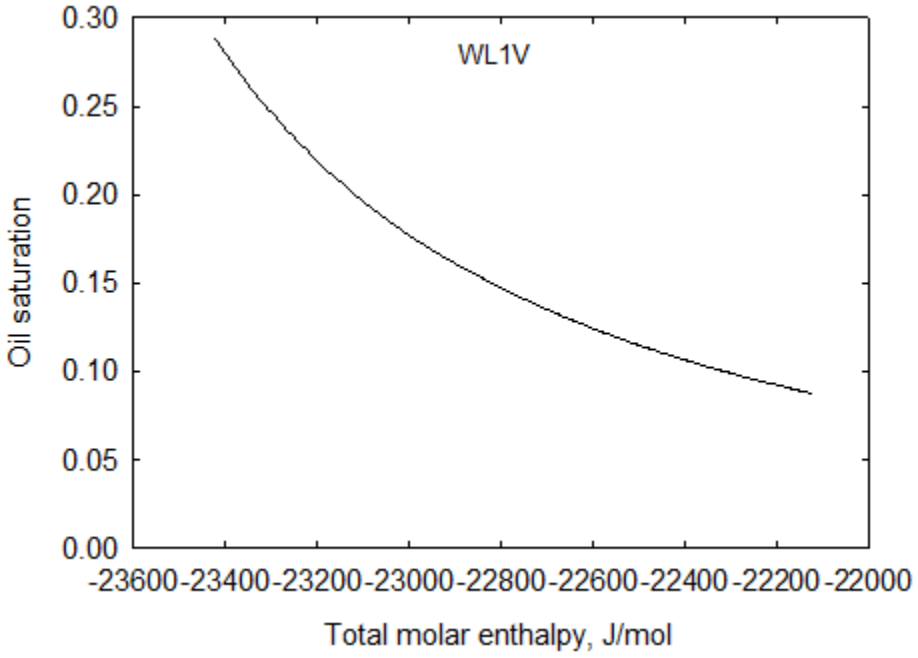

(3) n-C_8

Figure 3.31 Case study 2 analytical S_o changes with total molar enthalpy under 35 bars. C_4 and C_6 are Ternary Type 1 while C_8 is Ternary Type 2.

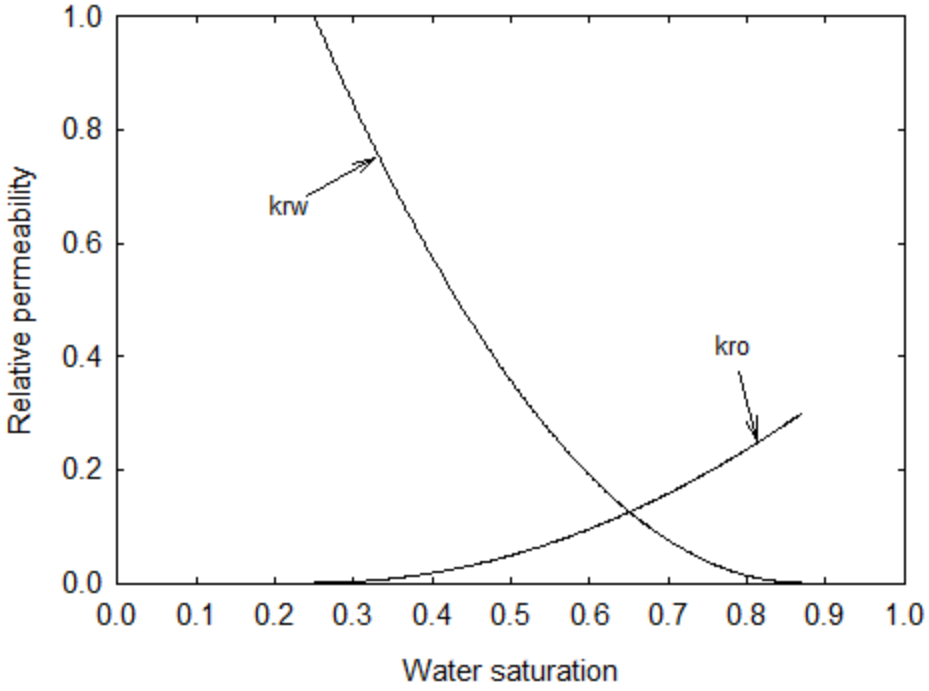

(1)

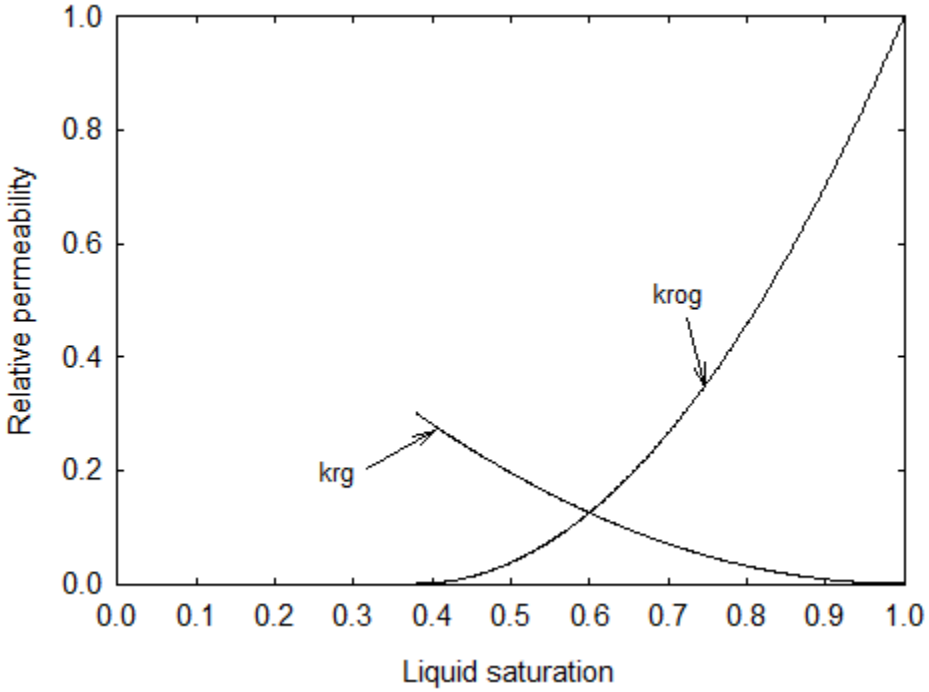

(2)

Figure 3.32 Simulation case study relative permeability curve.

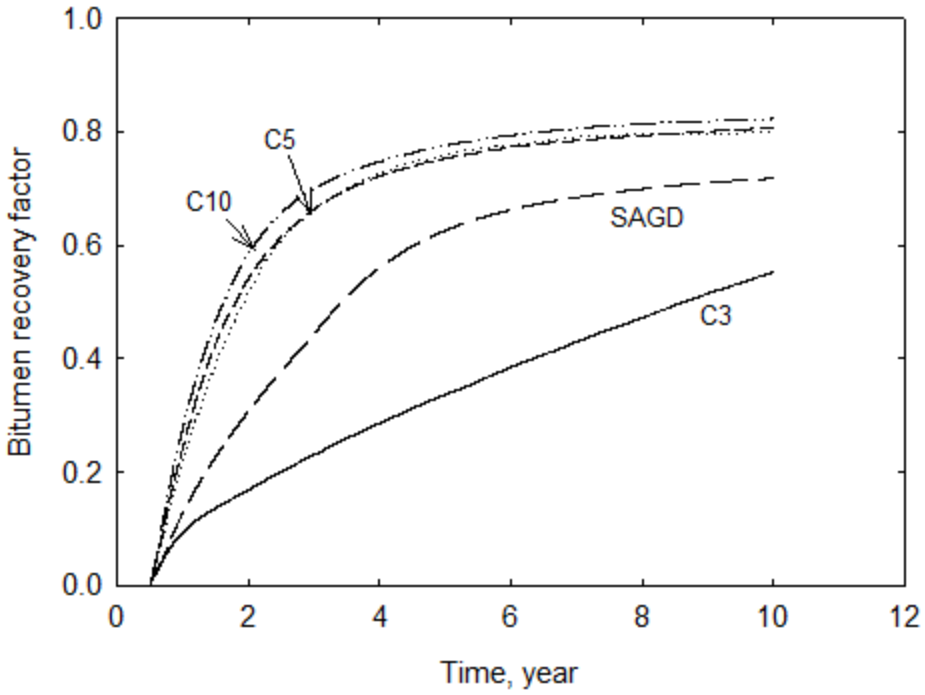

Figure 3.33 Recovery factor for steam/n-alkane coinjection simulation case study. 2 mol% of solvent is coinjected with steam throughout the simulation. Type 2 solvents (C_5, C_7 and C_{10}) can produce more bitumen faster than Type 1 solvent (C_3).

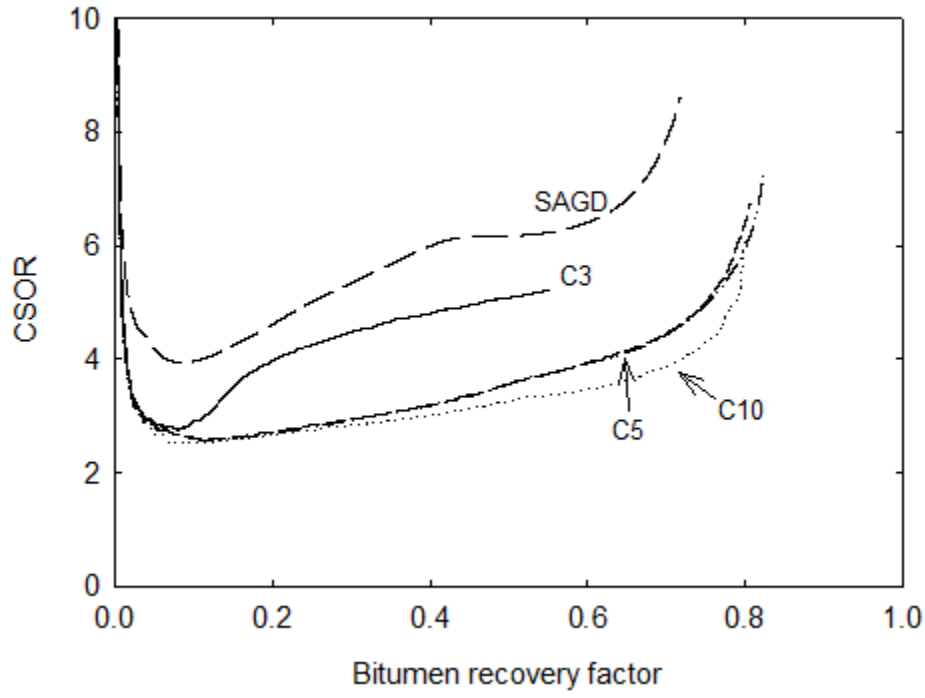

Figure 3.34 Cumulative steam-oil ratio for steam/n-alkane coinjection simulation study. 2 mol% of solvent is coinjected with steam throughout the simulation. Type 2 solvents (C_5 to C_{10}) generally require less steam injection to recover same amount of bitumen as Ternary Type 1 (C_3).

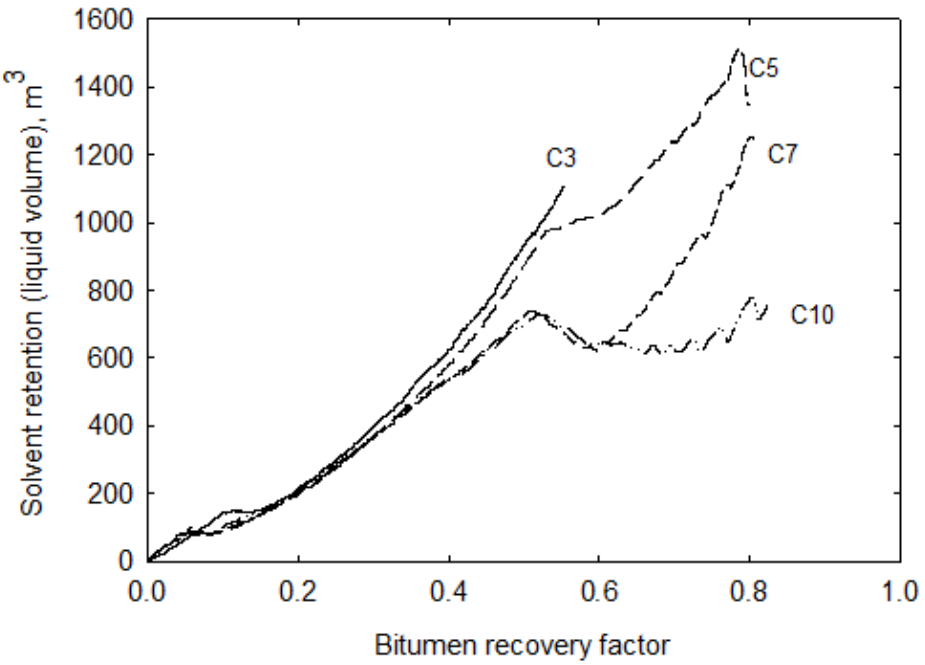

Figure 3.35 Solvent retention for steam/n-alkane coinjection simulation study. 2 mol% of solvent is coinjected with steam throughout the simulation. Ternary Type 2 solvents (C_5 to C_{10}) have less solvent retention to recover same amount of bitumen as TernaryType 1 solvent (C_3).

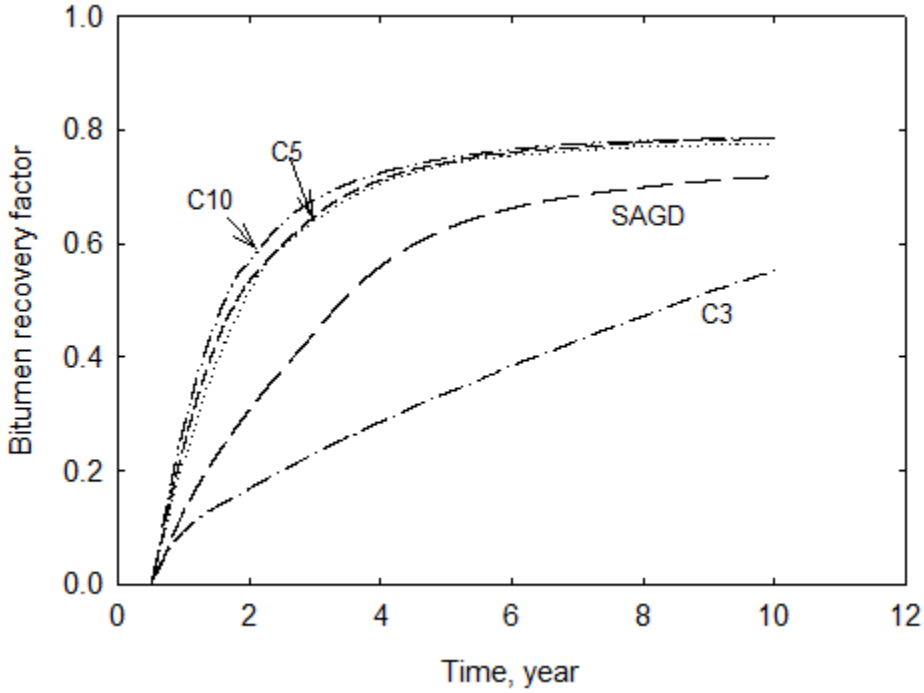

Figure 3.36 Recovery factor for steam/n-alkane coinjection simulation study. 2 mol% of solvent is first coinjected with steam and then steam is injected only.

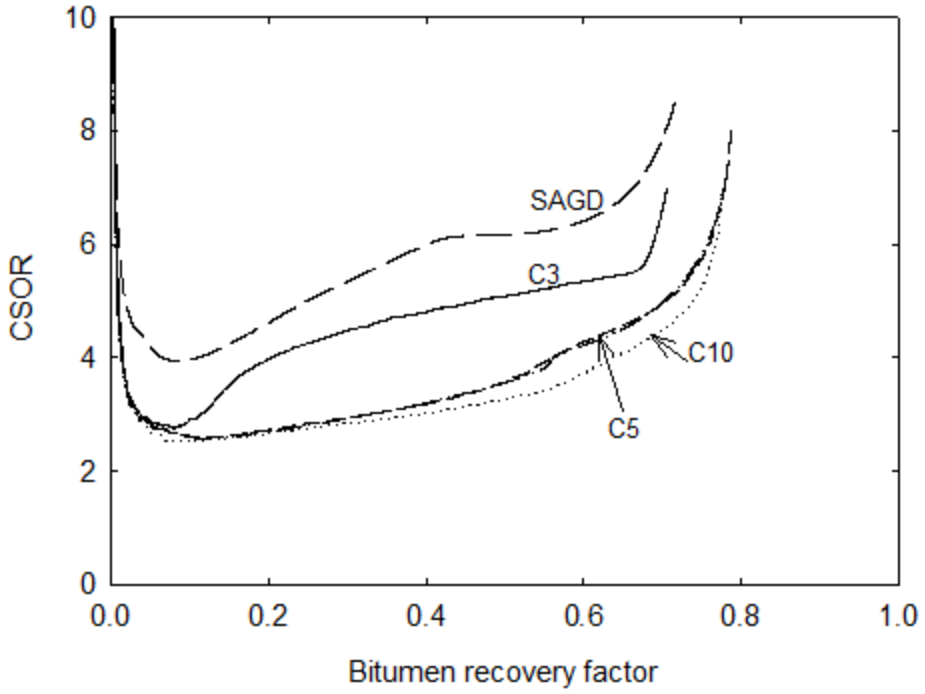

Figure 3.37 Cumulative steam-oil ratio for steam/n-alkane coinjection simulation study. 2 mol% of solvent is first coinjected with steam and then steam is injected only. C_3 case is prolonged to 20 years.

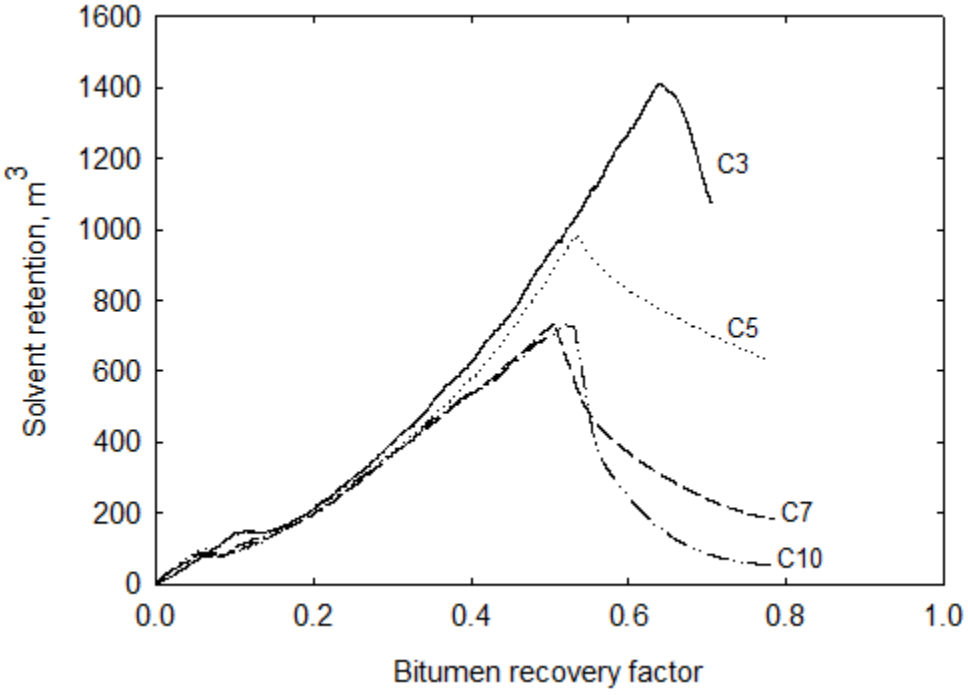

Figure 3.38 Solvent retention for steam/n-alkane coinjection simulation study. 2 mol% of solvent is first coinjected with steam and then steam is injected only. C_3 case is prolonged to 20 years.

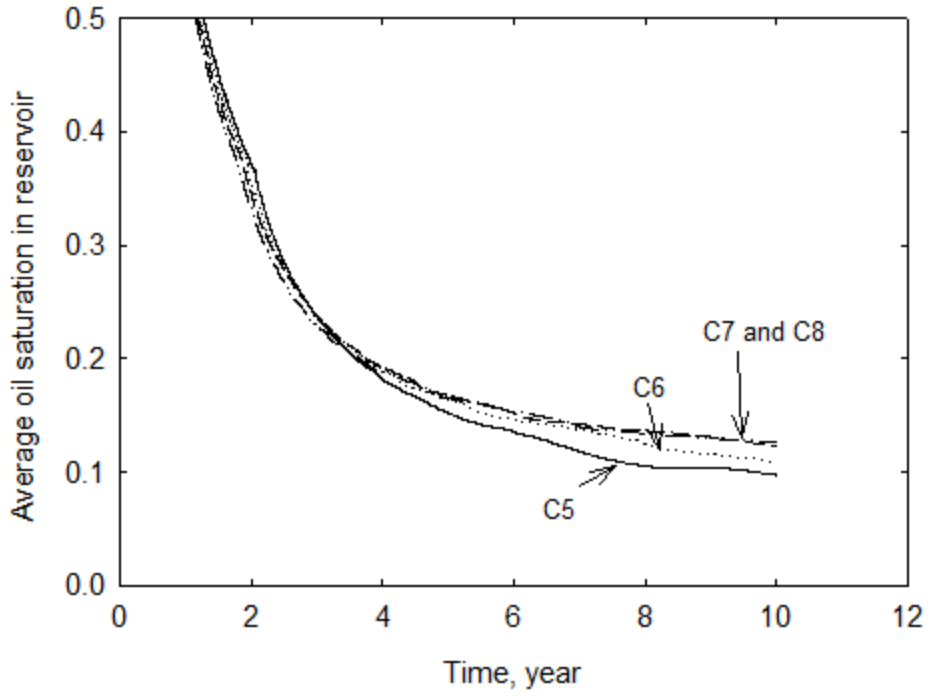

(1) Average oil saturation in reservoir at 35 bars

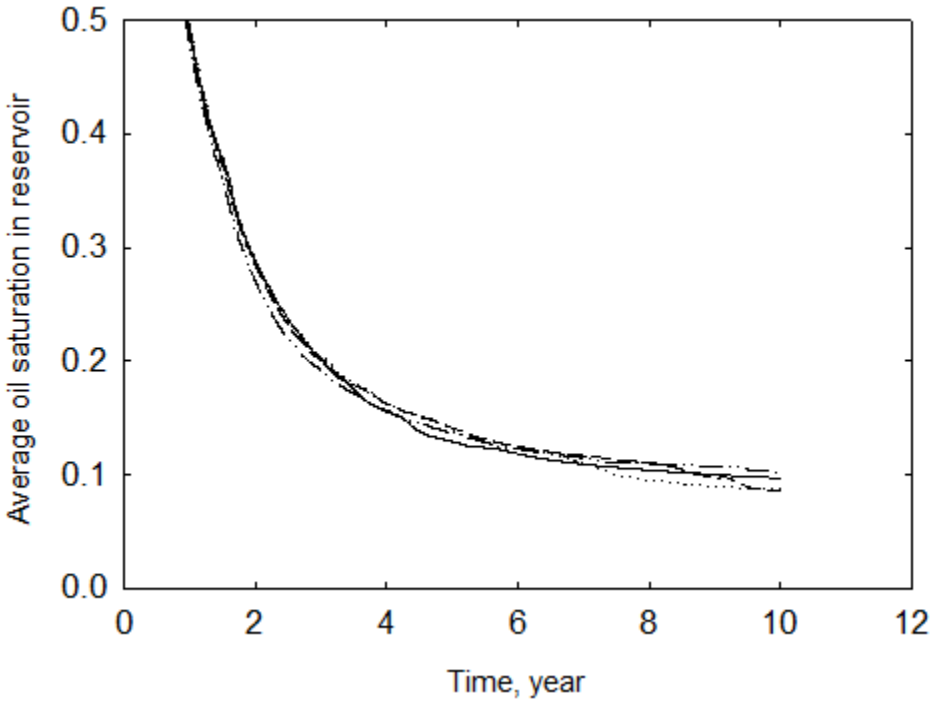

(2) Average oil saturation in reservoir at 60 bars

Figure 3.39 Qualitative validation of analytical solutions using simulation. Average oil saturation in reservoir is compared for 35 bars and 60 bars. At 35 bars, lighter solvents have better

displacement efficiency in the end. However, at 60 bars, the trend is not obvious, which is consistent with analytical prediction that all solvent essentially has almost the same S_{or} at 60 bars.

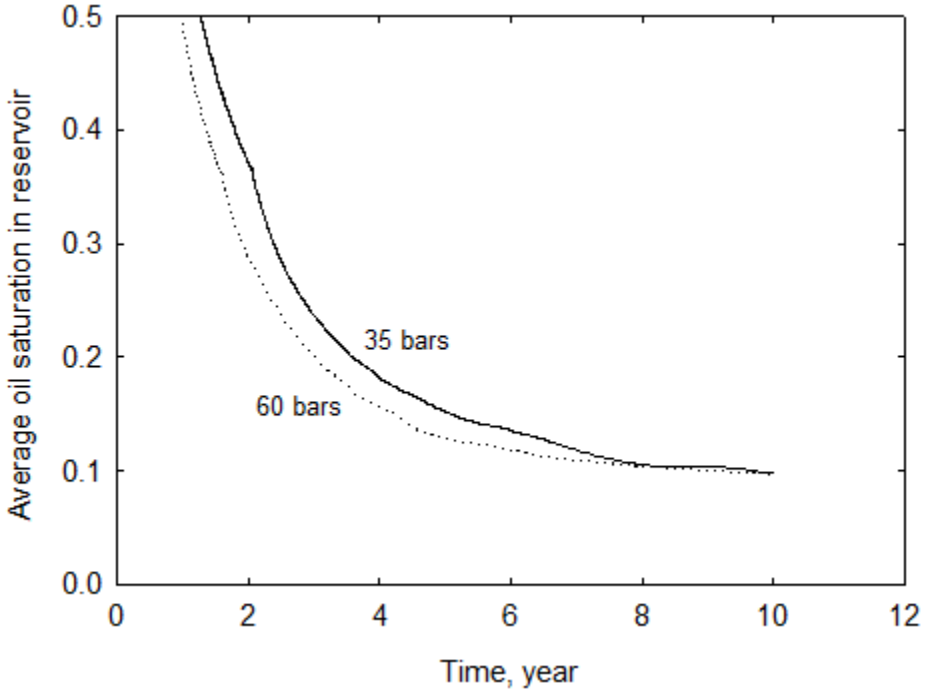

(1) C_5

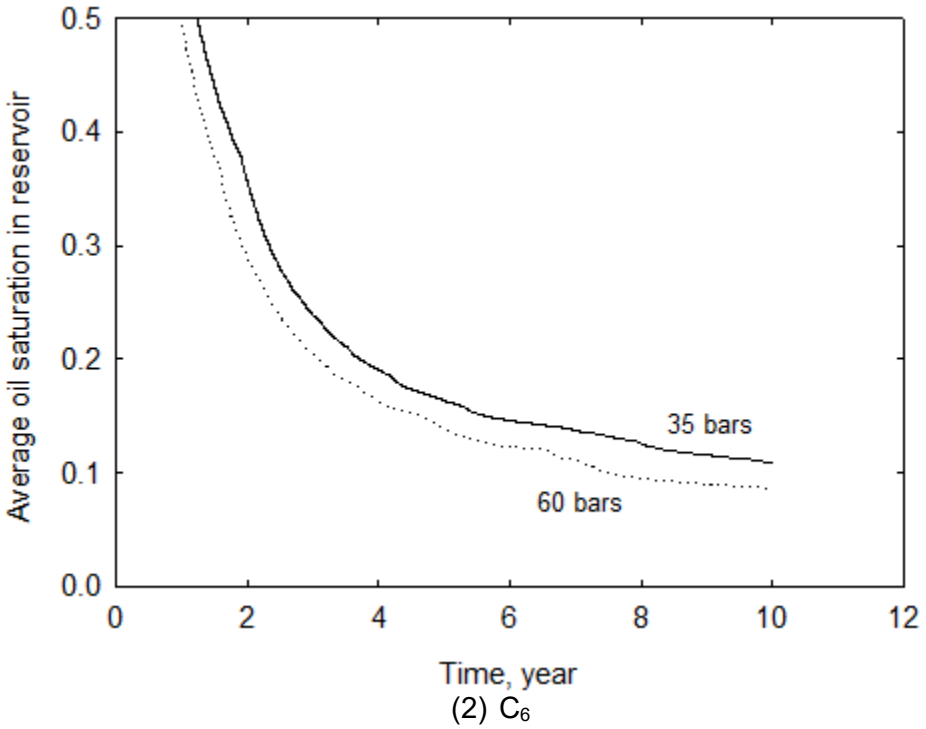

(2) C_6

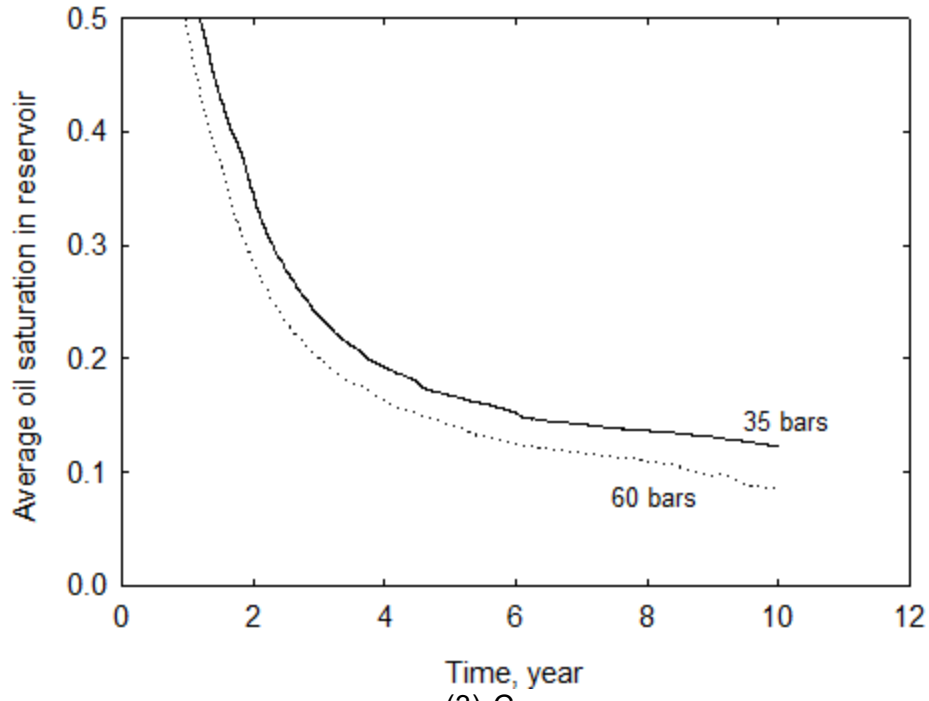

(3) C_7

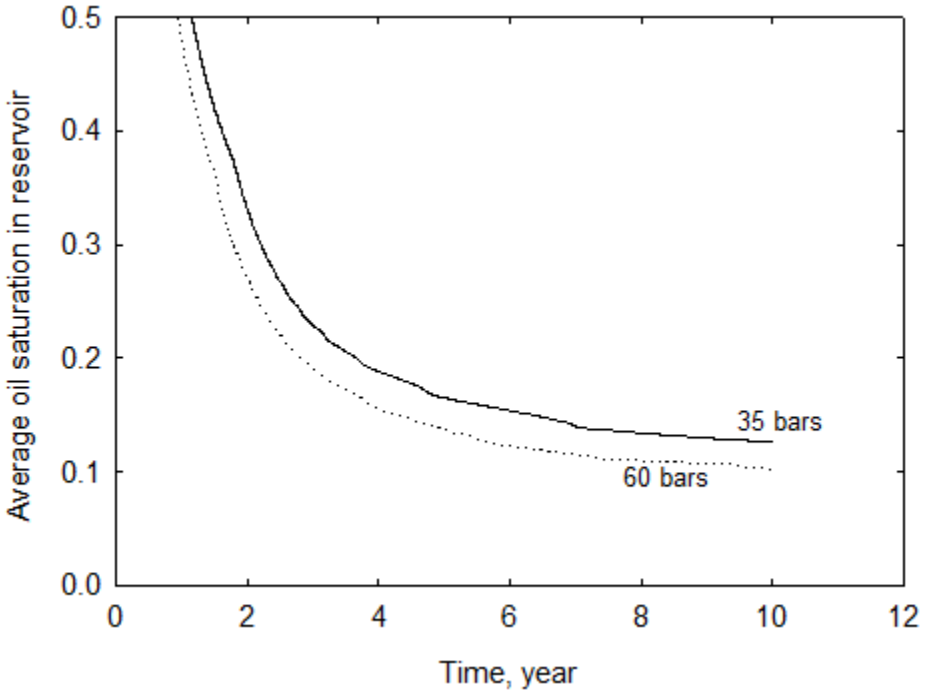

(4) C_8

Figure 3.40 Qualitative validation of analytical solutions using simulation. Average oil saturation in reservoir w.r.t. pressure is examined. Lighter solvent has smaller differences in S_{or} change if pressure is increased from 35 to 60 bars. This is consistent with analytical solution predictions.

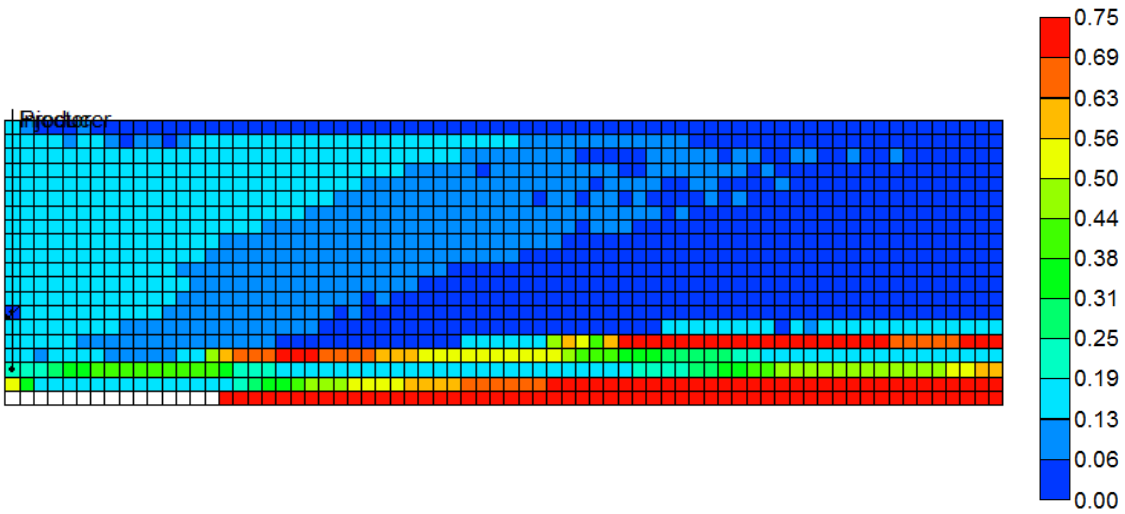

(1) Oil saturation profile

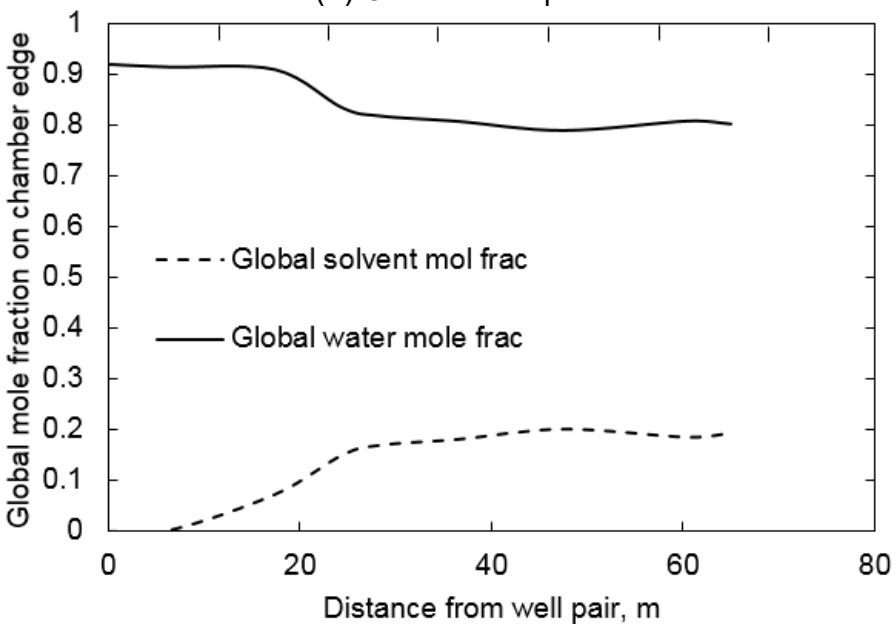

(2) Global concentration on the chamber edge for 12th row from the top

Figure 3.41 Qualitative validation of chamber edge overall composition impact on residual oil saturation. Lower solvent concentration and high water concentration on the chamber edge was found in the vicinity of the well pair, and therefore oil saturation is around 13%. However, deep inside the reservoir, solvent gradually accumulates and water concentration drops. Residual oil saturation correspondingly drops.

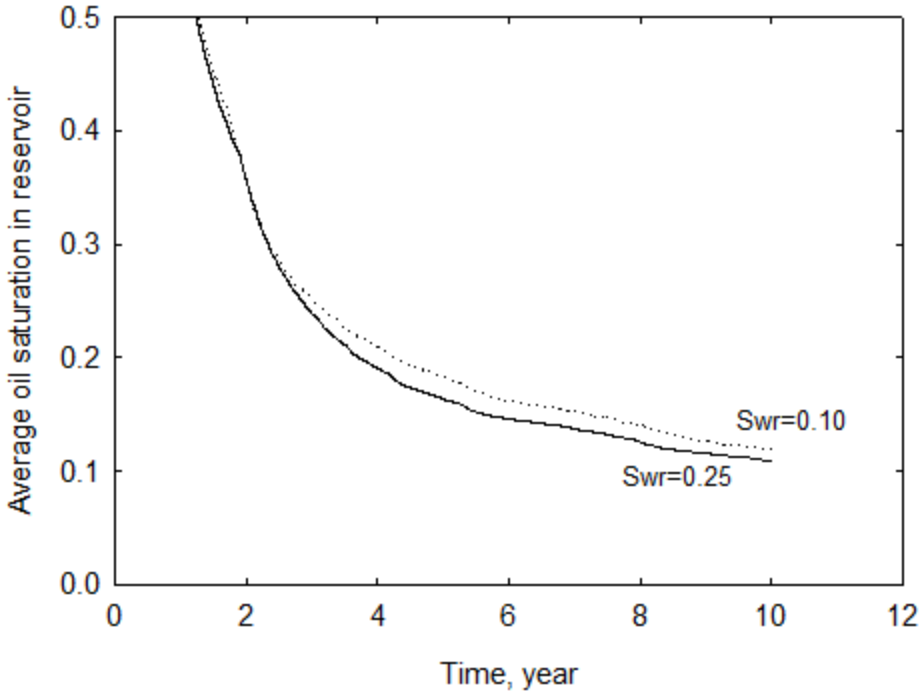

Figure 3.42 Qualitative validation of analytical solutions using simulation. Average oil saturation in reservoir w.r.t. S_{wr} for n-C_6 at 35 bars is examined. S_{wr} affects S_{or} in a much more complicated way than just phase behavior. Endpoint S_{wr} affects relative permeability curve and therefore affect flow in simulation.

Table 3.1 Conditions for the calculation of analytical S_{or} in sensitivity analysis for case study 1.

Case	Solvent	P, bars	z_{sol}, mol%	z_w, mol%	S_{wr}	S_{or}
Example calculation	n-C_5	35	1.2	98	0.25	0.13
Volatility sensitivity	C_3, C_5, C_7, C_{10}	35	1.2	98	0.25	0.13
Pressure sensitivity	C_3, C_5, C_7, C_{10}	15, 35, 60	1.2	98	0.25	0.13
z_{sol} sensitivity	C_3, C_5, C_7, C_{10}	35	0.9, 1.2, 1.5	98	0.25	0.13
z_w sensitivity	C_3, C_5, C_7, C_{10}	35	1:4 (bit/sol)	-	0.10, 0.25, 0.40	0.13
S_{wr} sensitivity	C_3, C_5, C_7, C_{10}	35	1.2	98	0.25	0.13
Case study 2	C_4, C_6, C_8	35	1:10 (bit/sol)	95	0.25	0.13

Table 3.2 Case study 1 example calculation. Beginning and ending temperature of n-C_5 distillation and analytical residual saturations.

	T_{edge}, K	T_{Swr}, K	S_{wr}	S_{or}	S_{gr}
n-C_5	463.73	500.52	0.2497	0.0595	0.6907

Table 3.3 Case study 1 analytical residual oil saturation sensitivity to solvent volatility.

	T_{edge}, K	T_{Swr}, K	S_{wr}	S_{or}	S_{gr}
C_3	374.68	498.77	0.2498	0.0579	0.6922
n-C_5	463.73	500.52	0.2497	0.0595	0.6907
n-C_7	492.85	503.07	0.2499	0.0633	0.6868
n-C_{10}	507.67	508.50	0.2489	0.0747	0.6763

Table 3.4 Case study 1 analytical residual oil saturation sensitivity to operation pressure.

	15 bars			35 bars			60 bars		
	T_{edge}, K	T_{Swr}, K	S_{or}	T_{edge}, K	T_{Swr}, K	S_{or}	T_{edge}, K	T_{Swr}, K	S_{or}
C_3	325.74	440.21	0.0589	374.68	498.77	0.0579	418.86	535.94	0.0578
n-C_5	414.66	445.82	0.0612	463.73	500.52	0.0595	502.36	536.85	0.0592
n-C_7	449.57	454.44	0.0674	492.85	503.07	0.0633	525.69	538.20	0.0620
n-C_{10}	465.65	465.81	0.0818	507.67	508.50	0.0747	538.75	540.96	0.0701

Table 3.5 Case study 1 analytical residual oil saturation sensitivity to chamber edge solvent concentration.

$z_{sol,}$, mol%	0.3	0.6	0.9	1.2	1.5	1.7
C_3	0.1214	0.1005	0.0794	0.0579	0.0363	0.0217
n-C_5	0.1221	0.1017	0.0809	0.0595	0.0377	0.0231
n-C_7	0.1230	0.1038	0.0840	0.0633	0.0415	0.0261
n-C_{10}	0.1250	0.1082	0.0911	0.0747	0.0570	0.0475

Table 3.6 Case study 1 analytical residual oil saturation sensitivity to chamber edge global water concentration.

z_w, mol%	C_3	n-C_5	n-C_7	n-C_{10}
99	0.0139	0.0142	0.0149	0.0178
98	0.029	0.0303	0.034	0.0525
97	0.0449	0.0481	0.0586	0.0888
96	0.0617	0.0685	0.0883	0.1227
95	0.0799	0.092	0.1212	-
94	0.0999	0.1188	-	-
93	0.1231	-	-	-

Table 3.7 Case study 1 analytical residual oil saturation sensitivity to irreducible water saturation (S_{wr}).

S_{wr}	C_3	n-C_5	n-C_7	n-C_{10}
0.10	0.0248	0.0251	0.0257	0.0279
0.25	0.0579	0.0595	0.0633	0.0747
0.40	0.0936	0.0985	0.1083	0.1264

Table 3.8 Case study 2 analytical residual oil saturation.

	T_{edge}, K	T_{Swr}, K	S_{wr}	S_{or}	S_{gr}
n-C_4	416.00	446.66	0.2500	0.0259	0.7241
n-C_6	474.33	477.10	0.2498	0.0486	0.7015
n-C_8	497.03	497.42	0.2491	0.0874	0.6634

Table 3.9 Case study 2 average total molar enthalpy change per unit oil saturation reduction for analytical S_{or} calculation. Average enthalpy in each phase region as well as on a whole are calculated.

Solvent	Type	Average total molar enthalpy change per unit So reduction, J/mol		
		W-L1-L2-V	W-L1-V	Average
n-C_4	Type 1	35.4	639.1	188.3
n-C_6	Type 1	36.6	139.7	64.2
n-C_8	Type 2	-	64.7	64.7

Table 3.10 Simulation case studies inputs for the CMG STARS (2013).

Property	Value
Porosity	33%
Horizontal permeability	4000 md
Vertical permeability	3000 md
Initial reservoir pressure at the depth of 500 m	15 bars
Initial reservoir temperature	286.15 K
Initial oil saturation	0.75
Initial water saturation	0.25
Three-phase relative permeability model (CMG, 2011)	Stone's model II
Formation compressibility	1.8E-05 1/kPa
Rock heat capacity (Keshavarz et al., 2014)	2600 kJ/m^3 K
Rock thermal conductivity (Keshavarz et al., 2014)	660 kJ/m day K
Over/underburden heat capacity (Keshavarz et al., 2014)	2600 kJ/m^3 K
Over/underburden thermal conductivity (Keshavarz et al., 2014)	660 kJ/m day K
Bitumen thermal conductivity	11.5 kJ/m day K
Gas thermal conductivity	2.89 kJ/m day K
Producer bottom-hole pressure (minimum)	15 bars
Steam quality	0.9

Table 3.11 Density coefficients used for solvent component in each simulation case.

Component	ρ_{ref}, kg/m^3	a_1	a_2	a_3	a_4
Water	998.5	0.00E+00	-1.67E-03	6.48E-06	0.00E+00
C1	320.15	5.13E-06	1.32E-03	5.77E-06	4.05E-08
C_3	651.83	3.02E-06	2.12E-04	5.46E-06	1.08E-08
n-C_5	823.47	2.20E-06	-8.87E-05	4.77E-06	2.88E-09
n-C_7	846.36	1.66E-06	-1.30E-04	3.79E-06	1.59E-09
n-C_{10}	869.99	1.22E-06	-1.17E-04	2.80E-06	7.75E-10

Table 3.12 Density coefficients used for bitumen component in each simulation case.

System	ρ_{ref}, kg/m^3	a_1	a_2	a_3	a_4
C_3	992.64	3.88E-07	-2.23E-05	9.09E-07	3.73E-09
n-C_5	992.64	3.85E-07	-1.95E-05	8.95E-07	4.72E-09
n-C_7	992.64	3.85E-07	-1.95E-05	8.96E-07	4.80E-09
n-C_{10}	992.64	3.86E-07	-2.03E-05	8.99E-07	4.78E-09

Chapter 4 Potential Application of Dimethyl Ether as an Additive for Improved SAGD

4.1 Introduction

Dimethyl ether, or DME, is the lightest organic in the ether family with the chemical formula of CH_3-O-CH_3. At atmospheric conditions, it is a colorless gas with mild sweet odor. It has the molecular weight of 46 g/mol and is heavier than air 1.23 g/L with the gas density of 1.97 g/L. DME can be synthesized in a variety of ways with low costs, for example, from methanol, organic waste, and biomass.

DME is useful in many industrial applications. It is an important starting material to synthesize chemicals, such as alkenes and other hydrocarbon catalysts (Ihmels and Lemmons, 2006). It is also a favorable propellant for machines using diesel engines because of DME's high cetane number, which is a combustibility indicator. For this reason, DME has been used as an additive and alternative to diesel and gasoline to reduce the emission of carbon and nitrogen oxides (Ohno et al., 2005).

DME's thermodynamic properties make it a good refrigerant and solvent. DME has high fusion heat for refrigerant. DME's optimal working temperature ranges from 5 to 45°C and it can be liquefied repeatedly under this temperature range by compressor (Park et al., 2007). Ganjdanesh et al. (2015) studied the applicability of DME in fractured shale gas production. They stated that the shale gas production rate was significantly improved, because DME could remove water blocks that impeded shale gas production as a result of DME good solubility in water and oil. Chernetsky et al. (2015) proposed the usage of DME to enhance waterflooding. They stated DME in the aqueous phase was capable of partitioning into the oleic phase at waterflooding fronts and therefore bitumen mobility could be efficiently improved. Ignasiak and Yamaoka (2010) proposed an injection strategy using pressurized and heated pure DME into a reservoir, instead of injecting

steam as in SAGD or CSS. They stated that the latent heat released by DME condensation as well as DME dissolution into bitumen could effectively reduce bitumen viscosity. They further stated DME can be recycled from produced bitumen and reinjected into reservoir. However, the applicability of steam-DME coinjection is not yet discussed in the literature.

Chapter 3 presented through analytical solutions the solvent distillation effect on displacement efficiency. C_3 has the potential to achieve the greatest displacement efficiency because of its high volatility. However, it requires much more temperature increase to fulfill its potential than heavier n-alkanes that tend to exhibit narrow-boiling behavior. Therefore, a desirable solvent in terms of the distillation mechanism would be as volatile as C_3, but should require a smaller increase in temperature to achieve low S_{or}.

Although the vapor pressures of DME and C_3 are similar to each other, their solubilities in the aqueous phase are quite different. This indicates that the interaction of DME with water is substantially different from that of C_3 with water. For example, experimental data show that the three-phase PT curve for water/DME is on the higher-temperature side of that for water/C_3 (Pozo and Streett, 1984), as will be discussed in this chapter. Therefore, steam-DME coinjection may result in higher operating temperatures than coinjection of other hydrocarbon solvents with similar volatility, such as C_3. The three-phase PT curve for a water/solvent binary is a good approximation for the lower bound for chamber-edge temperature when that solvent is coinjected with steam (**Chapter 2**).

For this reason, this chapter investigates the potential of DME as an additive for improved SAGD in terms of operating temperature distribution, which affects the gravity drainage rate of oil, steam requirement, and residual oil. Also, the DME injected can be recovered through the aqueous and oleic phases, unlike conventional hydrocarbons solvents that can only be recovered from the oleic phase. In the subsequent sections, phase behavior prediction of the water/bitumen/DME system is studied based on an EOS. Then, steam/DME coinjection is discussed via both analytical solution and numerical simulation. Its performance is compared with

n-alkane solvents in terms of energy efficiency and solvent retention. A simple economic analysis will be also presented.

4.2 Phase Behavior of Water/Bitumen/DME Mixtures

4.2.1 EOS Model

In this research, the PR EOS with the vdW mixing rules is used because only simple cubic EOSs, such as the PR EOS, are implemented in the commercial software to be used in this chapter. In order to more accurately describe phase behavior of DME-containing systems, however, it is desirable to use more advanced EOS and/or mixing rules, such as Wong and Sandler mixing rules (Wong and Sandler, 1992; Tallon and Fenton, 2010).

Only three components are considered in the system, water, DME, and the bitumen characterized as one pseudo component as described in Chapter 2. Critical properties of DME were experimentally determined by Tallon and Fenton (2006). The critical properties and acentric factors for the three components are summarized in **Table 4.1**.

The BIP correlation between water and bitumen remains the same as described in **Chapter 2**. However, due to limited BIP information between DME and other components, data from available publications and their reliability against experimental data are inspected. Here, Ganjdanesh et al.'s (2015) BIPs for water/DME and bitumen/DME are examined and calibrated to match experiments, as summarized in **Table 4.2**. Details of the calibration are explained below.

EOS predictions are compared with experimental data (Pozo and Streett, 1984) in terms of vapor-liquid-liquid equilibrium (VLLE) for the water/DME binary. They measured VLLE P-T data from 10 to 60 bars (**Table 4.3**), which caters to the operation range of SAGD and its variants. Both three-phase P-T curve and DME dissolution in the aqueous phase are considered for the calibration of the PR-EOS model. Average absolute relative deviation (AARD) in percentage and

average absolute deviation (AAD) are calculated and summarized in Table 4.6. AARD and AAD are defined as follows,

$$\text{AARD} = \frac{1}{n}\sum_{i=1}^{n}\left|\frac{x_{EOS} - x_{EXP}}{x_{EXP}}\right| \tag{4.1}$$

$$\text{AAD} = \frac{1}{n}\sum_{i=1}^{n}|x_{EOS} - x_{EXP}| \tag{4.2}$$

where x_{EOS} is an EOS predicted value, x_{EXP} experiment determined value, and n is the number of experiment data.

For the water/DME system, the PR EOS and the vdW mixing rules have limited ability to predict phase behavior, because the vdW mixing rules are not accurate for highly non-ideal mixtures such as water/DME solution. The BIP of -0.17 is the optimal value for the PR EOS with the vdW mixing rules. This BIP gives reasonably accurate predictions for water/DME three-phase P-T curve and DME solubility in water. As mentioned earlier, matching DME solubility in water is important because the distillation analysis indicates that a water-soluble solvent may increase chamber edge temperature.

By using the P_{3p} in **Table 4.3**, T_{3p} attained by EOS is compared with the corresponding experimental data. From 10 to 60 bars, AARD of EOS prediction is 4.91% and AAD is 19.92 K. AARD and AAD of EOS prediction at 35 bars is 3.83% and 14.8 K.

DME solubility in the aqueous phase is compared between EOS and experiment at three-phase conditions, by using the P_{3p} in **Table 4.3**. DME solubility from 10 to 60 bars predicted by the PR-EOS model with this BIP is on the same order of magnitude as experimental data. AARD of EOS prediction is 40.74% and AAD is 6.58 mol%. At 35 bars, EOS gives estimated 55% AARD and 4.5 mol% AAD.

Figure 4.1 shows deviations of EOS predictions from experiment data. In terms of three-phase curve, the EOS model generally gives overestimated values. In terms of DME solubility in

water, the EOS model underestimates below 50 bars and overestimates above 50 bars. By further adjusting BIP from -0.17, either DME solubility in water or three-phase P-T curve is more deviated. Decreasing the BIP from -0.17 results in more deviation in terms of three-phase P-T curve although DME solubility in water is increased. It also turns the water/DME binary into Type I of the K-S classification, which should be a Type III according to Pozo and Streett (1984). Increasing the BIP from -0.17 gives more accurate three-phase curve predictions; however, DME dissolution in water is underestimated by several orders of magnitude in comparison with experimental data. Therefore, the optimum BIP of -0.17 will give conservative results in terms of the effect of DME solubility in the aqueous phase because DME solubility in the aqueous phase is predicted to be lower than experimental data. Again, use of a more advanced EOS and/or mixing rules may improve the accuracy of phase behavior predictions; however, this is beyond the scope of this thesis.

The BIPs of DME with hydrocarbons are difficult to obtain. The only relevant data that are available in the literature are the PVT data for n-C_{10}/DME and n-C_{12}/DME by Park et al. (2007), as summarized in **Table 4.4** and **Table 4.5**. A BIP of 0.015 gives AARD around 1%, which is in good agreement with the experiment data. The BIP of DME with bitumen is expected to be different from this value based on Park et al.'s data for n-C_{10} and n-C_{12}. Due to the unavailability of more data, however, the BIP of 0.015 is used for bitumen/DME in this chapter. All the AARDs and AADs for the calibration of BIPs for water/DME and hydrocarbon/DME are shown in **Table 4.6**.

4.2.2 Ternary Phase Behavior of Water/Bitumen/DME

As mentioned in **Chapter 2**, ternary phase behavior can be classified based on solvent solubility in bitumen within three-phase temperature of water/n-alkane and water/bitumen. If there can be a L2 besides L1 within that temperature range for bitumen/solvent, the corresponding ternary system shows may show W-L1-L2 on the chamber edge. Previously, phase behavior of

water/bitumen/n-alkane system was studied based on bitumen/n-alkane binary behavior. Bitumen/n-alkane is a Type III_m binary of the K-S classification. At T_{3p} of water/n-alkane, bitumen/n-alkane always shows L1 one phase or L1-L2 two phases. Therefore, the existence of phase boundaries between two-phase regions of oil/solvent binary within coinjection operation temperature range determines classification of corresponding ternary systems. Two ternary types are classified based on whether L1 or L2 can coexists within the steam-solvent coinjection temperature range.

DME-containing reservoir fluids can be classified by following the same logic. For the water/bitumen/DME system described in **§4.2.1**, bitumen/DME is a Type III_m of the K-S classification. See **Figure 4.2** for vapor pressure curves and three-phase curve of water/bitumen/DME system. The volatility of DME is between C_3 and n-C_4. Also see **Table 4.7** for comparison of binary pairs for n-alkane containing system and DME containing system. It would be interesting to see the phase behavior of bitumen/DME binary at the three-phase temperature of water/DME at a specific pressure to see the corresponding water/bitumen/DME ternary classification.

Figure 4.3 shows T-x diagrams at 35 bars for water/DME and bitumen/DME. (1) Water/DME at 35 bars shows similar T-x diagram as water/n-alkane. Unlike water/n-alkane, three-phase line of water/DME is to the right of DME vapor curve so that three-phase temperature in **Figure 4.3** (1) is higher than DME saturated temperature. In contrast, three-phase temperature of water/n-alkane is always lower than n-alkane saturated temperature. (2) Since there is not L2 within the temperature range for bitumen/DME, the corresponding ternary system should show Ternary Type 2 behavior on the chamber edge.

Figure 4.4 demonstrates ternary phase behavior of water/bitumen/DME at 35 bars. In (1) and (2), when temperature is low, only W-L1-L2 three-phase region exists. In (3), a second three-phase region, V-L1-L2 starts to coexist with W-L1-L2 when temperature is greater than saturated temperature of DME. In (4) and (5), complex three-phase transition happens. L2 exists when

temperature is equal to or lower than three-phase temperature of water/DME. W-L1-L2 merges with V-L1-L2 into W-L1-V as temperature increases. L2 disappears the instant two three-phase regions merge. From (6) to (8), as temperature keeps increasing, L1 swings towards water/bitumen edge, as n-alkane systems, and finally three-phase regions disappears onto water/bitumen edge. As can be seen that, W-L1-L2 is only possible below the lowest temperature bound, the three-phase temperature of water/DME. This is a Ternary Type 2 system.

Much higher DME solubility in water compared to n-alkanes may be beneficial in steam-solvent coinjection. **Figure 4.5** shows ternary diagrams at the chamber edge conditions for water-soluble solvents like DME and water-insoluble solvents like n-alkane. The operation pressure is 35 bars, and global water concentration on the chamber edge is 95 mol% and solvent concentration is 4 mol%. DME case has higher chamber edge temperature than Ternary Type 1 n-alkane cases, however lower than Ternary Type 2 n-alkane cases. For the same overall composition on a chamber edge, the L vertex of W-L-V for water-soluble solvent case is closer to the water/bitumen edge, which gives a higher chamber-edge temperature than when the solvent is insoluble in water. The following sections will provide a more detailed study of increased chamber-edge temperature.

4.3 Steam/DME coinjection

In this section, coinjection of DME with steam into a bitumen reservoir is numerically studied. Firstly, the algorithm developed in Chapter 3 for residual oil saturation after distillation is applied to steam-DME coinjection. Then, steam-DME coinjection is simulated with the CMG STARS simulator (Computer Modelling Group Ltd., 2013). Its performance is compared with n-alkanes in terms of energy efficiency and economic performance.

4.3.1 Liquid DME Density

Before performing the analytical solution to estimate the distillation effect on residual oil saturation, it is important to obtain a reliable density model for liquid DME. Modified Rackett equations were used by Ihmels and Lemmon (2006) for accurate representation of liquid DME density from 10 to 400 bars and 273 to 523 K. The liquid density prediction of this model gives 0.039% AARD from experimental data. The modified Rackett equations are,

$$\rho = \frac{\rho_0}{[1 - C_T \ln((B_T + P)/(B_T + P_0))]} \tag{4.2}$$

$$\rho_0 = \frac{A_R}{B_R^{[1+(1-\frac{T}{C_R})]^{D_R}}} \tag{4.3}$$

$$B_T = B_{T0} + B_{T1}\frac{T}{E_T} + B_{T2}(\frac{T}{E_T})^2 \tag{4.4}$$

where ρ is the liquid density of DME, C_T=0.0834042, B_{T0}=284.304, B_{T1}=-130.021, B_{T2}=14.4194, E_T=100, A_R=55.6001, B_R=0.236704, C_R=401.406 and D_R=0.243368. The CMG STARS simulator uses the liquid density model described in **Appendix B**, instead of Rackett ones. Therefore, the model was regressed to match Rackett's model by adjusting the five parameters, ρ_{iref} and α_1 *to* α_4. The regression results have an R-square index of 0.9998, and are given in **Table 4.8**.

4.3.2 Liquid DME Viscosity Model

Steam-solvent coinjection reduces bitumen viscosity by solvent dilution and steam latent heat. In numerical simulation, viscosity has to be reasonably modeled.

CMG STARS (Computer Modelling Group Ltd., 2013) using logarithmic linear or non-linear mixing of pure component viscosities for oleic phase viscosity. Non-linear logarithmic mixing is recommended because viscosity of bitumen and volatile solvent mixture is highly non-linear to solvent concentration in bitumen (Venkatramani and Okuno, 2016).

The saturated liquid DME viscosity correlation developed by Wu et al. (2003) is used to generate viscosity-temperature table at DME subcritical conditions for STARS. The correlation is as follows:

$$\log_{10}\mu = -5.7282 + \frac{631.031}{T} + 0.01453T + 1.8225 \times 10^{-5}T^2 \quad (4.5)$$

where μ is viscosity in mPa·s and T is temperature in K. This correlation gives 0.5% AARD to the experimental data measured from 227 to 343 K. DME becomes supercritical at temperatures greater than 427.4 K. However, supercritical DME viscosity data has not yet been measured to my knowledge. Supercritical viscosity of C_4 is used in this research for DME under supercritical conditions. Comparison of viscosity-temperature curves between n-alkanes and DME are shown in **Figure 4.6**. DME shows similar viscosity to n-C_4. However, DME viscosity is not as sensitive to temperature as n-C_4. DME is more viscous than n-C_4 if temperature is greater than 400 K.

In the absence of experimental viscosity data for water/DME and bitumen/DME mixtures, a sensitivity analysis should be done in terms of the coefficients used for the non-linear logarithmic mixing rule. In the simulation case study in **§4.3.4**, viscosity mixing coefficients of C_4 are used for DME. Then **§4.3.5**, a sensitivity analysis is conducted on the impact of viscosity model on simulation results. Details of how non-linear coefficients are obtained for bitumen and n-alkanes can be found in the research of Venkatramani and Okuno (2016).

4.3.3 Analytical Solution Study

The algorithm for analytical S_{or} is performed with the PR-EOS model presented in **§4.2.1.** Liquid density model for water and bitumen is the same as in **Chapter 3**. The liquid density model for DME in **§4.3.1** is used.

Figure 4.7 shows the result of DME comparison with C_3 in terms of S_{or} under the condition of 35 bars, the overall water concentration of 98 mol% and the S_{wr} of 0.25. A number of overall solvent concentrations on the chamber edge were used to get a series of calculated S_{or}. Results

show that DME is only slightly better than C_3 to reduce oil saturation due to distillation effect. Besides, DME and C_3 show a similar sensitivity of the calculated S_{or} to the overall solvent accumulation on the chamber edge.

In **Chapter 2**, it was shown that C_3 has the greatest potential to reduce S_{or} among the solvents studied. However, several disadvantages of C_3 greatly impede its potential, such as low chamber edge temperature, poor solvent mixing because of oleic-phase separation, and a large temperature increase to achieve S_{or}. By investigation of the distillation process of DME, **Figure 4.8** shows the beginning and the end of the distillation process by demonstration of ternary phase diagrams on the chamber edge and at the temperature of lowest oil saturation. The L-phase composition does not change much during the distillation. However, the chamber-edge temperature is so much increased because of the DME solubility in water. **Figure 4.9** shows S_o reduction comparison between C_3 and DME during distillation. The temperature at which distillation starts (T_{edge}) for DME is much higher than that of C_3 for the conditions examined. The incremental temperature (ΔT), i.e. T_{Swr}-T_{edge}, for distillation of DME is much smaller than that of C_3. At 35 bars with 98 mol% overall water, 1.2 mol% solvent and 0.25 S_{wr} (**Figure 4.8**), the C_3 case needs a temperature increase of 124.9 K to achieve the S_{or} of 0.058, while DME only needs the temperature increase of 8.6 K to achieve a similar S_{or} of 0.056.

Figure 4.10 and **Figure 4.11** show the ΔT of the DME case compared to n-alkanes as well as water and DME distillation compared to n-alkanes. 4.2 mol% of water evaporates in the DME case, almost the same as the amount of water evaporated in C_{10} case. 0.6 mol% of DME evaporates from the L phase, which is less than C_8 but more than C_{10}. More water evaporates from liquid phases than light n-alkanes with smaller ΔT. Because of the DME partitioning inside the W phase, DME can evaporates from both the W and L phases during distillation. DME's enhanced displacement efficiency is different from n-alkanes in that the volume shrinkage of the L phase is a result of both solvent distillation from the L phase and water evaporation from the W phase. In DME case, however, what may make DME good in displacement efficiency is primarily

the aqueous phase evaporation that minimizes oleic phase saturation. The DME evaporated from the aqueous phase makes the aqueous phase more volatile.

Figure 4.12 shows water and solvent evaporated from both aqueous and oleic phases during distillation for the DME and n-alkane cases. For increased solvent accumulation, the water evaporated is not much affected. The increased ΔT and DME distillation accounts for extra oil saturation reduction.

Besides solvent accumulation, sensitivity analysis is also done for pressure, chamber edge water concentration and endpoint water saturation of reservoir. All the explanations of enhanced displacement efficiency resemble the ones shown in **Figure 4.10** to **Figure 4.12.**

In **Figure 4.13**, three different pressures, 15, 35 and 60 bars, are used to calculate residual oil saturation analytical solutions while global water concentration, solvent concentration and S_{wr} remain 98 mol%, 1.2 mol% and 0.25 respectively. Unlike heavier n-alkane solvents such as C_7 of which S_{or} can be significantly decreased by increasing operation pressure, DME has very similar sensitivity to pressure as C_3. For both DME and C_3, S_{or} does not vary much with pressure change. Increased pressure generally increases the ΔT of DME. Also, solvent distillation is more pronounced if pressure is higher. DME has limited capacity to further distill solvent, just like C_3.

In **Figure 4.14**, sensitivity of S_{or} to chamber edge water concentration is shown. Pressure, solvent concentration and S_{wr} are set to 35 bars, 1.2 mol% and 0.25 respectively. Again, due to similar volatility, DME and C_3 have similar sensitivity to water concentration. 1 mol% of water increase results in significant oil saturation reduction, mainly because of lowered chamber edge oil saturation.

In **Figure 4.15**, sensitivity of analytical S_{or} to endpoint water saturation is shown. Pressure is set to 35 bars. Water and solvent concentration on chamber edge are 98 and 1.2 mol% respectively. Analytical S_{or} decreases as Swr decreases. Same as other n-alkane solvents, DME distillation can be more profound for reservoirs with lower residual water saturation as a result of increased ΔT.

4.3.4 Comparison between DME and n-alkanes

This section presents the comparison between DME and n-alkanes in steam/solvent coinjection through simulation studies. The solvent efficiency, which is measured by bitumen recovery, SOR, and solvent retention, is first compared. Then, a simple economic analysis is presented.

A single-sided reservoir model is used as described for n-alkanes in **§3.5** to compare DME and n-alkanes in terms of bitumen recovery, SOR, and solvent retention. All other reservoir parameters and operation conditions are the same as in Chapter 3. At 35 bars, 2 mol% of solvent is coinjected with steam until the steam chamber reaches the outer reservoir boundary.

Figure 4.16 compares DME with n-alkanes in terms of bitumen-recovery predictions. The DME case can produce bitumen faster than C_3 (Ternary Type 1) and achieve the bitumen recovery that is close to those with light n-alkanes within Ternary Type 2 by the end of production. As explained by analytical solutions in **§4.2.2**, improved chamber-edge conditions because of water dissolution may account for improved drainage rate compared to C_3. However, bitumen drainage rate of the water-DME coinjection case is similar to SAGD. This can be a result of underestimated chamber-edge temperature in this simulation, due to the underestimated DME solubility in the aqueous phase by use of the EOS model. The DME solubility in water predicted by the EOS model is only half of what was observed in the experiment of Pozo and Streett (1984). Figure 4.16 also shows that the ultimate recovery is higher for the DME case than the SAGD case because of enhanced displacement efficiency in the DME case.

In **Figure 4.17**, the temperature profiles in the simulated reservoir are compared among C_3, DME and C_5 when the same amount of bitumen was recovered. C_3 has the lowest inside-chamber temperature. DME and heavy n-alkanes have higher inside-chamber temperature. Ternary Type 2 solvents require less temperature increase to achieve S_{or}. C_3 may take longer time to achieve its highest temperature and lowest S_{or}.

The chamber-edge conditions are now examined in simulation. **Figure 4.18** compares the temperature distribution between DME and selected n-alkanes near a chamber edge. At 35 bars, DME shows an increased chamber-edge temperature than C_3 and C_4. This increased chamber-edge temperature is a result of the DME solubility in the aqueous phase and the three-phase temperature of water/DME that is higher than the DME condensation temperature at the pressure of interest. The L phase in the DME case has higher bitumen-to-solvent ratio than C_3 and C_5. However, DME still has lower chamber-edge temperature than C_5. As mentioned before, DME solubility is underestimated with the current PR-EOS model; therefore, a chamber-edge temperature for the DME case can be underestimated as well. **Figure 4.19** and **Figure 4.20** compare DME with selected n-alkanes in terms of the L1-phase composition near a chamber edge. The increased chamber-edge temperature in the DME case results in the DME concentration in the L1 phase that is similar to the C_3 case, but a higher concentration of water than the C_4 case.

Figure 4.21 and **Figure 4.22** compares the DME and n-alkane cases in terms of CSOR and solvent retention, respectively. For both DME and n-alkane cases, solvent retention first reaches a highest level, and then declines as only steam is injected when steam chamber reaches the outer reservoir boundary. In terms of the highest level of solvent retention, the DME case is the lowest. The DME case exhibits a similar or even lower CSOR and solvent retention as Ternary Type 2 solvents; however, DME is cheaper than Ternary Type 2 n-alkanes according to the data source referenced in this research. **Figure 4.23** shows the production (or recovery) of DME. Due to the solubility of DME in the aqueous and oleic phases at reservoir conditions, DME can be recovered by the flow of the aqueous and oleic phases. In contrast, n-alkanes can be recovered only by the flowing oleic phase.

DME is likely cheaper than heavy Ternary Type 2 n-alkanes. A simple economic analysis is presented to show the economic potential of the use of DME as an additive to steam. A reservoir with dimensions of 142×500×20 (m) is divided into 71×1×20 gridblocks. The well length is 500 m

and horizontal well pair is placed as shown in **Figure 4.24**. Other reservoir simulation parameters are the same as aforementioned single-sided reservoir in Chapter 3. Solvent injection is ceased immediately after steam chamber reaches the outer reservoir boundary. **Table 4.9** summarizes time when chamber edge reaches reservoir boundary for each case. Net present value (NPV) is calculated for DME and n-alkane solvents (Table 4.10). Bitumen price is an average reference price from January 2015 to February 2016 of Alberta provincial government statistics. Due to the lack of latest solvent prices in the literature, solvent prices in the market for industrial usage purposes are used. The solvent prices are roughly averaged from December 2015 to April 2016. The formulation for NPV and other inputs refer to Keshavarz et al. (2015). The formulation is shown below.

Net Present Value (NPV) [USD] = (cumulative oil × oil price) × (1.0 – discount rate) [USD]

– capital cost of exploration

– capital cost of well pair [USD]

– water treatment equipment [USD]

– steam generator cost [USD]

– capital cost of solvent distribution [USD]

– administration and head office [USD]

– blending and transportation [USD]

– production years × well pair and field operation [USD/year]

– production years × solvent handling [USD/year]

– cumulative steam injection [m^3 CWE] × (generator operation [USD/m^3 CWE] + fuel cost [USD/m^3 CWE])

– cumulative water production [m^3] × treatment of production water [USD/m^3]

– (cumulative solvent injection [m^3] – cumulative solvent production [m^3]) × solvent price [USD/m^3]

(4.6)

Figure 4.25 compares NPVs for the DME and n-alkane cases. Maximum NPV and the time for the maximum achieved for each case are summarized in **Table 3.2**, which indicates when the project should stop. C_{10} has the highest maximum NPV, followed by DME, C_7, SAGD, C_5 and C_3. For the C_{10} case, a deficit is expected for the first several years, and later on the project starts to make profit by recycling C_{10} via steam-only injection. The time that the maximum NPV is achieved could be numerically simulated, but it may be risky to use C_{10} considering the substantial importance of recovering C_{10} for achieving the highest NPV. Although Ternary Type 2 solvents produce bitumen faster early in the process, the loss of expensive n-alkanes may totally counter the advantages of Ternary Type 2 solvents. N-alkane cases are only more profitable than SAGD if solvents can be effectively recycled. In contrast, the DME case makes profit steadily before the chamber edge reaches the outer reservoir boundary. Although it is making profits slower than SAGD in the beginning, it results in a higher maximum NPV than SAGD and most n-alkanes cases. Therefore, if making profit quickly at a lower risk is the objective, DME and light Ternary Type 2 solvents can be good choices of solvent to be coinjected with steam. Under a higher oil-price environment, the advantage of steam-solvent coinjection over SAGD may be more pronounced.

Around 4.3 years, the DME case reaches the reservoir boundary. Steam-only injection helps further improve the profit by recycling DME from the water and oleic phases by increasing temperature, as was illustrated previously in **Figure 4.22**. Further, the NPV of the DME case is less sensitive to the injection strategy change compared to heavy Ternary Type 2 solvents such as C_{10}, i.e., there is no obvious turning point in the NPV curve for the DME case when solvent injection is stopped. There is a good reason for this. The distillation of C_{10} requires less ΔT, and is more sensitive to overall water concentration as illustrated in Chapter 3. It is important to recover expensive solvent like C_{10} by stopping injecting solvent to make ES-SAGD profitable. The

indication behind this is that, it can be economically beneficial if a solvent like DME is used that is less expensive, easier to recover from the reservoir, and efficient to produce bitumen.

4.3.5 Sensitivity of DME Simulation Results to Viscosity Model

Since no data is available for viscosities of DME containing mixtures, a sensitivity analysis is performed for the viscosity models used in simulation to show how viscosity modelling can affect simulation results. The DME-saturated liquid viscosity mentioned in **§4.3.2** with the mixing coefficients of C_3, C_4 and C_5 for bitumen/DME mixture viscosity is used as in Venkatramani and Okuno (2016). Also, viscosity of C_3, C_4 and C_5 are used for DME are used as well with C_4 coefficients.

Five sets of viscosity models are used for DME simulation. Their bitumen recovery at the first five years and average bitumen drainage rate are compared with that of SAGD. Here, single-sided reservoir as described in Section 3.5 is used. Steam and solvent are coinjected throughout the simulation. Five sets of viscosity models are:

(1) DME saturated liquid viscosity in **§4.3.2** and non-linear logarithmic mixing coefficients of C_3 for oleic phase;
(2) DME saturated liquid viscosity in **§4.3.2** and non-linear logarithmic mixing coefficients of C_4 for oleic phase;
(3) DME saturated liquid viscosity in **§4.3.2** and non-linear logarithmic mixing coefficients of C_5 for oleic phase;
(4) C_4 saturated liquid viscosity and non-linear logarithmic mixing coefficients of C_3 for oleic phase; and
(5) C_4 saturated liquid viscosity and non-linear logarithmic mixing coefficients of C_5 for oleic phase.

Figure 4.26 shows bitumen recovery for the first five years. **Figure 4.27** shows average bitumen drainage rate at 4 years for each case. In general, if C_3 viscosity and/or mixing

coefficients for heavier solvents are used, bitumen can be recovered faster than SAGD case. The drainage rate in the early years directly determines the economic performances and solvent efficiency, of which the analysis is based on recovery of bitumen and solvent in early years. More work should be done on the viscosity model of DME-containing hydrocarbon mixtures to more reasonably evaluate the performance of steam-DME coinjection.

4.4 Conclusions

This chapter presented the potential benefits of using DME in ES-SAGD, which partitions into the water and oleic phases at operating conditions. The phase-behavior analysis given in Chapter 2 was first applied to the coinjection of DME with steam. Then, the analytical estimation of S_{or} after distillation and numerical simulations for steam-DME coinjection were performed to investigate the potential of DME as an additive for improved SAGD in terms of bitumen recovery, SOR and solvent retention. An economic analysis was also conducted for the DME-steam coinjection.

- At 35 bars, the water/bitumen/DME system is classified as Ternary Type 2 since there is no L2 phase between the operation temperature range for bitumen/DME binary.
- Phase behavior study of water/bitumen/DME indicates that DME dissolution in the aqueous phase may result in higher chamber-edge temperature than Ternary Type 1 n-alkanes at the same pressure.
- Solvent efficiency analysis using numerical simulation shows that the DME case can achieve a final bitumen recovery that is similar to those with light n-alkanes within Ternary Type 2, such as n-C_5, although the drainage rate is similar to SAGD in the first several years. Cumulative steam-oil ratio in the DME case was simulated to be similar to those with light n-alkanes within Ternary Type 2. Besides, DME low retention was

simulated in the simulation. DME can be recycled from both water and oleic phases, unlike n-alkanes which can only be recycled from the oleic phase.

- Economic analysis indicates that the DME case is as profitable as light n-alkanes with in Ternary Type 2, and can make more profit than SAGD even before DME is recycled by steam-only injection. This is mainly because DME is less expensive than Ternary Type 2 n-alkanes, but also because it yields less in-situ retention and similar SOR and bitumen recovery as Ternary Type 2 solvents.
- A more reliable of evaluation of DME performance in numerical simulation requires more reliable experiment data for the viscosity and phase behavior for bitumen/DME mixtures.

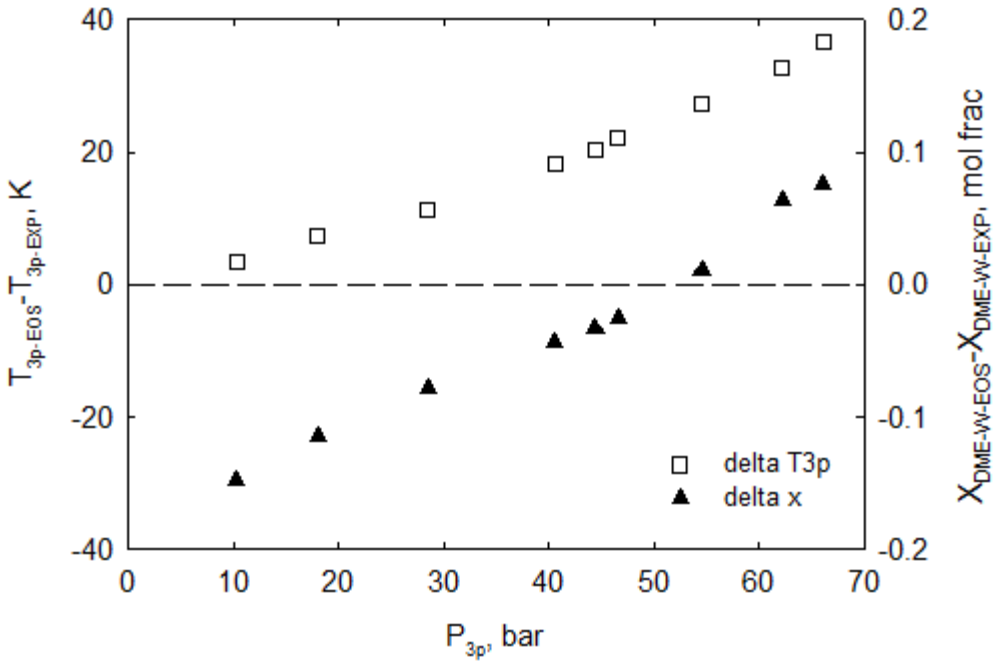

Figure 4.1 Deviation of EOS prediction from Pozo and Streett (1984) experimental data for water/DME BIP of -0.17. three-phase curve is generally overestimated, while DME solubility in water is underestimated at lower pressures.

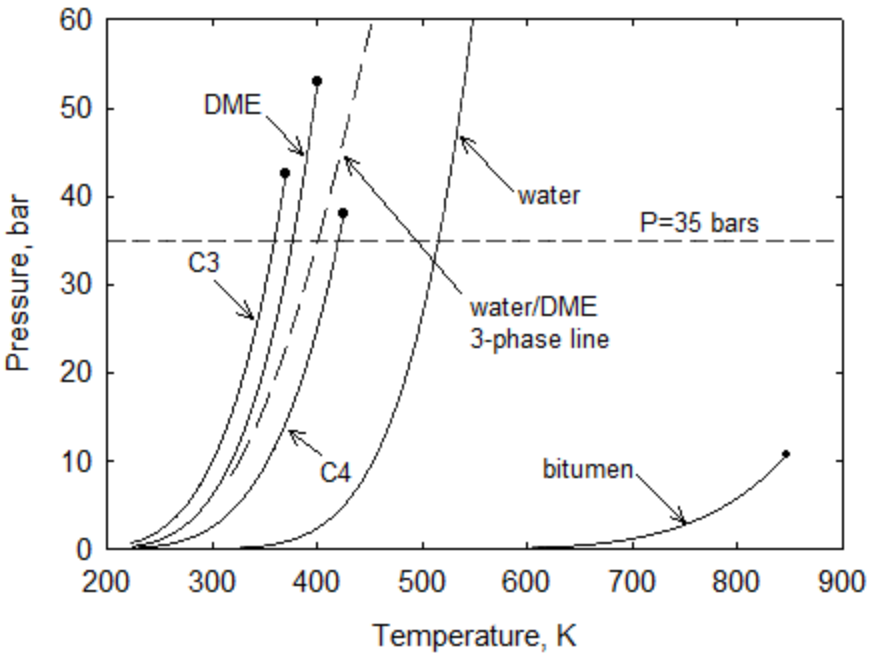

(1)

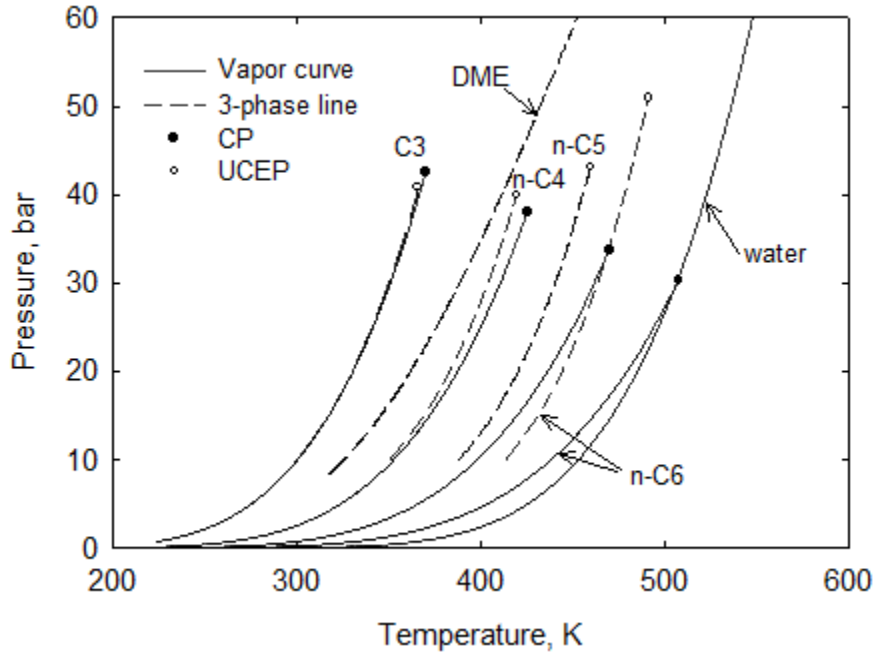

(2)

Figure 4.2 P-T diagrams of water/bitumen/DME system. (1) DME vapor pressure curve is compared with C_3 and C_4. Water/DME three-phase curve is to the right of DME vapor pressure curve, which is a Type III_m K-S binary. (2) three-phase curves for DME and n-alkanes are compared.

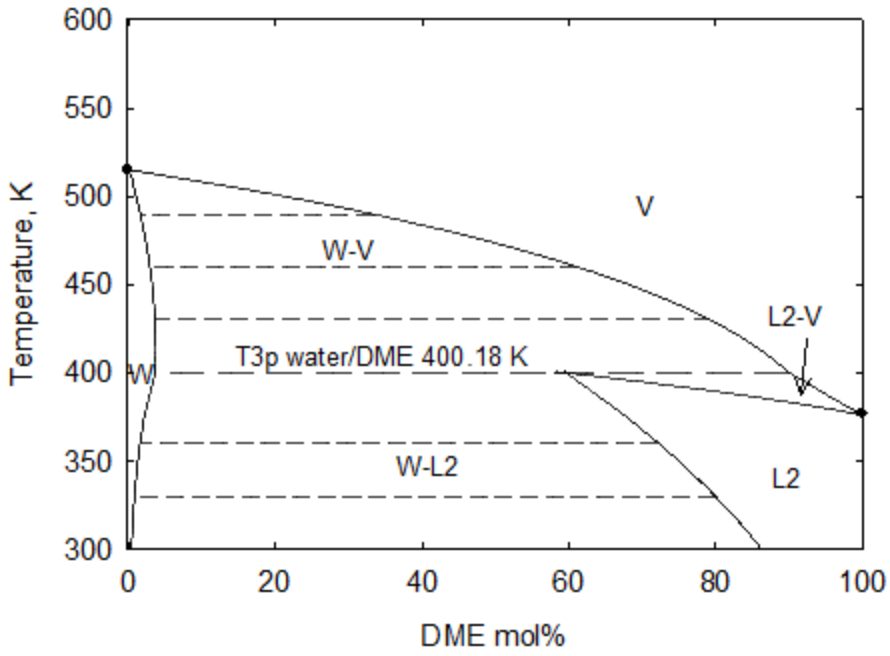

(1) Water/DME at 35 bars

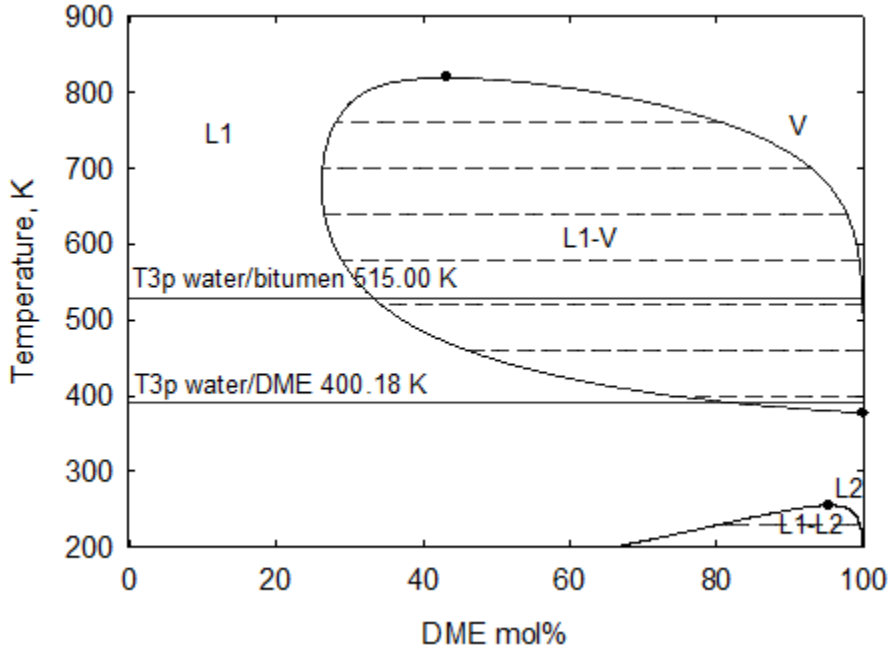

(2) Bitumen/DME at 35 bars

Figure 4.3 T-x diagrams of water/DME and bitumen/DME binaries at 35 bars. L1 represents bitumen-rich oleic phase while L2 represents DME-rich oleic phase. Solid dots are critical points or saturated points.

P = 35 bars
T = 200 K

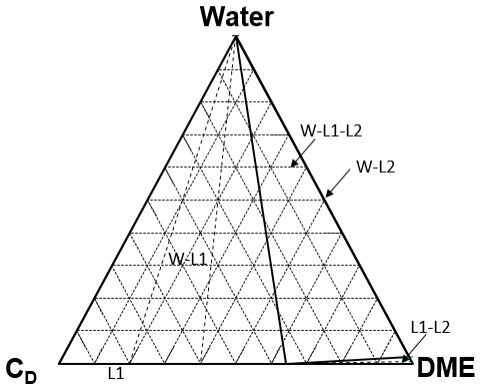

(1)

P = 35 bars
T = 300 K

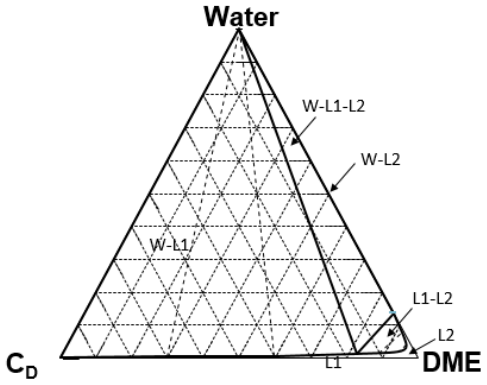

(2)

P = 35 bars
T = 393 K

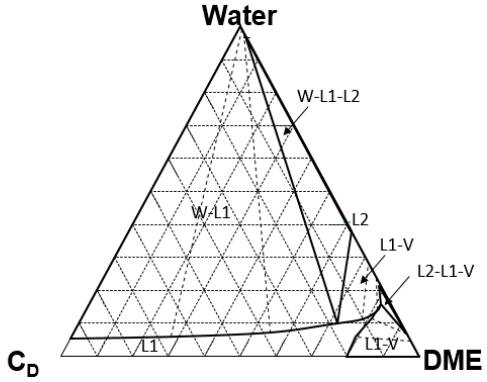

(3)

P = 35 bars
T = 400.17 K

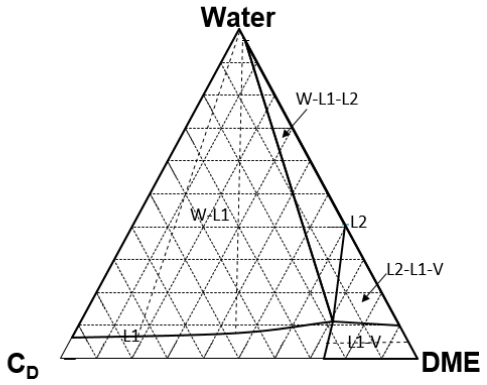

(4)

P = 35 bars
T = 400.18 K
T3p of water/DME

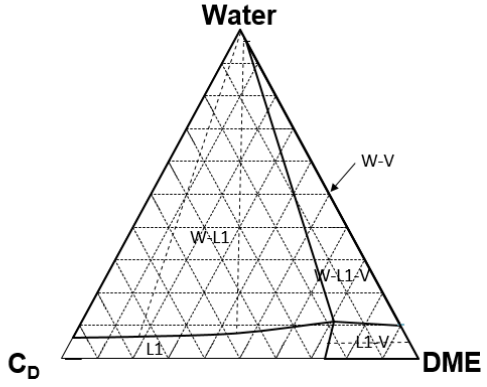

(5)

P = 35 bars
T = 450 K

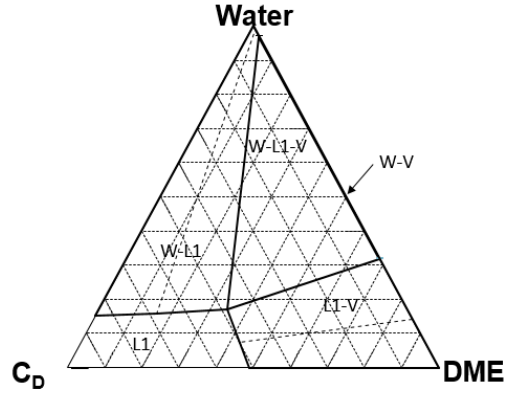

(6)

P = 35 bars
T = 490 K

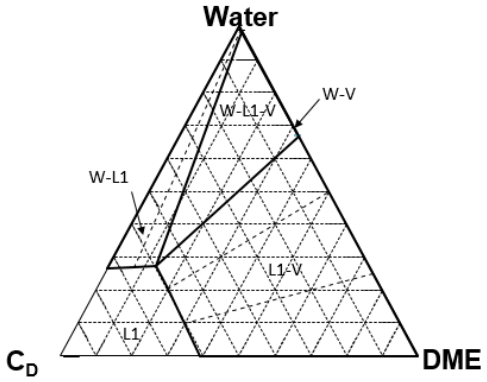

(7)

P = 35 bars
T = 515 K

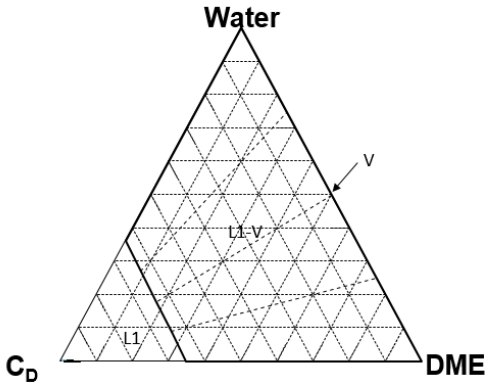

(8)

Figure 4.4 Water/bitumen/DME ternary diagrams at 35 bars. W represents the aqueous phase, while L1 the bitumen-rich oleic phase, L2 the DME-rich oleic phase and V the vapor phase.

P = 35 bars
T = 358.47 K

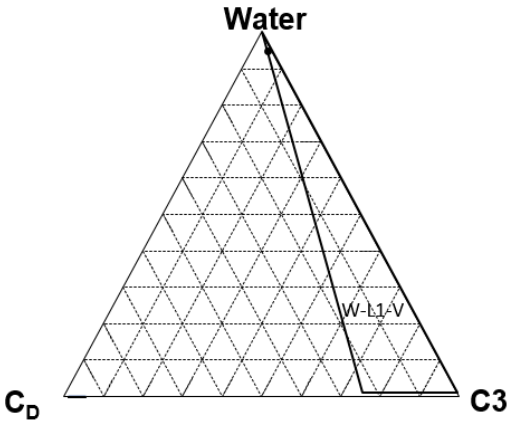

(1)

P = 35 bars
T = 416.20 K

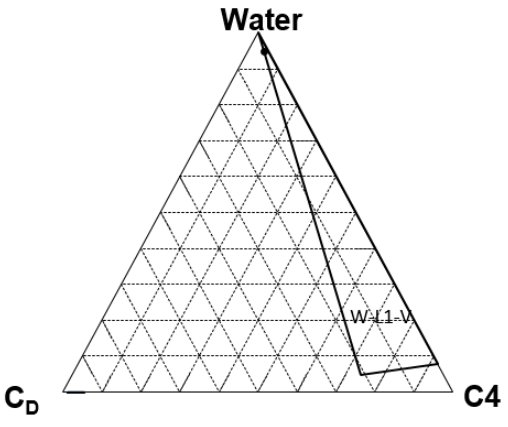

(2)

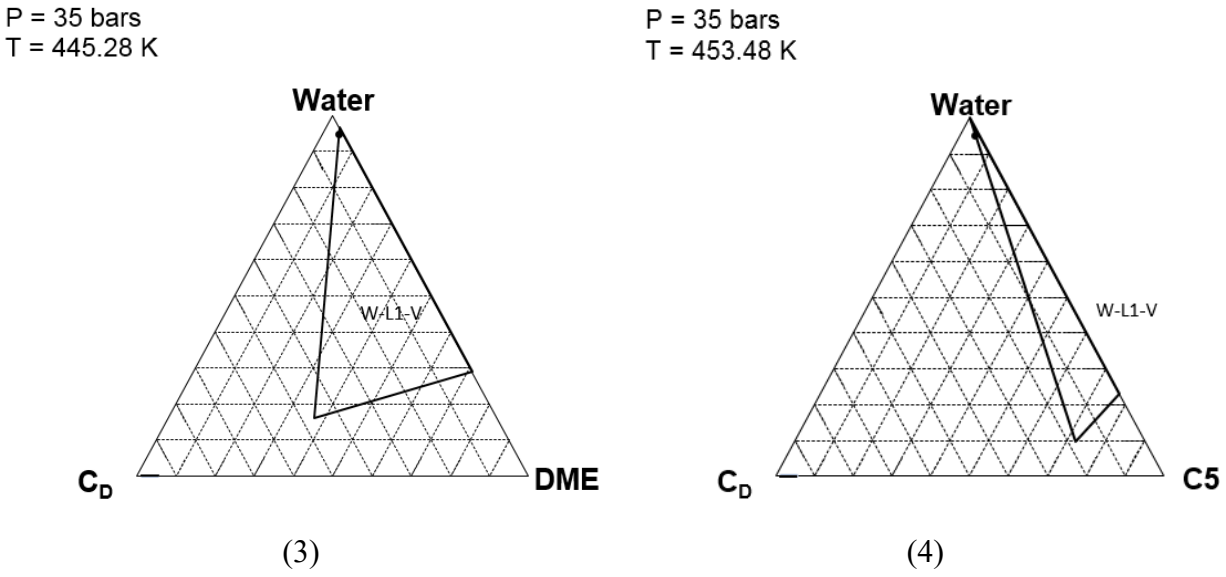

Figure 4.5 Chamber edge condition comparison between water-insoluble solvent like n-alkane and water soluble solvent like DME. Solid dot is the composition accumulation on chamber edge. Injection pressure is 35 bars. Overall water and solvent concentration are 95 mol% and 4 mol%. The water and bitumen properties are the same as case study 1, the water/bitumen/n-alkane ternary EOS model.

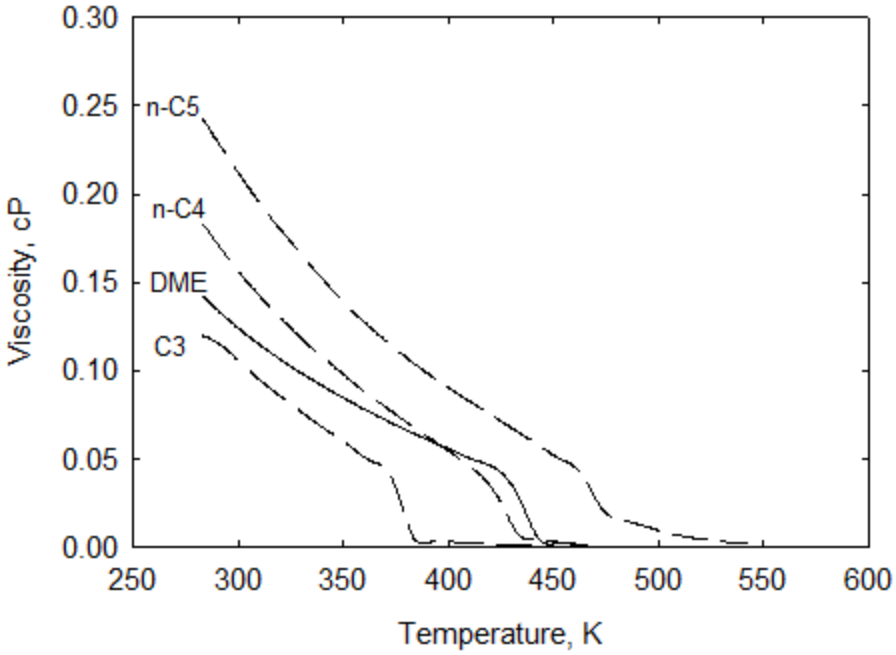

Figure 4.6 Saturated liquid viscosity of DME (Wu et al., 2013). Supercritical C4 viscosities are used for supercritical DME viscosities due to lack of supercritical DME viscosity data. DME has similar viscosity to n-C_4 but is less sensitive to temperature compared to n-C_4.

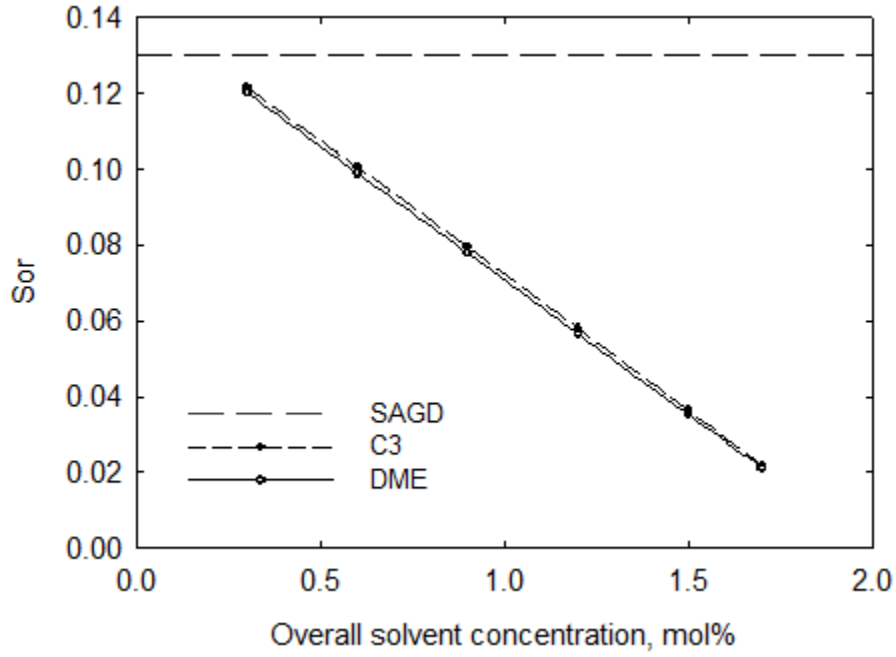

Figure 4.7 Analytical solution to residual oil saturation due to solvent distillation. Chamber edge solvent concentration sensitivity analysis. Analytical solution is performed at 35 bars and 98 mol% water on the chamber edge. S_{wr} is set to 0.25. DME has slightly better potential to reduce oil saturation as C_3.

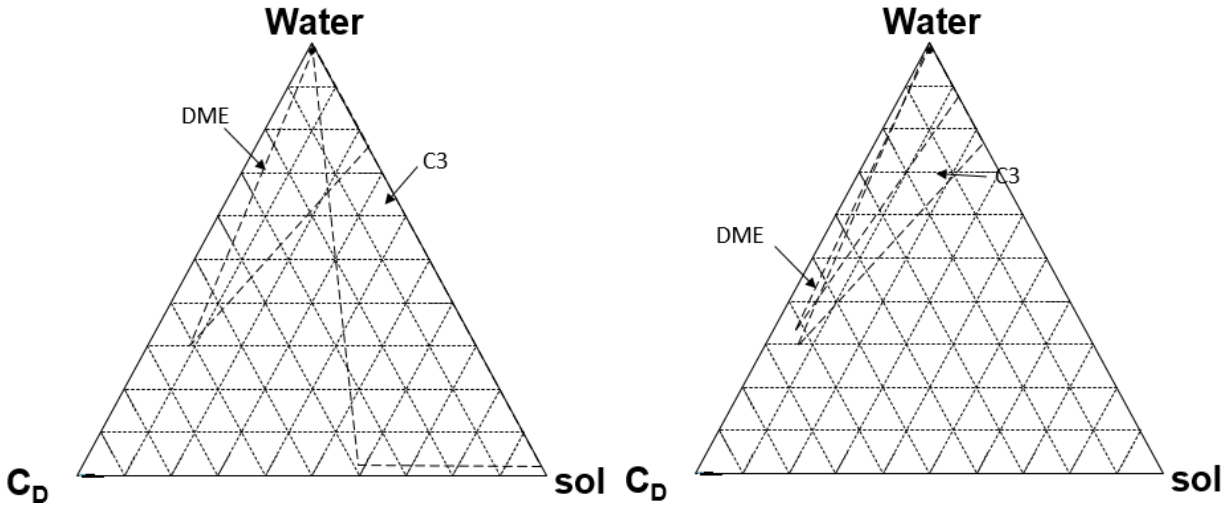

Figure 4.8 Ternary diagrams at chamber edge and S_{wr}. 98 mol% water and 1.2 mol% solvent are used. Pressure is 35 bars and Swr is 0.25. It can be seen for DME case that because of DME solubility in water, its chamber edge temperature is rather high. Water phase saturation diminishes even faster with soluble solvents inside. DME does not need as much temperature variation as C_3 to achieve rather low S_{or}.

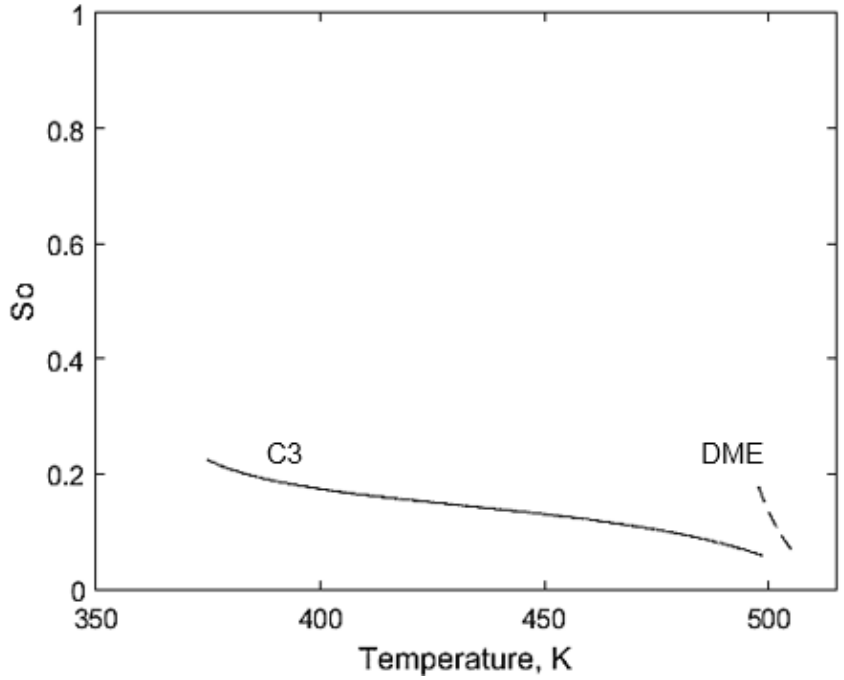

Figure 4.9 Oil saturation reduction during DME distillation. DME is compared with C_3. Pressure is 35 bars with 1.2 mol% overall DME accumulation and 98 mol% overall water. S_{wr} is 0.25.

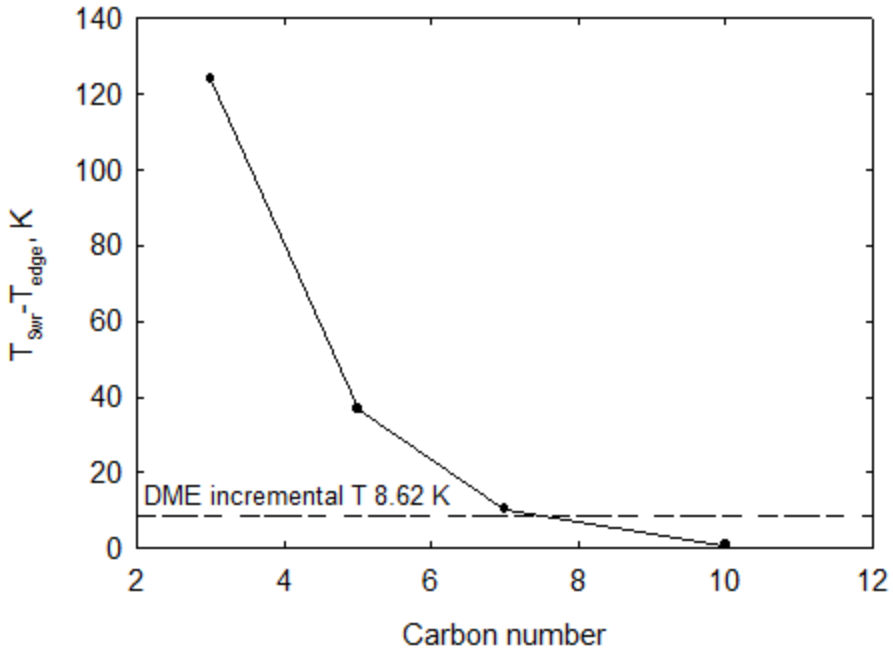

Figure 4.10 DME incremental temperature (ΔT) during distillation compared to n-alkanes. Pressure is 35 bars with 1.2 mol% overall DME accumulation and 98 mol% overall water. S_{wr} is 0.25.

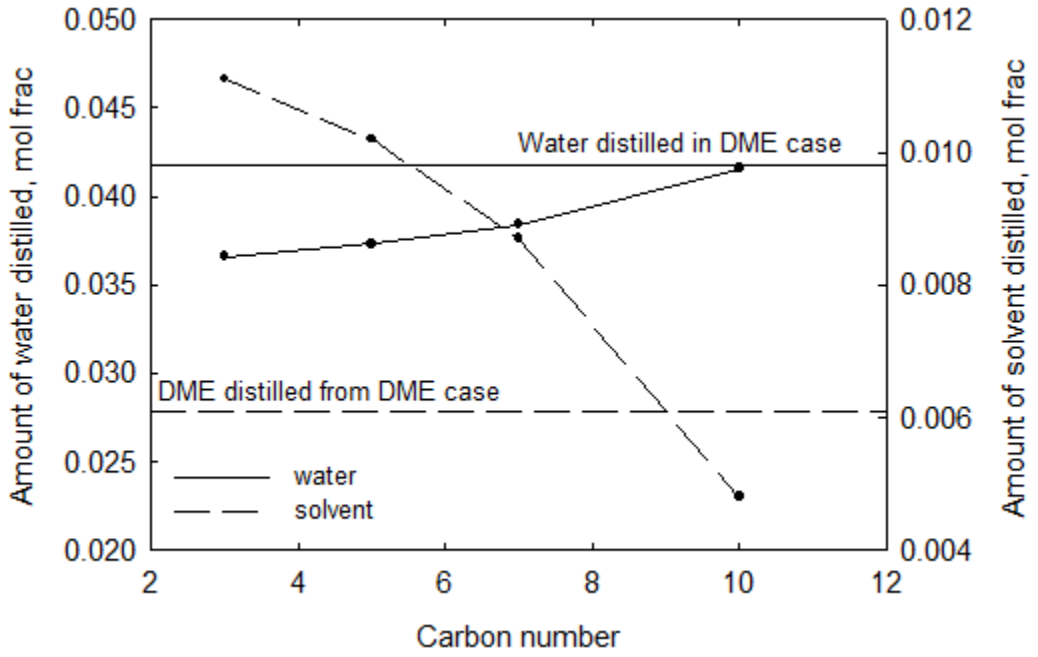

Figure 4.11 Water evaporation and solvent distillation comparison between DME and n-alkane cases. Pressure is 35 bars with the overall DME concentration of 1.2 mol% and overall water concentration of 98 mol%. S_{wr} is 0.25.

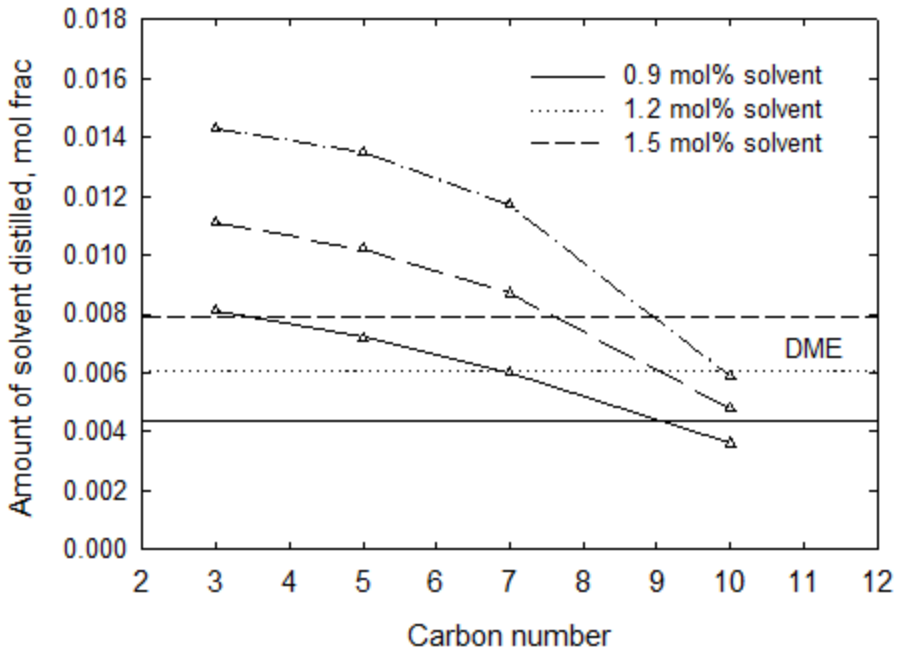

(1)

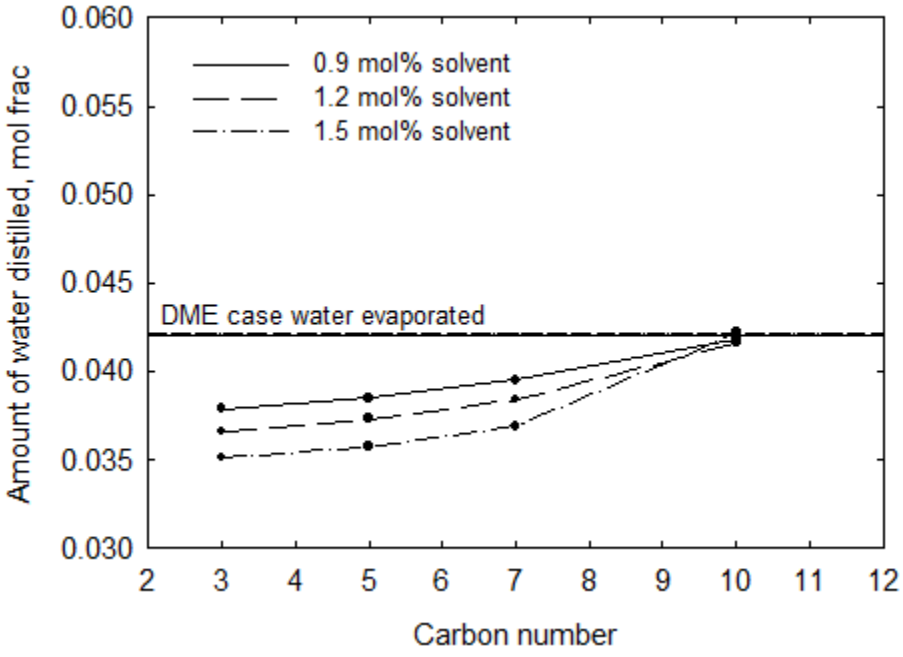

(2)

Figure 4.12 Solvent concentration sensitivity analysis for DME and n-alkanes.

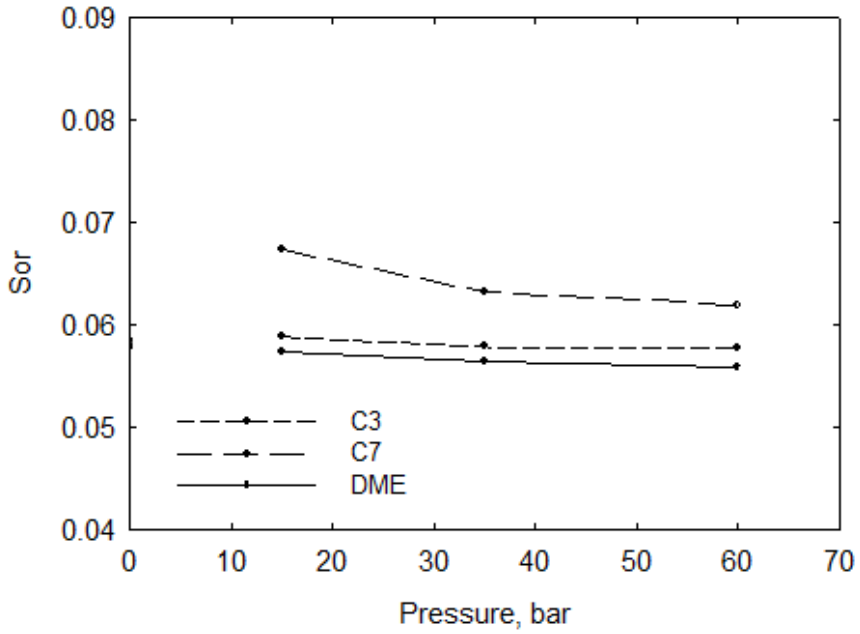

Figure 4.13 Sensitivity analysis for operation pressure influence on analytical solution to S_{or} due to solvent distillation. 98 mol% water and 1.2 mol% solvent are used. S_{wr} is 0.25. Under the same conditions, increased pressure results in lowered S_{or} for DME case as in other n-alkane cases, but the change in S_{or} due to the increased pressure is small.

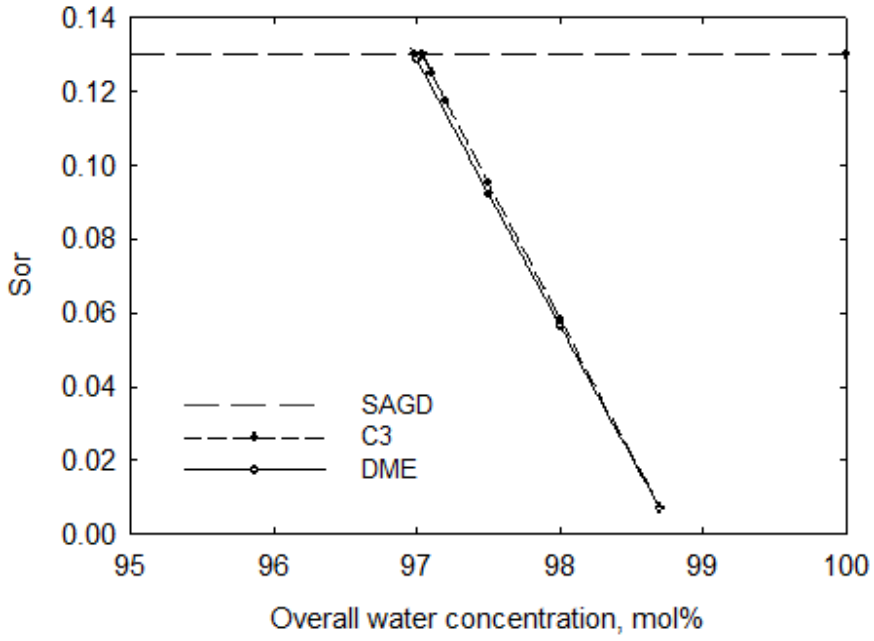

Figure 4.14 Sensitivity analysis for chamber edge water concentration on analytical solution to Sor due to solvent distillation. 1.2 mol% solvent is considered. Operation pressure is 35 bars and S_{wr} 0.25. Due to the similarity of DME and C_3 in terms of volatility, it shows similar sensitivity of S_{or} to water concentration as C_3 in water concentration.

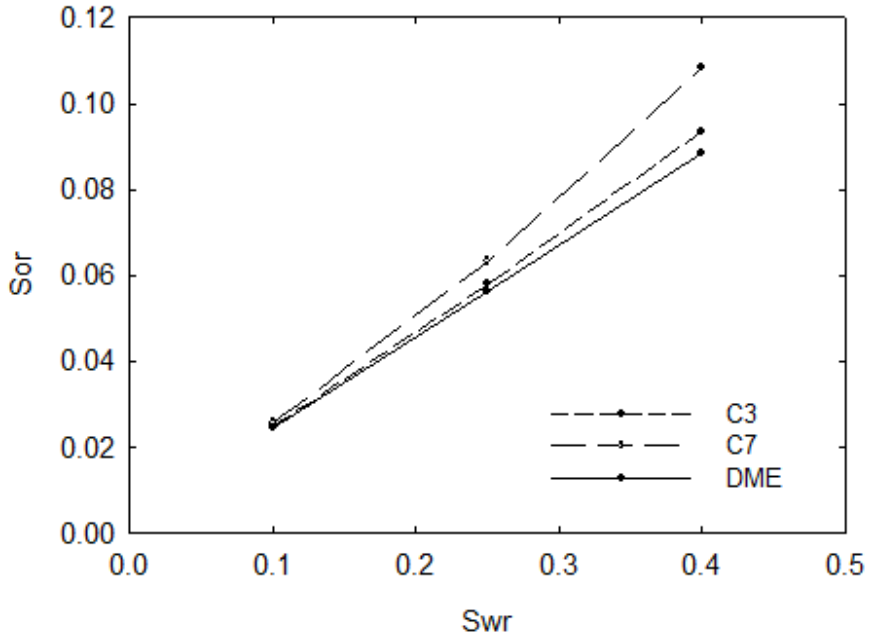

Figure 4.15 Sensitivity analysis for Swr influence on analytical solution to S_{or} due to solvent distillation. 98 mol% water and 1.2 mol% solvent are used. Operation pressure is 35 bars. DME is less sensitive than heavy n-alkane solvent.

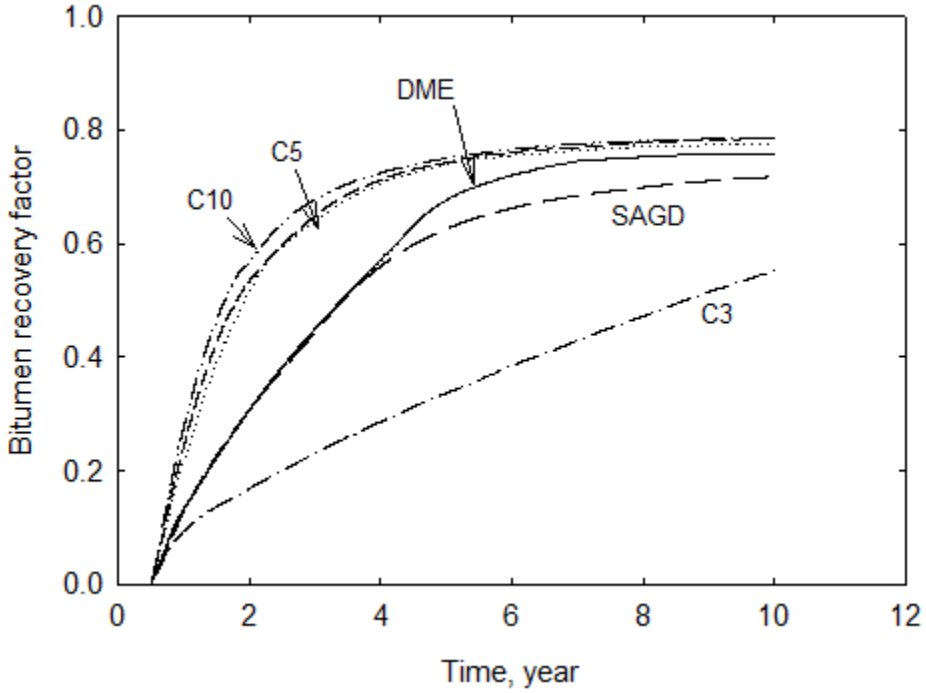

Figure 4.16 DME comparison with n-alkane in terms of bitumen recovery. Steam and solvent are coinjected first and then steam alone is injected. DME can produce bitumen faster than C_3 mainly because of improved chamber edge conditions as a result of DME solubility in aqueous phase.

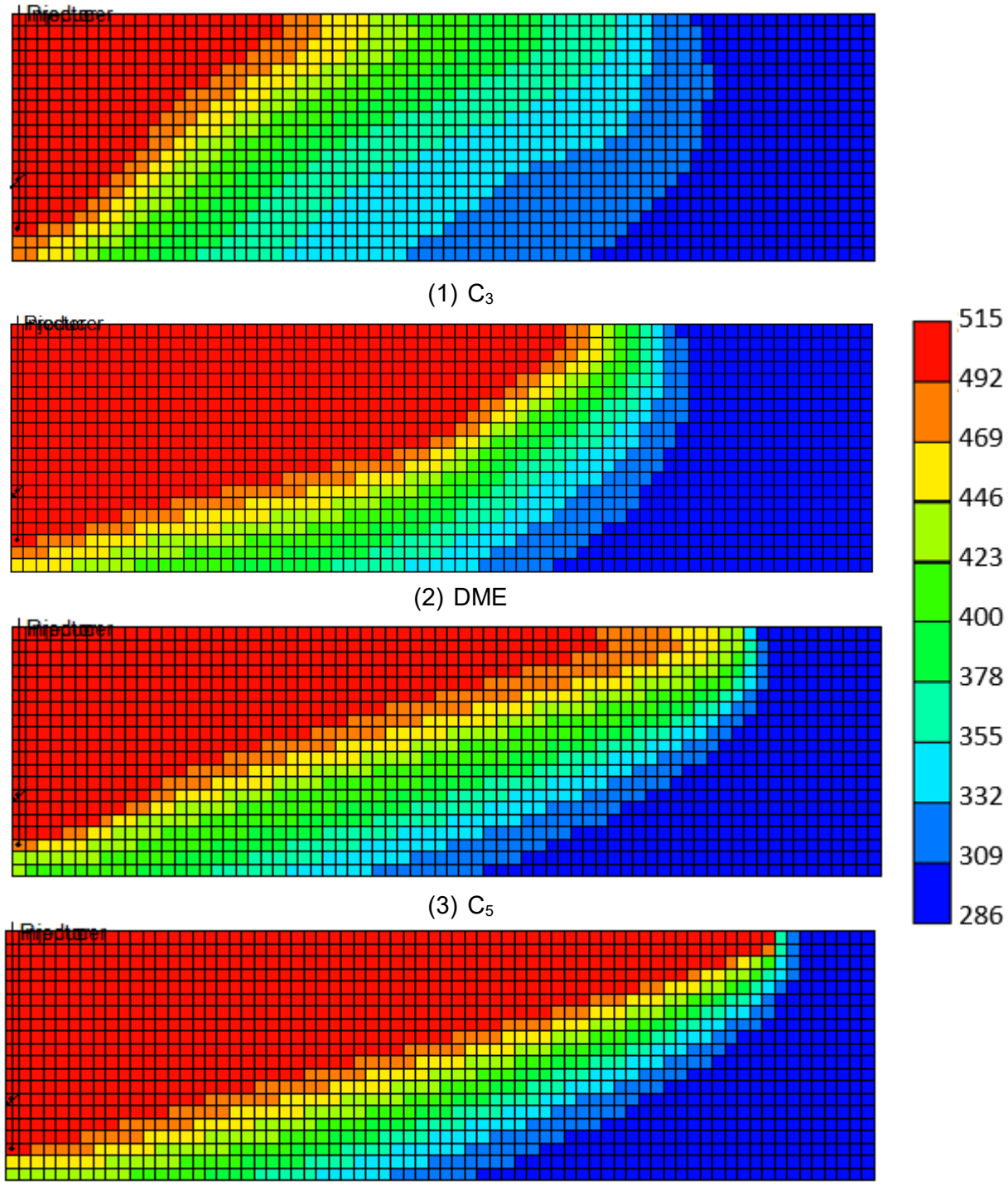

Figure 4.17 Temperature profile (K) comparison between n-alkanes and DME when 6000 m^3 of bitumen is recovered. Well pair is located at the left most of reservoir. Times of temperature profile snapshots are 7.83, 3.10, 1.75 and 1.50 years.

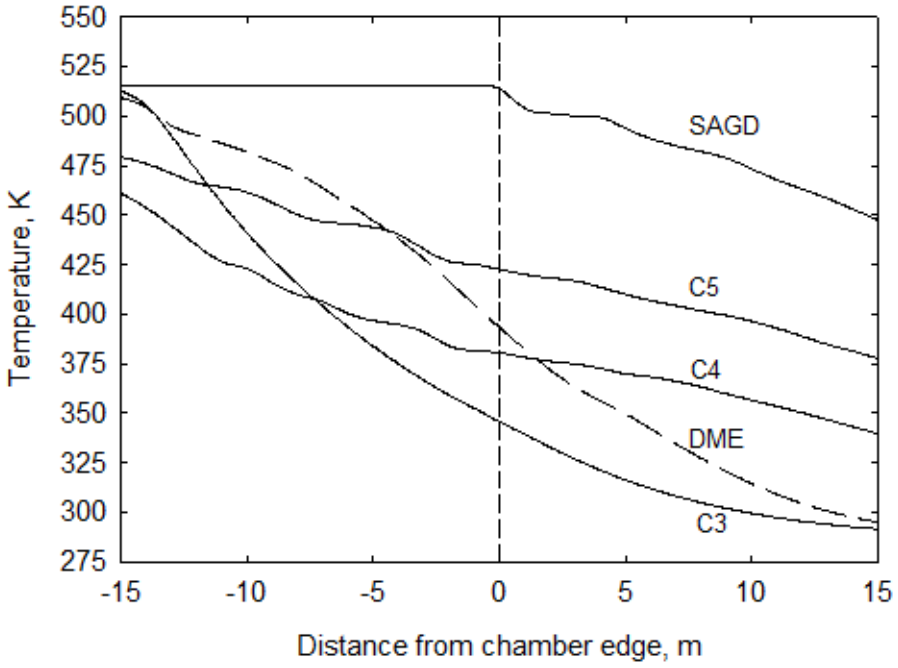

Figure 4.18 Chamber edge temperature comparison between DME and selected n-alkanes in simulation. 12th row from the top of the reservoir is chosen when chamber edge condition is stable. DME shows enhanced chamber edge temperature compared to C_3.

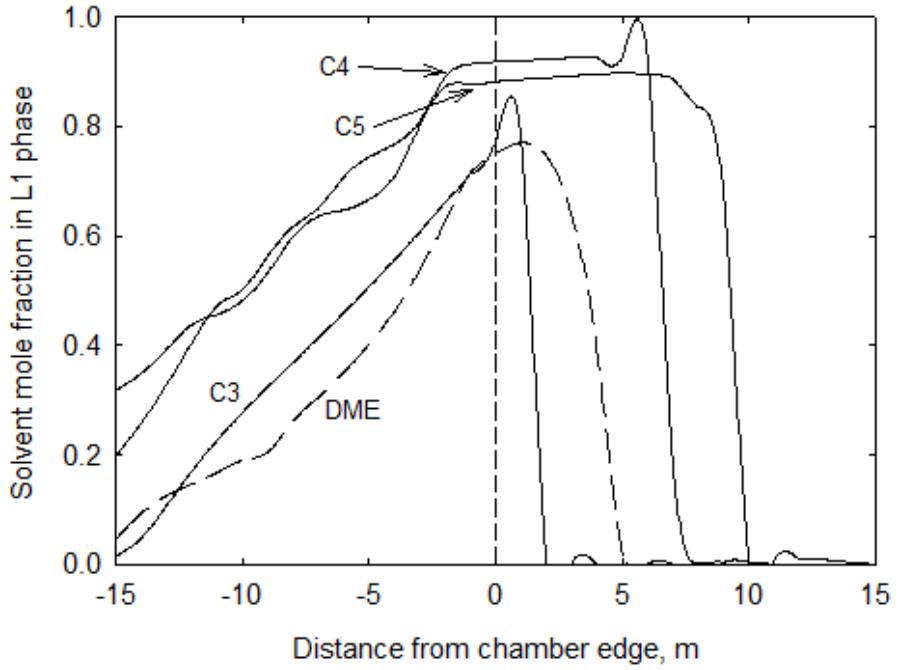

Figure 4.19 Solvent concentration in oleic phase in the vicinity of chamber edge. 12th row from the top of the reservoir is chosen when chamber edge condition is stable. DME shows less solvent concentration on chamber edge. This is a result of DME dissolution in the aqueous phase.

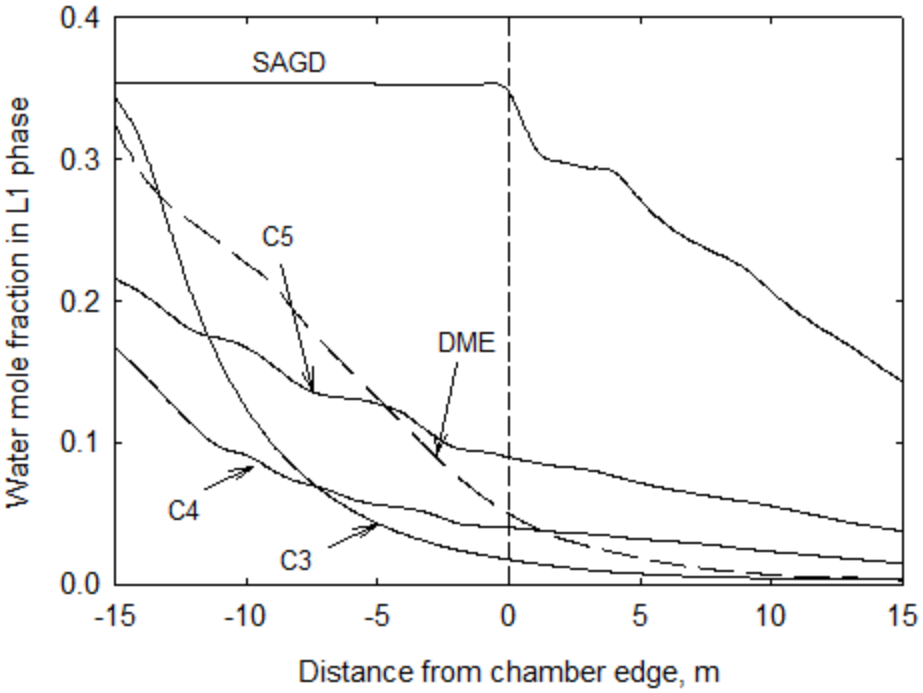

Figure 4.20 Water concentration in oleic phase in the vicinity of chamber edge. 12th row from the top of the reservoir is chosen when chamber edge condition is stable. DME shows water concentration between C_3 and C_5 on the chamber edge.

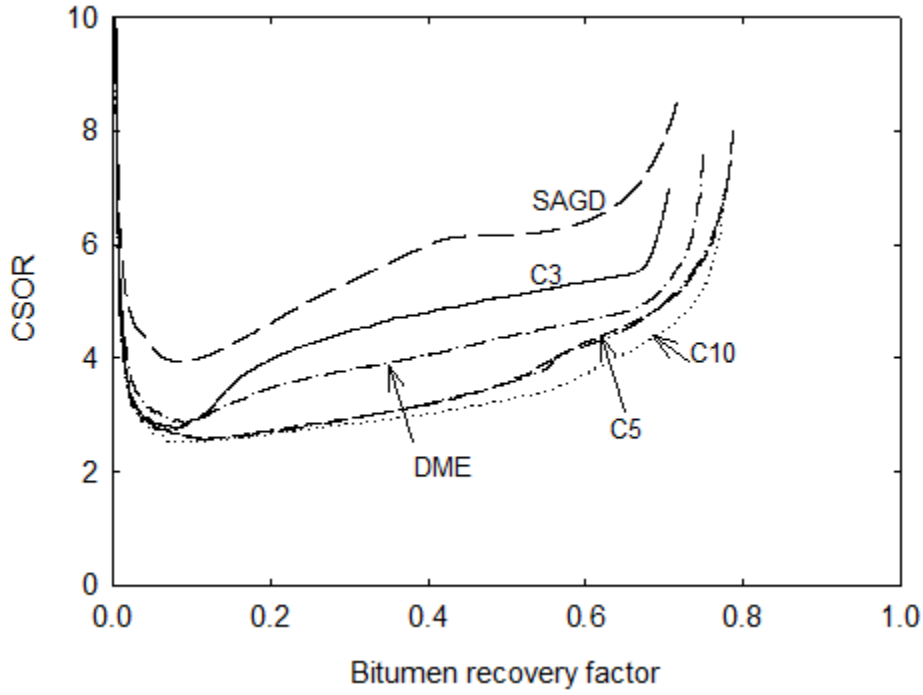

Figure 4.21 DME comparison with n-alkane in terms of CSOR. Steam/solvent are coinjected first and then steam alone is injected. DME has very similar performance as light Ternary Type 2 n-alkanes.

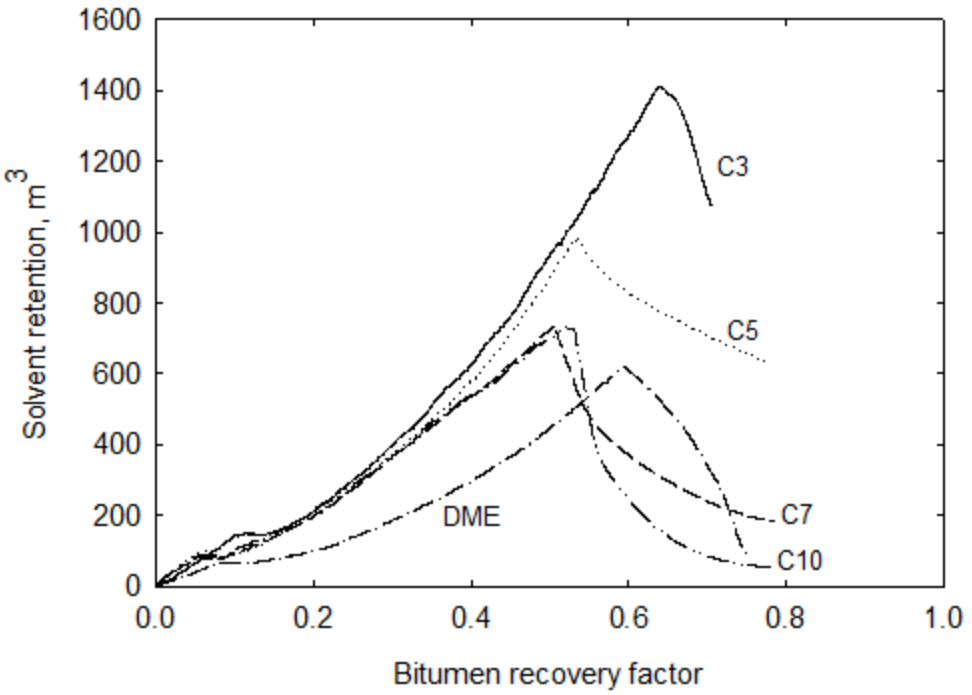

Figure 4.22 DME comparison with n-alkane in terms of solvent retention. The abscissa represents the bitumen recovery factor. Steam-solvent are coinjected first and then steam alone is injected. DME has similar or even less solvent retention to recover same amount of bitumen compared to n-alkanes.

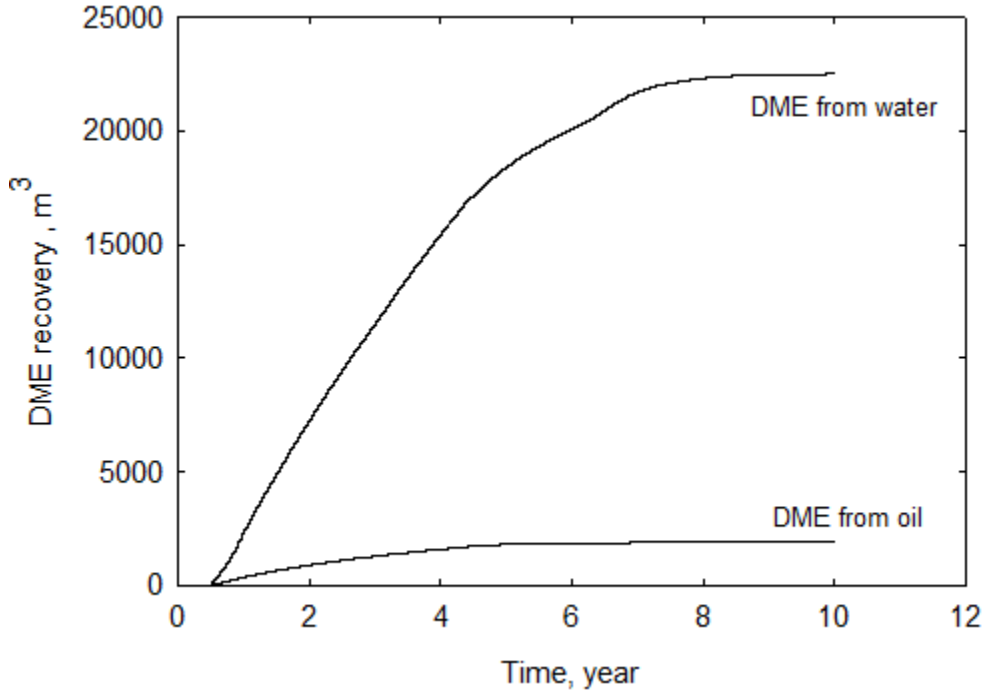

Figure 4.23 DME recovery curves in both water and oil produced. DME volume is measured in saturated liquid volume at the reservoir conditions.

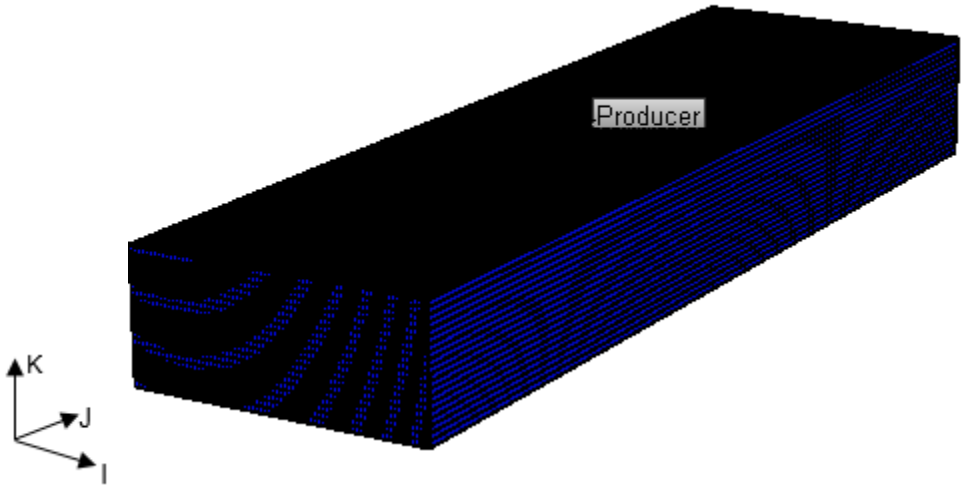

(1) 3-D reservoir

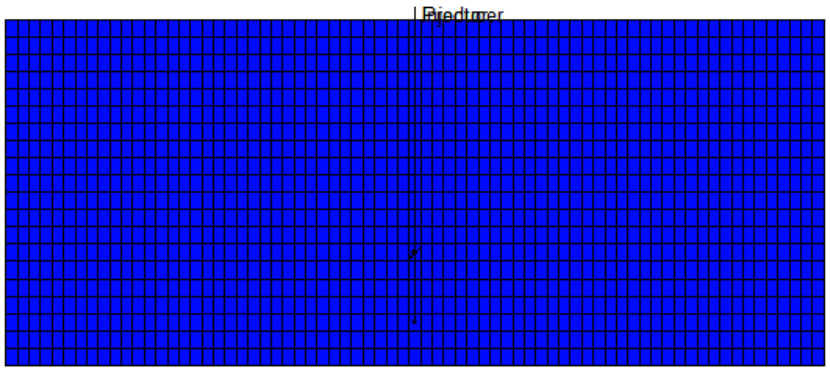

(2) Reservoir projection on the I-K plane

Figure 4.24 Reservoir dimensions for economic analysis. Producer is placed 2 m above the lower reservoir boundary. Injector is 4 m above the producer. Well pair length is 500 m.

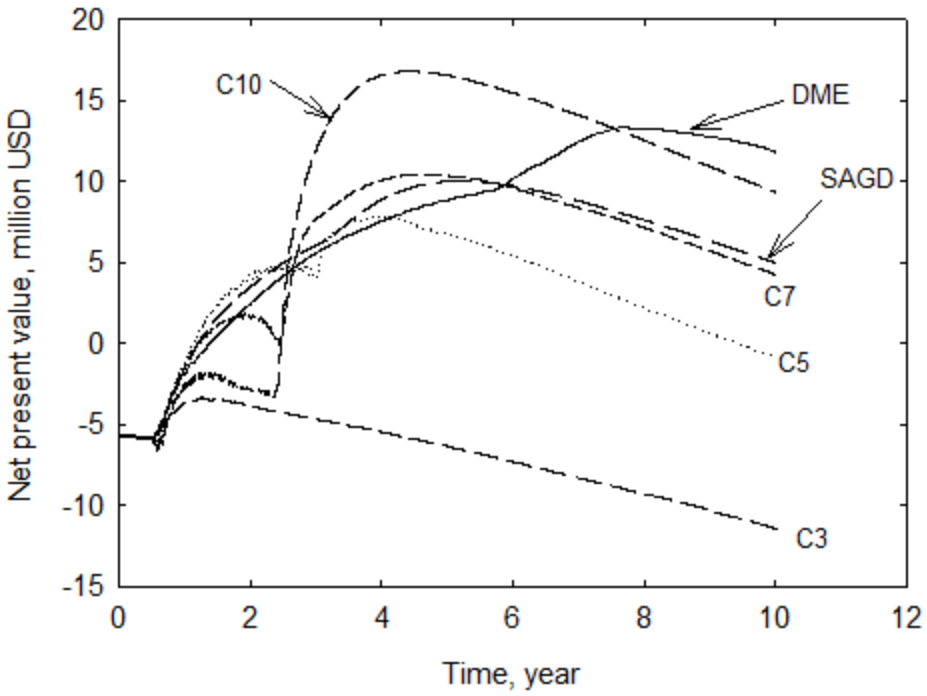

Figure 4.25 Net present value comparison. C_{10} has the maximum NPV, followed by DME, C_7, SAGD, C_5 and C_3.

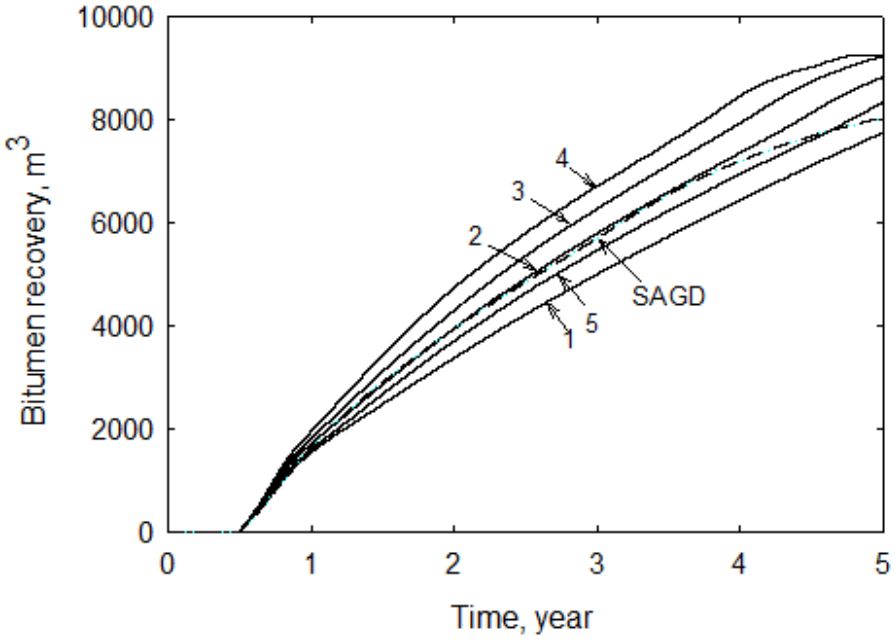

Figure 4.26 Bitumen recovery for the first 5 years using different viscosity models. Case 1: DME viscosity with C_3 coefficients. Case 2: DME viscosity with C_4 coefficients. Case 3: DME viscosity with C_5 coefficients. Case 4: C_3 viscosity with C_4 coefficients. Case 5: C_5 viscosity with C_4 coefficients.

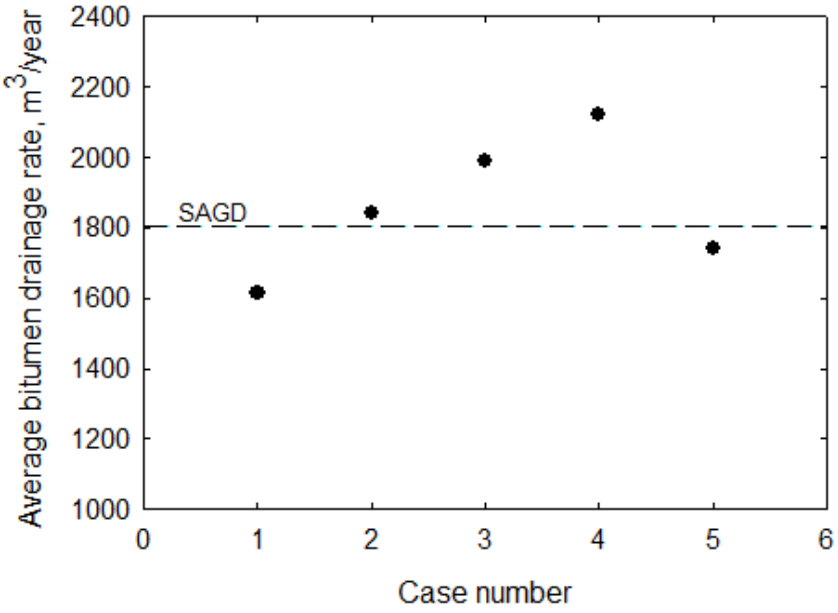

Figure 4.27 Average drainage rate by using different viscosity models for DME. Case 1: DME viscosity with C_3 coefficients. Case 2: DME viscosity with C_4 coefficients. Case 3: DME viscosity with C_5 coefficients. Case 4: C_3 viscosity with C_4 coefficients. Case 5: C_5 viscosity with C_4 coefficients.

Table 4.1 Critical properties and molecular weights for water/bitumen/DME ternary system.

	Tc, K	Pc, bar	ω	MW
Water	647.10	220.64	0.3433	18.01
CD	847.17	10.64	1.0406	530.00
DME	400.50	52.92	0.2000	46.07

Table 4.2 BIPs for water/bitumen/DME for the PR EOS. Ganjdanesh et al.'s (2015) BIPs are adjusted to better match experimental data.

	Water	CD	DME
Water	0		
CD	0.169	0	
DME	-0.170	0.075	0

Table 4.3 Water/DME VLLE experiment data from Pozo and Streett (1984).

T, K	P, bar	x_DME_W	x_DME_L	x_DME_V
323.15	10.27	0.155	0.814	0.958
348.15	18.00	0.128	0.781	0.936
373.26	28.48	0.104	0.755	0.910
394.21	40.54	0.090	0.727	0.901
400.49	44.40	0.089	0.725	0.879
403.26	46.61	0.087	0.721	0.862
414.00	54.54	0.081	0.705	0.844
423.5	62.19	0.093	0.736	0.832
427.4	66.05	0.104	0.755	-

Table 4.4 DME and n-C_{10} VLE experiment data from Park et al. (2007) at 323.15 K.

P, bar	X_DME_L	P, bar	X_DME_L	P, bar	X_DME_L
0.0118	0	6.9302	0.6065	10.5442	0.9331
0.4214	0.0361	7.1749	0.6285	10.7261	0.9476
1.0284	0.0923	7.4478	0.6535	10.8867	0.9601
1.8317	0.1674	7.7211	0.6787	11.0195	0.9702
2.5537	0.2328	7.9177	0.6970	11.1274	0.9783
2.9252	0.2655	7.9959	0.7043	11.2147	0.9848
3.2081	0.2900	8.2660	0.7296	11.2749	0.9892
3.5784	0.3215	8.6044	0.7614	10.8867	0.9601
4.6748	0.4133	8.9313	0.7919	11.3175	0.9923
5.4953	0.4820	9.2424	0.8206	11.3452	0.9944
5.965	0.5219	9.5400	0.8476	11.3761	0.9966
6.3743	0.5573	9.8215	0.8725	11.4052	0.9987
6.6677	0.5831	10.0853	0.8952	11.4231	1

Table 4.5 DME and n-C_{12} VLE experiment data from Park et al. (2007) at 323.15 K.

P, bar	X_DME_L	P, bar	X_DME_L	P, bar	X_DME_L
0.002	0	6.9709	0.6133	10.1592	0.8970
1.4515	0.1428	7.2175	0.6342	10.3951	0.9175
1.8914	0.1843	7.4722	0.6559	10.6101	0.9357
2.4681	0.2371	7.7524	0.6801	10.8083	0.9520
3.0536	0.2889	8.0324	0.7046	10.9675	0.9648
3.404	0.3191	8.3081	0.7290	11.1092	0.9758
3.7226	0.3461	8.5744	0.7530	11.2296	0.9850
4.2166	0.3873	8.7167	0.7659	11.3265	0.9922
5.1833	0.4666	9.0362	0.7950	11.3767	0.9959
5.9576	0.5296	9.3456	0.8234	11.4036	0.9978
6.3484	0.5616	9.6344	0.8498	11.4239	0.9993
6.6918	0.5900	9.906	0.8744	11.4339	1

Table 4.6 AARD between EOS prediction and experiment data with the calibrated EOS model.

	Water/DME X_DME_W	Water/DME T three-phase	n-C_{10}/DME X_DME_L	n-C12/DME X_DME_L
AARD, %	40.74	4.91	1.14	1.68
AAD	6.58 mol%	19.92 K	0.62 mol%	0.65 mol%

Table 4.7 Binary type summary according to classification of van Konynenburg and Scott (1980).

	Water/bitumen	Water/solvent	Bitumen/solvent
Water/bitumen/n-alkane	III HA	III HA	III_m
Water/bitumen/DME	III HA	III_m	III_m

Table 4.8 Regression results on liquid DME density for analytical solution and numerical simulation.

Reference density, kg/m3	678
a1	1.596e-03
a2	3.183e-05
a3	3.397e-06
a4	-2.330e-09
R-square	0.9998

Table 4.9 Time when steam chamber reaches reservoir boundary for each case. Reservoir for Net present value calculation purpose. C_3 case cannot reaches reservoir within 10-year simulation span.

	C_3	n-C_5	n-C_7	n-C_{10}	DME	SAGD
time, yr	Never	3.0	2.5	2.4	4.3	2.9

Table 4.10 Inputs for economic analysis.

Item	Values	Units
Bitumen	35	USD/barrel
DME	0.44	USD/kg
C_3	0.46	USD/kg
C_5	0.61	USD/kg
C_7	0.82	USD/kg
C_{10}	1.09	USD/kg
Exploration	200000	USD
Well-pair completion	4800	USD/m
well length	500	m
Steam generator	2260000	USD
Water-treatment equipment	1000000	USD
Well-pair and field operation	150000	USD/yr

Administration and head office	7.48	USD/m3 oil
Blending and transportation	6.29	USD/m3 oil
Steam-generator operation	2.83	USD/m3 CWE
Fuel for steam generator	10.1	USD/m3 CWE
Treatment of water production	1.96	USD/m3 CWE
Solvent distribution line	100000	USD
Solvent handling	2000	USD/yr

Table 4.11 Maximum NPV and time achieved for each solvent coinjection. Solvent injection is ceased immediately after steam chamber reaches the reservoir boundary.

	C_3	n-C_5	n-C_7	n-C_{10}	DME	SAGD
Max NPV, mil USD	-3.35	7.86	10.45	16.78	16.46	10.02
Time, yr	1.3	4.0	4.6	4.4	6.0	5.2

Chapter 5 Conclusions and Recommendations

This research has presented a systematic analysis on enhanced oil displacement efficiency by steam-solvent coinjection based on thorough phase behavior study. This chapter summarizes conclusions of previous chapters and gives suggestions for future works based on the observations in this research.

5.1 Conclusions

In this research, a systematic phase behavior study for water/bitumen/solvent was given and a classification method was proposed. The significance of this classification method is to understand the ability of solvent mixing with bitumen on the steam chamber edge. The bitumen mixing with solvent is the essential difference that makes coinjection different from SAGD. Then, an algorithm was given to quantify the residual oil saturation for distillation based on the phase behavior study. This algorithm used only thermodynamics to explain the residual oil saturation due to the distillation, instead of solving mass balance or energy transfer equations as in numerical simulation. The algorithm also provides a unified way to explain the differences in the displacement efficiency by using different solvent or other conditions in coinjection. Finally, the classification method and algorithm was applied to the coinjection of steam/DME, which is not much studied so far.

Here are the key conclusions in this research:

- Water/bitumen/solvent system can be classified into Ternary Types 1 and 2, depending on whether solvent is completely miscible with bitumen without the appearance of a second oleic phase L2. If solvent cannot completely mix with bitumen and form L2, it is classified as Ternary Type 1. If within the operation temperature range, only L1 exists, it is classified as Ternary Type 2.

- Ternary Type 1 is unfavorable, because the solvent-rich L2 phase on the steam chamber indicates poor solvent mixing with bitumen. Also, the L2 phase may extract light components from the bitumen and impedes the flow of L1.
- The distillation mechanisms can be explained in a unified way: the temperature increase during distillation, and competition between solvent and water transfer from the W and L phases to the V phase.
- Lower residual oil saturation can be achieved if temperature increase is high, more solvent and/or less water can be transferred from liquid to vapor during the distillation.
- Lighter solvents, greater operation pressure and more solvent accumulation on the chamber edge are favored in terms of displacement efficiency.
- A preliminary research on the water/bitumen/DME system shows it is a Ternary Type 2 solvent at 35 bars. Because of the DME dissolution inside the water phase, steam/DME coinjection may achieve higher chamber edge temperature than other Ternary Type 1 n-alkanes. As a result, the drainage rate may be improved.

5.2 Recommendations

Throughout this research, accurately modeled phase behavior has been the key to explain enhanced displacement efficiency by steam-solvent coinjection compared to SAGD. For non-polar molecules as in the n-alkane models based upon latest experiment results, the PR EOS and the vdW EOS were able to predict phase behavior accurately. However, the study regarding DME in this research gives rather conservative results because of limitations of phase behavior study using the PR EOS and the vdW mixing rules in dealing with mixtures containing DME. With the current EOS model, the prediction of either three-phase temperature of water/DME or DME dissolution in water is sacrificed however the BIP between water/DME is adjusted. Therefore, to

improve the understanding of ES-SAGD using DME, more advanced EOS model should be used to accurately model both three-phase curve and solvent solubility in water.

Further, DME was classified as a Ternary Type 2 solvent at 35 bars in this research because DME has limited ability to dissolve in bitumen at three-phase temperature of water/DME. However, the phase behavior for bitumen/DME mixtures is still missing in the literature. PVT experiments to determine the thermodynamics properties of DME-containing hydrocarbon systems should be done in the future.

Also, the viscosity model in the simulations greatly impacts flows in the vicinity of chamber edge and therefore impacts analysis involving drainage rate in this study. A lack of viscosity data for DME-containing hydrocarbon mixtures created uncertainties in the discussion of DME performance in coinjection. In the future, viscosity models for DME-containing mixtures can be established by experiments to better understand the flow in steam-DME coinjection.

The whole research was focused on the phase behavior in steam-solvent coinjection. The classification method was specifically developed to help explain the distillation and enhanced displacement efficiency. However, it is possible to develop a more general classification method for ternary system that is not limited to the practice of steam-solvent coinjection, for the pure interest of theoretical study.

References

Amani, M.J., Gray, M.R. and Shaw, J.M., 2013. Phase behavior of Athabasca bitumen+ water mixtures at high temperature and pressure. The Journal of Supercritical Fluids, 77, pp.142-152.

Amani, M.J., Gray, M.R. and Shaw, J.M., 2013. Volume of mixing and solubility of water in Athabasca bitumen at high temperature and pressure.Fluid Phase Equilibria, 358, pp.203-211.

Blevins, T.R., Aseltine, R.J. and Kirk, R.S., 1969. Analysis of a steam drive project, Inglewood Field, California. Journal of Petroleum Technology, 21(09), pp.1-141.

Blevins, T.R. and Billingsley, R.H., 1975. The Ten-Pattern Steamflood, Kern River Field, California. Journal of Petroleum Technology, 27(12), pp.1-505.

Boshkov, L.Z., 1987. On the description of closed-loop phase-diagrams of 2-component solutions, based on the one-fluid equation of state. DOKLADY AKADEMII NAUK SSSR, 294(4), pp.901-905.

Brunner, E., 1988. Fluid mixtures at high pressures VI. Phase separation and critical phenomena in 18 (n-alkane+ ammonia) and 4 (n-alkane+ methanol) mixtures. The Journal of Chemical Thermodynamics, 20(3), pp.273-297.

Brunner, E., 1990. Fluid mixtures at high pressures IX. Phase separation and critical phenomena in 23 (n-alkane+ water) mixtures. The Journal of Chemical Thermodynamics, 22(4), pp.335-353.

Brunner, E., Thies, M.C. and Schneider, G.M., 2006. Fluid mixtures at high pressures: Phase behavior and critical phenomena for binary mixtures of water with aromatic hydrocarbons. The Journal of supercritical fluids, 39(2), pp.160-173.

Butler, R.M., 1997. Thermal recovery of oil and bitumen, publ. GravDrain Inc.(2nd printing), Calgary, Alberta, 528pp.

Chernetsky, A., Masalmeh, S., Eikmans, D., Boerrigter, P.M., Fadili, A., Parsons, C.A., Parker, A., Boersma, D.M., Cui, J., Dindoruk, B. and te Riele, P.M., 2015, November. A Novel Enhanced Oil Recovery Technique: Experimental Results and Modelling Workflow of the DME Enhanced Waterflood Technology. In Abu Dhabi International Petroleum Exhibition and Conference. Society of Petroleum Engineers.

Computer Modelling Group, 2013. STARS version 2013 user's guide. Computer Modelling Group, Calgary, Alberta, Canada.

Computer Modelling Group, 2013. WINPROP version 2013 user's guide. Computer Modelling Group, Calgary, Alberta, Canada.

Connolly, J.F., 1966. Solubility of Hydrocarbons in Water Near the Critical Solution Temperatures. Journal of Chemical and Engineering data, 11(1), pp.13-16.

Constantinou, L. and Gani, R., 1994. New group contribution method for estimating properties of pure compounds. AIChE Journal, 40(10), pp.1697-1710.

Constantinou, L., Gani, R. and O'Connell, J.P., 1995. Estimation of the acentric factor and the liquid molar volume at 298 K using a new group contribution method. Fluid Phase Equilibria, 103(1), pp.11-22.

Deiters, U.K. and Kraska, T., 2012. High-Pressure Fluid Phase Equilibria: Phenomenology and Computation (Vol. 2). Elsevier.

Dong, L., 2012. Effect of vapour–liquid phase behaviour of steam–light hydrocarbon systems on steam assisted gravity drainage process for bitumen recovery. Fuel, 95, pp.159-168.

Ganjdanesh, R., Rezaveisi, M., Pope, G.A. and Sepehrnoori, K., 2015, September. Treatment of Condensate and Water Blocks in Hydraulic Fractured Shale Gas-Condensate Reservoirs. In SPE Annual Technical Conference and Exhibition. Society of Petroleum Engineers.

Gao, J., Okuno, R. and Li, H.A., 2016, June. An Experimental Study of Multiphase Behavior for n-Butane/Bitumen/Water Mixtures. In SPE Canada Heavy Oil Technical Conference. Society of Petroleum Engineers.

Gates, I.D., 2007. Oil phase viscosity behaviour in expanding-solvent steam-assisted gravity drainage. Journal of Petroleum Science and Engineering,59(1), pp.123-134.

Govind, P.A., Das, S.K., Srinivasan, S. and Wheeler, T.J., 2008, January. Expanding solvent SAGD in heavy oil reservoirs. In International Thermal Operations and Heavy Oil Symposium. Society of Petroleum Engineers.

Gupta, S.C. and Gittins, S.D., 2006. Christina Lake Solvent Aided Process Pilot. Journal of Canadian Petroleum Technology, 45(09).

Ignasiak, B.L., Yamaoka, K., 2010. In-situ recovery of bitumen or heavy oil by injection of di-methyl ether. https://www.google.ca/patents/CA2652930A1?cl=en. Google Patents.

Ihmels, E.C. and Lemmon, E.W., 2007. Experimental densities, vapor pressures, and critical point, and a fundamental equation of state for dimethyl ether. Fluid Phase Equilibria, 260(1), pp.36-48.

Jha, R.K., Kumar, M., Benson, I. and Hanzlik, E., 2013. New insights into steam/solvent-coinjection-process mechanism. SPE Journal, 18(05), pp.867-877.

Keshavarz, M. and Chen, Z., 2014, October. Modeling Displacement Efficiency Improvement During Solvent Aided-SAGD. In SPE Annual Technical Conference and Exhibition. Society of Petroleum Engineers.

Keshavarz, M., Okuno, R. and Babadagli, T., 2014. Efficient oil displacement near the chamber edge in ES-SAGD. Journal of Petroleum Science and Engineering, 118, pp.99-113.

Keshavarz, M., Okuno, R. and Babadagli, T., 2015 (a). A semi-analytical solution to optimize single-component solvent coinjection with steam during SAGD. Fuel, 144, pp.400-414.

Keshavarz, M., Okuno, R. and Babadagli, T., 2015 (b). Optimal Application Conditions for Steam/Solvent Coinjection. SPE Reservoir Evaluation & Engineering, 18(01), pp.20-38.

Kumar, A., 2016. Characterization of Reservoir Fluids based on Perturbation from n-Alkanes. ERA thesis of University of Alberta.

Kumar, A. and Okuno, R., 2015, September. A New Algorithm for Multiphase Fluid Characterization for Solvent Injection. In SPE Annual Technical Conference and Exhibition. Society of Petroleum Engineers.

Kumar, A. and Okuno, R., 2016. Reliable characterization of bitumen based on perturbation from n-alkanes for steam-solvent coinjection simulation.Fuel, 182, pp.141-153.

Leaute, R.P., 2002, January. Liquid addition to steam for enhancing recovery (LASER) of bitumen with CSS: Evolution of technology from research concept to a field pilot at Cold Lake. In SPE International Thermal Operations and Heavy Oil Symposium and International Horizontal Well Technology Conference. Society of Petroleum Engineers.

Leaute, R.P. and Carey, B.S., 2007. Liquid addition to steam for enhancing recovery (LASER) of bitumen with CSS: Results from the first pilot cycle.Journal of Canadian Petroleum Technology, 46(09).

Li, W., Mamora, D.D. and Li, Y., 2011a. Solvent-type and-ratio impacts on solvent-aided SAGD process. SPE Reservoir Evaluation & Engineering,14(03), pp.320-331.

Li, W., Mamora, D. and Li, Y., 2011b. Light-and heavy-solvent impacts on solvent-aided-SAGD process: a low-pressure experimental study. Journal of Canadian Petroleum Technology, 50(04), pp.19-30.

Nasr, T.N. and Ayodele, O.R., 2006, January. New hybrid steam-solvent processes for the recovery of heavy oil and bitumen. In Abu Dhabi International Petroleum Exhibition and Conference. Society of Petroleum Engineers.

Nasr, T.N., Beaulieu, G., Golbeck, H. and Heck, G., 2003. Novel Expanding Solvent-SAGD Process" ES-SAGD". Journal of Canadian Petroleum Technology, 42(01).

Nghiem, L.X. and Li, Y.K., 1984. Computation of multiphase equilibrium phenomena with an equation of state. Fluid Phase Equilibria, 17(1), pp.77-95.

Ohno, Y., Inoue, N., Okuyama, K. and Yajima, T., 2005, January. New clean fuel DME. In International Petroleum Technology Conference. International Petroleum Technology Conference.

Okuno, R., Johns, R. and Sepehrnoori, K., 2010. A new algorithm for Rachford-Rice for multiphase compositional simulation. SPE Journal, 15(02), pp.313-325.

Orr, B., 2009, January. ES-SAGD; Past, Present and Future. In SPE Annual Technical Conference and Exhibition. Society of Petroleum Engineers.

Park, S.J., Han, K.J. and Gmehling, J., 2007. Isothermal phase equilibria and excess molar enthalpies for binary systems with dimethyl ether at 323.15 K. Journal of Chemical & Engineering Data, 52(5), pp.1814-1818.

Park, K.J., Seo, T. and Jung, D., 2007. Performance of alternative refrigerants for residential air-conditioning applications. Applied energy,84(10), pp.985-991.

Pozo, M.E. and Streett, W.B., 1984. Fluid phase equilibria for the system dimethyl ether/water from 50 to 220. degree. C and pressures to 50.9 MPa.Journal of Chemical and Engineering Data, 29(3), pp.324-329.

Prats, M., 1982. Thermal recovery.

Qian, J.W., Privat, R. and Jaubert, J.N., 2013. Predicting the Phase Equilibria, Critical Phenomena, and Mixing Enthalpies of Binary Aqueous Systems Containing Alkanes, Cycloalkanes, Aromatics, Alkenes, and Gases (N2, CO2, H2S, H2) with the PPR78 Equation of State. Industrial & Engineering Chemistry Research, 52(46), pp.16457-16490.

Rebert, C.J. and Kay, W.B., 1959. The phase behavior and solubility relations of the benzene-water system. AIChE Journal, 5(3), pp.285-289.

Riazi, M.R. and Daubert, T.E., 1987. Characterization parameters for petroleum fractions. Industrial & engineering chemistry research, 26(4), pp.755-759.

Schneider, G.M., 2002. Aqueous solutions at pressures up to 2 GPa: gas–gas equilibria, closed loops, high-pressure immiscibility, salt effects and related phenomena. Physical Chemistry Chemical Physics, 4(6), pp.845-852.

Scott, R.L. and van Konynenburg, P.H., 1970. Static properties of solutions. Van der Waals and related models for hydrocarbon mixtures. Discussions of the Faraday society, 49, pp.87-97.

Tallon, S. and Fenton, K., 2010. The solubility of water in mixtures of dimethyl ether and carbon dioxide. Fluid Phase Equilibria, 298(1), pp.60-66.

van Konynenburg, P.H. and Scott, R.L. 1980. Critical lines and phase equilibria in binary van der Waals mixtures. Philosophical Transactions of the Royal Society of London A: Mathematical, Physical and Engineering Sciences 298(1442): 495-540.

Venkatramani, A.V. and Okuno, R., 2014, June. Modeling of Multiphase Behavior for Water/n-Alkane Mixtures by Use of the Peng-Robinson EOS. In SPE Heavy Oil Conference-Canada. Society of Petroleum Engineers.

Venkatramani, A.V. and Okuno, R., 2015. Characterization of water-containing reservoir oil using an EOS for steam injection processes. Journal of Natural Gas Science and Engineering, 26, pp.1091-1106.

Venkatramani, A.V. and Okuno, R., 2016, June. Compositional Mechanisms in SAGD and ES-SAGD With Consideration of Water Solubility in Oil. In SPE Canada Heavy Oil Technical Conference. Society of Petroleum Engineers.

Volek, C.W. and Pryor, J.A., 1972. Steam distillation drive-Brea field, California. Journal of Petroleum Technology, 24(08), pp.899-906.

Willman, B.T., Valleroy, V.V., Runberg, G.W., Cornelius, A.J. and Powers, L.W., 1961. Laboratory studies of oil recovery by steam injection. Journal of Petroleum Technology, 13(07), pp.681-690.

Wong, D.S.H. and Sandler, S.I., 1992. A theoretically correct mixing rule for cubic equations of state. AIChE Journal, 38(5), pp.671-680.

Wu, J., Liu, Z., Bi, S. and Meng, X., 2003. Viscosity of saturated liquid dimethyl ether from (227 to 343) K. Journal of Chemical & Engineering Data,48(2), pp.426-429.

Appendices

Appendix A. Peng-Robinson Equation of State and van der Waals Mixing Rules

Peng and Robinson (1978) suggested cubic EOS for pure component in the following form,

$$P = \frac{RT}{\underline{V} - b} - \frac{a(T)}{\underline{V}(\underline{V} + b) + b(\underline{V} - b)} \quad \text{(A.1)}$$

where,

$$a(T) = 0.45724\ \frac{R^2 T_c^2}{P_c}\alpha(T) \quad \text{(A.2)}$$

$$\alpha(T) = \left(1 + m\left(1 - \sqrt{\frac{T}{T_c}}\right)\right)^2 \quad \text{(A.3)}$$

$$m = 0.37464 + 1.54226\omega - 0.26992\omega^2 \quad (\omega < 0.49) \quad \text{(A.4a)}$$

$$m = 0.379642 + 1.48503\omega - 0.164423\omega^2 + 0.016666\omega^3 \quad (\omega > 0.49) \quad \text{(A.4b)}$$

$$b = \frac{0.07780 RT_c}{P_c} \quad \text{(A.5)}$$

For mixtures, pure component a and b should be mixed according to certain rules, such as the vdW mixing rules shown as follows,

$$a = \sum_1^{Nc}\sum_1^{Nc} x_i x_j \sqrt{a_i a_j}\text{(1-BIP)} \quad \text{(A.6)}$$

$$b = \sum\nolimits_1^{Nc} x_i b_i \quad \text{(A.7)}$$

Appendix B. Liquid Density Correlations of the CMG STARS (2013)

In the CMG STARS (2013), liquid phase density such as aqueous and oleic phase is calculated by linear mixing of pure component density,

$$\rho_j = \sum_{i=1}^{Nc} x_{ij}\rho_{\mathrm{ij}} , \tag{B.1}$$

where,

ρ_j, molar density of liquid phase j,

x_{ij}, mole fraction of component i in liquid phase j,

ρ_{ij}, density of component i in phase j at T and P, which can be calculated in the following way.

$$\rho_{\mathrm{ij}} = \rho_{iref}\exp[-\alpha_1(T - T_{ref}) - \frac{1}{2}\alpha_2(T^2 - {T_{ref}}^2) + \alpha_3(P - P_{ref}) + \alpha_4(P - P_{ref})(T - T_{ref})] \tag{B.2}$$

where,

P_{ref}, the reference pressure, 1.01325 bars.

T_{ref}, the reference temperature, 288.15 K.

ρ_{iref}, pure component i molar density at reference pressure and temperature.

α_1, the first coefficient of the thermal expansion correlation of component i, $\frac{1}{K}$.

α_2, the second coefficient of the thermal expansion correlation of component i, $\frac{1}{K^2}$.

α_3, liquid compressibility at constant temperature of component i, $\frac{100}{bar}$.

α_4, pressure-temperature cross term for liquid density of component i, $\frac{100}{bar.K}$.